Title
The Engineering of Triggerable Nanocarriers: Surface Charge Converters (SCC) and Fusogenic and Triggerable Phosphopeptide Displaying Liposomes (FTP)

Author
Motion, J.P. Michael

Publication Date
2012

Peer reviewed|Thesis/dissertation

The Engineering of Triggerable Nanocarriers:

Surface Charge Converters (SCC) and

Fusogenic and Triggerable Phosphopeptide Displaying Liposomes (FTP)

By

J.P. Michael Motion

DISSERTATION

Submitted in partial satisfaction of the requirements for the degree of

DOCTOR OF PHILOSOPHY

in

Bioengineering

in the

GRADUATE DIVISION

of the

UNIVERSITY OF CALIFORNIA, BERKELEY

and

UNIVERSITY OF CALIFORNIA, SAN FRANCISCO

ACKOWLEDGEMENTS

First and foremost, I would like to express my gratitude towards my dissertation mentor and advisor, Dr. Francis C. Szoka, Jr. His novel ideas, deep perspectives on science, and enthusiastic outlook on research were invaluable for the completion of this dissertation. It has been a pleasure learning from a highly skilled and detail oriented drug delivery expert.

I would like to express my appreciation to the faculty members that served on my dissertation committee: Dr. Francis C. Szoka Jr., Dr. Tejal Desai, Dr. Song Li, and Dr. Brian K. Shoichet. I would also like to express my appreciation to the faculty members that served on my qualifying oral examination committee: Dr. Tejal Desai, Dr. Song Li, Dr. Christopher Cullander, and Dr. Tanja Kortemme.

Additionally, I would like to express my gratitude to all those who have made contributions to the research in this dissertation including: Dr. Juliane Nguyen for her guidance and assistance with cell cytotoxicity assays, as well as with encapsulation methods; Dr. Justin Chan and Dr. David Pham for their assistance with peptide synthesis; Dr. Zhaohua Huang, Dr. Bo Chen, Dr. Justin Chan, and Dr. Vincent Venditto for sharing their chemistry knowledge, and know-how; Dr. Grace Huynh for her insights on convection and retro-convection enhanced delivery; and Dr. Ronald Siegel for his mentorship and guidance throughout the modeling of brain infusion techniques.

I would also like to thank my laboratory mates: Dr. Juliane Nguyen, Dr. Justin Chan, Dr. Zhaohua Huang, Dr. Bo Chen, Dr. Vincent Venditto, Dr. Emily Perttu, Dr. Kareen Riviere, Dr. Grace Huynh, Dr. Virginia Platt, Dr. Richard Cohen, Jonathan Sockolosky, Colin Walsh, Matthew Tiffany, and Aditya Kohli for collegial conversations and suggestions about my research.

I express my profound gratitude to my mother, Josiane, and grandparents, Raymond and Germaine, who have always believed in my potential and encouraged my academic career. In addition, I express my appreciation to all of my academic mentors at MIT who encouraged me to pursue a PhD. Finally, I am most thankful for the love, support, and encouragement of my wife, Carenina, who provided me with the additional daily energy and motivation to finish this dissertation.

My dissertation is dedicated to my grandparents and my mother. They have been a great source of strength and motivation and to them I am forever indebted for all of their sacrifices.

This work was funded by NIH Grant R01 CA107268-01, the NIGMS Fellowship (NIGMS-IMSD grant R25-GM56847), and by the UC Berkeley Chancellor's Fellowship.

The Engineering of Triggerable Nanocarriers:

Surface Charge Converters (SCC) and

Fusogenic and Triggerable Phosphopeptide Displaying Liposomes (FTP)

By

J.P. Michael Motion

ABSTRACT

A plethora of drug delivery systems (DDS) have been designed over the years to maximize drug payload at tumor sites and reduce the off-target side effects associated with chemotherapeutics. DDS are generally classified by their mode of action and include: passive targeting, active targeting, and/or triggered release. Passive targeted DDS exploit the increased vascular permeability of hypoxic, inflamed, and cancerous tissues for tissue accumulation. Active targeted DDS incorporate targeting ligands that preferentially bind to over expressed receptors in cancer cells providing increased specificity. Nevertheless, off-target side effects still occur due to the lack of spatial control over drug release.

Triggered DDS provide a solution to uncontrolled drug release by eliciting release upon exposure to a disease associated stimuli. The degree of sophistication built into triggers varies by design, but the preference is for engineering simple and robust triggers that are disease-specific and can take advantage of the microenvironment cues of the diseased tissue. Although a number of triggerable systems have been engineered over the last two decades, there is ample opportunity for expanding the arsenal of triggers for drug delivery. In this thesis, I focused my efforts on designing triggerable delivery systems that are substrates for phosphatases, which are enzymes that can be over expressed in life-threatening diseases such as brain and prostate cancer. I report the design and engineering of novel phosphatase triggerable systems that mediate cytosolic delivery through the use of substrate masking and charge conversion.

The phosphatase triggerable systems were designed for cytosolic delivery of drugs. Two different triggering schemes were engineered. The first triggering mechanism was inspired by the fusion machinery of viruses. It was hypothesized that a phosphatase triggerable system could be engineered by masking the hydrophobic and membrane destabilizing segments of fusogenic peptides. Triggering would expose the full peptide sequence, which would partition into adjacent membranes. This membrane insertion event would provide enough enthalpic energy to drive membrane fusion and/or content release of drugs.

In order to design this mechanism, I first had to gain control over the membrane destabilizing properties of fusion peptides. In Chapter 2, it was hypothesized that phosphate substitutions would inactivate the membrane destabilizing properties of these peptides by masking their hydrophobicity. Moreover, phosphatase catalyzed dephosphorylation would regenerate the peptides and trigger lipid mixing and content release. Strategically positioned phosphate moieties were found to be effective at inactivating the fusion peptides, with two phosphates needed for complete loss of activity. The phosphopeptides were excellent substrates for phosphatases, which acted on them to regenerate their membrane destabilizing properties. This robust trigger mechanism was then used to design triggerable fusogenic liposomes.

In Chapter 3, it was hypothesized that fusogenic liposomes could be designed with surface-bound phosphopeptides, and that phosphatases would trigger these peptides to promote lipid mixing, cellular accumulation, and cytosolic content delivery. Fusogenic liposomes, termed FTP for fusogenic and triggerable phosphopeptide displaying liposomes, were found to be excellent substrates for phosphatases. Moreover, phosphatase triggering led to content release and lipid mixing of neighboring liposomes. In addition, FTP exhibited enhanced cellular accumulation as compared to non-triggerable liposomes and were able to mediate cytosolic delivery of their cargos. Although fusogenic liposomes derived from viral proteins provide an

interesting template for triggerable DDS, they are complex in nature and might invoke an immune response upon repeated administration.

The second triggering mechanism exploited phosphatase catalyzed dephosphorylation as a method for converting an anionic liposome into a cationic liposome. Inspired by my electrical engineering background, surface charge converters (SCC) were engineered using inverse-phosphocholine lipids (CP) for triggered anionic-to-cationic charge conversion by phosphatases. Charge conversion was observed upon exposure of SCC to alkaline or acid phosphatases. A rapid increase in zeta potential was observed for SCC formulated with inverse-phosphocholine lipid DOCP. The net gain in zeta potential conversion was +80 mV, which is impressive for an enzyme triggered system. This surface charge conversion mechanism was exploited to design liposomes with enhanced content release and lipid mixing capabilities. SCC formulated with phosphatidylethanolamine and cholesterol were effective at lipid mixing with anionic membranes and delivering macromolecules into the cytoplasm of cells.

In Chapter 5, I provide mathematical insights for the use of infusion technique, such as convection and retro-convection, which can enable the delivery of phosphatase triggerable liposomes to the brain. I also provide mathematical justifications to support key assumptions that have been postulated for modeling these systems in the brain. I conclude by showing how multi-catheter arrays can be used for compartmentalizing drugs delivered into the brain interstitial area.

The thesis is divided into six chapters:

Chapter 1 provides background information on drug delivery systems, reviewing the major classes of delivery systems: passive, active, and triggerable. Furthermore, the chapter provides an overview of enzymatically-active systems, with a particular emphasis on phosphatase triggering.

Chapter 2 presents research that was completed to engineer fusogenic gp41 phosphopeptides. The biophysical and structural characterization of these peptides is presented.

Chapter 3 presents formulation and characterization studies for fusogenic and triggerable phosphopeptide displaying liposomes (FTP). I present formulation schemes as well as biophysical and *in vitro* cellular characterization.

Chapter 4 describes research performed to formulate and characterize surface charge converting liposomes. I present formulation schemes as well as biophysical and *in vitro* cellular characterization.

Chapter 5 provides insights into how mathematical modeling can set the limits for using advanced drug infusion and fluid removal techniques.

Chapter 6 provides a summary of this thesis, as well as recommendations for future designs of phosphatase triggerable systems.

TABLE OF CONTENTS

LIST OF TABLES

LIST OF FIGURES

Abbreviations

AND	Conjunctional Logic Gate
AP	Alkaline Phosphatase
CD	Circular Dichroism
CED	Convection Enhanced Delivery
CF	Carboxyfluorescein
$CHCl_3$	Chloroform
CHEMS	Cholesteryl Hemisuccinate
Chol	Cholesterol
CIP	Calf Intestinal Alkaline Phosphatase
CP	Inverse Phosphocholine Lipid
DAPI	4',6-Diamidino-2-phenylindole
DCC	Dicyclohexylcarbodiimide
DCM	Dichloromethane
DDS	Drug Delivery System(s)
DMF	Dimethylformamide
DMPG	Dimyristoylphosphatidylglycerol
DMSO	Dimethyl Sulfoxide
DNA	Deoxyribonucleic Acid
DOCP	Dioleoylcholinephosphate
DOCPe	Dioleoylcholinephosphoester
DOPE	Dioleoylphosphatidylethanolamine
DORI	1,2-Dioleoyl-3-dimethyl-hydroxyethyl Ammonium Bromide
DOTAP	N-1[1-(2,3-Dioleoyloxy)propyl]-N,N,N-trimethylammonium
DPPG	Dipalmitoylphosphatidylglycerol
DSPC	Distearoylphosphatidylcholine
DSPE	Distearoylphosphatidylethanolamine
ECM	Extracellular Matrix
EPR	Enhanced Permeability and Retention Effect
FACS	Fluorescence-activated Cell Sorting
FBS	Fetal Bovine Serum
FITC	Fluorescein Isothiocyanate
FITC-Dextran	Fluorescein Isothiocyanate-Dextran
FMOC/HBTU/HOBT	Fluorenylmethyloxycarbonyl/o -benzotriazole- N,N,N,N- tetramethyl -uronium -hexafluoro-phosphate/n-hydroxybenzotriazole
FP	Fusion Peptide
FRET	Fluorescence Resonance Energy Transfer
FSC/SSC	Forward Scatter/Side Scatter
FTP	Fusogenic and Triggerable Phosphopeptide Displaying Liposome
HA	Hyaluronic Acid

HAP	Human Alkaline Phosphatase (Placenta)
HBSS	Hank's Buffered Saline Solution
HIV	Human Immunodeficiency Virus
HPLC	High-Performance Liquid Chromatography
Hr	Hour
ISF	Interstitial Fluid
L/P	Lipid to peptide ratio
LP	Lysophospholipid
MALDI-MS	Matrix-assisted laser desorption/ionization Mass Spectrometer
MDCC	*N*-[2-(1-maleimidyl)ethyl]-7-(diethylamino) coumarin-3-carboxamide
MeOH	Methanol
MMP	Matrix Metalloproteinases
MPS	Mononuclear Phagocytic System
MTT	Dimethyl Thiazolyl Diphenyl Tetrazolium Salt
mV	Milivolts
MW	Molecular Weight
NBD	Nitro-benzoxadiazole
NBD-PE	1,2-Dipalmitoyl-*sn*-glycero-3-phosphoethanolamine-N-(7-nitro-2-1,3-benzoxadiazol-4-yl) (ammonium salt)
NHS	*N*-hydroxysuccinimide
nm	Nanometer
nmol	Nanomole
PC	Phosphatidylcholine
PDE	Partial Differential Equation
PDI	Polydispersity Index
PE	Phosphatidylethanolamine
PEG	Polyethylene Glycol
PEG-DSPE	polyethylene glycol distearoylphosphatidylethanolamine
PG	Phosphatidylglycerol
POPC	Palmitoyloleoylphosphatidylcholine
POPE	Palmitoyloleoylphosphatidylethanolamine
POPG	Palmitoyloleoylphosphatidylglycerol
PP1	Protein Phosphatase 1
PPI	Propidium Iodide
PS	Phosphatidylserine
R-CED	Retro Convection Enhanced Delivery
RES	Reticuloendothelial System
RHO-PE	1,2-Dipalmitoyl-*sn*-glycero-3-phosphoethanolamine-N-(lissamine rhodamine B sulfonyl)
RNA	Ribonucleic Acid
SCC	Surface Charge Converter

Sec	Seconds
siRNA	Short Interfering Ribonucleic Acid
$sPLA_2$	Phospholipase A_2
Std.	Standard Deviation
TFA	Trifluoroacetic Acid
TFE	Trifluoroethanol
VEGFR	Vascular Endothelial Growth Factor Receptor

Chapter 1: The Engineering of Bioactive Liposomes: A Review of Passive, Active, and Triggerable Targeting Strategies

1.1 Abstract

For over half a century, many drug delivery systems (DDS) have been designed to address the shortcomings associated with systemically administered drugs. Combinatorial libraries of lipids, polymers, and peptides have been used to create a myriad of nanocarriers with unique properties [1-3]. Out of these, liposomes, or lipid-based nanoparticles, offer unparalleled versatility for triggered drug release.

Liposomes are designed to take advantage of leaky vasculatures within pathological disease sites (such as in inflammatory diseases and cancer). In addition, liposomes can actively target tissues with surface anchored ligands that bind to receptors over expressed at the site of disease, and can be triggered to provide spatial and temporal control over drug release. The goal of liposomes is to prolong the half-life and circulation time of drugs, increase drug accumulation at pathological sites, and specifically target disease tissue. This chapter describes the requirements that liposomes must possess to be effective drug carriers. In addition, it provides a summary of passive, active, and triggerable targeting strategies and an overview of enzymatically triggerable systems.

1.2 Design and Engineering Challenges of Drug Delivery Systems

In the early twentieth century, the German bacteriologist Paul Ehrlich coined the term "magic bullet", referring to a molecule capable of selectively fighting disease without harming healthy tissue. When designing drug delivery systems based on the notion of the "magic bullet", several engineering factors must be considered. First, a "magic bullet" must contain an active targeting moiety that differentiates between healthy and diseased tissues. It must also have release mechanisms that allow for temporal and spatial control of drug release. In addition, it must be stable in circulation and reach the target tissue at adequate concentrations to perform its therapeutic effect. Finally, the "magic bullet" must be superior to the free drug, have a better therapeutic index, and reduced side effects.

Drug delivery engineers need to understand the limitations of each component, as well as the limitations and challenges that the delivery system faces upon systemic administration. The engineering considerations of multi-component drug delivery systems can be broken down into four parts (Figure 1.1):

1) An active biological agent that inhibits or activates cellular functions,

2) A carrier capable of protecting the biological agent and reducing its systemic toxic effects,

3) A targeting ligand that can target and identify the diseased tissue,

4) A chemical or biological trigger that elicits controlled drug release at the pathological site of interest upon stimuli.

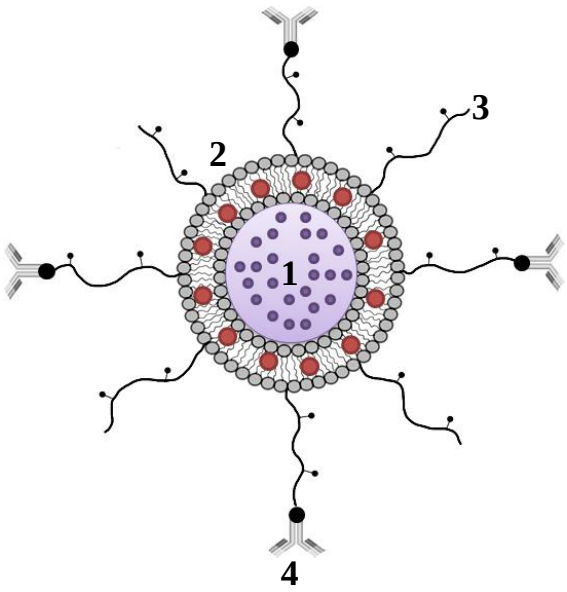

Biological Agent (1)	**Carrier Layer (2)**	**Targeting Layer (3)**	**Trigger Layer (4)**
Small Molecules	*Lipids*	*Peptides*	*pH Triggers*
Proteins	*Polymers*	*Antibodies*	*Redox Triggers*
Biopolymers	*Peptides*	*Polymer*	*Light Triggers*
DNA	*Dendrimers*	*Carbohydrates*	*Magnetic Triggers*
siRNA	*Composites*	*Small Molecules*	*Enzyme Triggers*

Figure 1.1: Schematic Illustration of Multi-component Drug Delivery Nanocarriers. Nanocarriers, such as liposomes, can be engineered with different elements for passive or active targeting and/or triggering at the disease site.

Delivery systems are suitable for therapeutic drugs that are limited by poor bioavailability and/or high toxicity. For instance, dose-limiting toxicities and acquired multi-drug resistance limits the clinical use of doxorubicin and paclitaxel as chemotherapeutics [4-6]. To overcome multi-drug resistance, the standard of care calls for an elevated drug dose regimen, but this has toxic implications and causes a variety of side effects. These limitations can be solved by the use of a liposomal delivery system.

Liposomes can mediate the delivery of lipophilic or water soluble drugs. The lipophilic drug is usually bound to the lipid bilayer or dissolved in the lipid phase, while the water soluble compound is encapsulated within the aqueous compartment. While many types of molecules can be encapsulated in liposomes, the lipid composition as well as the physico-chemical properties of the drug influences the stability and the encapsulation of the formulation. For instance, the chemotherapeutic paclitaxel requires high a concentration of toxic emulsifying agents, such as Cremophor®, to solubilize the drug for parenteral administration. Replacing the emulsifying agent with a liposomal formulation greatly improved paclitaxel solubility and bioavailability and, in turn, its clinical utility [5, 7].

The carrier surface is also responsible for improving the pharmacokinetics of the drug. The properties of the carrier must be selected to sustain the stress imposed by circulation, protect the cargo from systemic exposure, and prevent drug leakage that could lead to side effects [8]. Furthermore, the components of the carrier must be selected for optimal drug release kinetics in order to achieve the therapeutic index of the drug [3].

Preventing cytotoxicity and immune activation are major goals of the carrier for oncology applications. Materials with high cytotoxicity profiles are thus discouraged as primary components of the carrier. The carrier must be biocompatible and biodegradable and have minimal toxicity. For instance, liposomes made of zwitterionic lipids such as phosphatidylcholine

are biocompatible and cause minimal immune or antigenic reactions [9], whereas positively charged cationic lipids are immunogenic and react towards a number of proteins in circulation. This promotes blood clots, inflammation, immune stimulus, and disruption of the blood brain barrier [10-12]. Nevertheless, skillful craftsmanship of the carrier composition can enable the design of cationic systems with great therapeutic potential and minimal cytotoxicity. For instance, Silence Therapeutics has designed a cationic siRNA lipoplex formulation (Atu027) that effectively targets protein kinase N3 and knocks down its activity in several animal models. Surprisingly, the formulation has been well tolerated in both animals and humans without the use of immune suppressants [13, 14].

The physiological barriers of the diseased tissue are of relevance to the carrier design since they impose physico-chemical constraints. Intuitively, the targeted tissue imposes limits on the size, shape, and charge of the carriers. Carriers have to be designed with a diameter cutoff of 500 nm if the end goal is to extravasate from circulation and accumulate at tumor sites. The sweet spot diameter for tumor targeting lies in the range of 100-200 nm [8, 15]. On the other hand, kidney targeting requires the particle diameter to be in the range of 50-100 nm [16]. The size of the carrier also influences its biodistribution. Lipid vesicles in the range of 25-50 nm exhibited reduced liver uptake as compared to larger vesicles in the range of 200-300 nm [17]. At the same time, vesicles with diameters greater than 100 nm experience increased clearance rate by the phagocytic system, which limits their circulation half life [18]. Charge also influences the biodistribution of particles. Monocytes and macrophages preferentially recognize anionic vesicles, since the negative surface charges interact with scavengers receptors on the surface of macrophages [19].

Intravenous injection is the most common route of administration for targeted delivery [8]. Nanocarriers administered via this route face significant delivery challenges for tissue accumulation and on-site drug release. Nanocarriers must remain in circulation long enough in

order to extravasate into the tissue and must be triggered at the site of disease to minimize off-target side effects. Active targeting strategies have been developed to improve the internalization and targeted accumulation of nanocarriers. A large number of site-specific ligands, including antibodies, peptides, hormones, and sugars, have been utilized with great success to target tissues and improve internalization [20]. Nonetheless, active targeting does not address the uncontrolled drug release of nanocarriers in circulation that is responsible for off-target side effects [8].

To gain temporal and spatial control over drug release profiles and kinetics, trigger release strategies can be incorporated into delivery systems. The ideal trigger is location and/or cell type specific and takes advantage of the microenvironmental cues of the diseased tissues. Various trigger modalities have been successfully designed to react to changes in redox potential [21], pH [8], enzyme concentrations [22], temperature [23, 24], light [25, 26], magnetic fields [27], and electrical fields [28]. This thesis will focus on expanding the uses of phosphatases as triggers for liposomes.

1.3 Liposomal Drug Delivery Systems

Liposomes are vesicles formed by the self-assembly of lipids in water into lipid bilayers. Liposomes were first observed in the 1960s studies of Alec Bangham, in which Bangham and Horne showed electron microscope images of liquid-crystalline multilamellar phospholipid bilayer structures resembling lipid spherules [29, 30]. The term liposomes was coined by Gerald Weissmann in 1968 [31], and has been used ever since to define these artificial lipid vesicles.

Liposomes are biocompatible, biodegradable, and have low immunogenicity, making them ideal drug carriers [9]. They are primarily composed of natural or nature-inspired lipids, such as phosphatidylcholine (PC), phosphatidylethanolamine (PE), phosphatidylglycerol (PG), phosphatidylserine (PS), and cholesterol (Chol). The method of preparation as well as the lipid

composition influences their shape, diameter, polydispersity, and drug loading ability [32]. Liposomes can be prepared in diameters ranging from 25 nm to greater than 50 μm with a single or multiple bilayers [9], and have been formulated to encapsulate a wide range of hydrophilic and hydrophobic molecules including small molecules, like doxorubicin, and macromolecules, such as DNA and RNA [33]. Their primary goal is to improve the bioavailability, biodistribution, and circulation time of drugs [9].

Over the last forty years, liposomes have been one of the leading areas of research for drug delivery systems with 42,000 Pubmed research articles published on the topic (data as of February 2012). Liposomes have had wide adoption in the pharmaceutical and biotechnology industry as carriers for cosmetics and drug therapies, including FDA-approved drugs for the treatment of cancer (Doxil®/Caelyx®), fungal infections (Ambisome®), and infantile respiratory distress syndrome [34, 35].

1.4 Passive Targeting

Passive targeting refers to the ability of macromolecules to accumulate in tissues as a result of the increased permeability of the endothelial lining around inflamed and hypoxic tissues [36] including tumors [36-38] and infarcts [39]. This phenomenon is known as the enhanced permeability and retention effect (EPR) and accounts for the increased accumulation of macromolecules in tumors [37].

The EPR effect in tumors relates to the increased vascular permeability as a result of the tumor neoangiogenic process [37]. Because of large fenestrations in tumor microvessels, liposomes extravasate from circulation into the interstitial fluid of the tumor [20]. In addition, the lack of functional lymphatic drainage and filtration prevents the outflow of liposomes, allowing liposomes to accumulate over time and release drug in a controlled manner [20]. EPR-mediated

drug delivery is well suited for macromolecules, liposomes, and other nanoparticles, but is of limited use for small molecular agents, which can readily diffuse back into circulation [40]. In addition, the low rate of particle extravasation into healthy tissue results in reduced cytotoxicity [20].

Passive targeting to tumors is affected by a number of systemic and formulation factors. These include rapid clearance by physiological systems, saturation of Kupffer cells, and the diameter, shape, charge, and stability of the formulation [20]. Rapid clearance of the liposomes is a rate limiting factor for extravasation. Increasing the circulation time of the liposomes leads to higher tumor tissue accumulation. To increase the circulation time of liposomes, liposomes must avoid opsonization by plasma proteins and rapid clearance by the mononuclear phagocytic system (MPS) and/or reticuloendothelial system (RES) after systemic administration [41].

The surface charge of liposomes also plays a critical role in clearance. Neutral liposomes show prolonged circulation times compared to anionic vesicles. Vesicles composed of anionic lipids like dimyristoylphosphatidylglycerol (DMPG) and dipalmitoylphosphatidylglycerol (DPPG) experience rapid opsonization with a number of circulating proteins and rapid clearance by the RES [42-45]. Therefore, techniques that mask the surface charges as well as the carrier surface are important for passive targeting. Surface-grafting of the liposome with water-soluble polymers, such as polyethylene glycol (PEG) [46], provides a strategy to shield the surface charge, while protecting against opsonizations and rapid clearance by the mononuclear phagocytic system [47].

The diameter of the liposomes is another critical factor for passive targeting. In order to extravasate the endothelial barrier, lipid vesicles must be formulated with a mean diameter below 500 nm [48]. The role of particle diameter is further exemplified by the fact that liposomes with a diameter greater than 200 nm have reduced circulation time and are quickly cleared by the MPS

and RES, whereas liposomes with diameters smaller than 200 nm have increased circulation and tumor accumulation [49]. A lower particle size limit is imposed by excretion from the kidneys, which can readily eliminate particles smaller than 4 nm [50]. Finally, it must be noted that the rate limiting step of drug bioavailability for passive drug targeting is drug release. Nonetheless, liposomes with passive drug targeting capabilities are successful in the clinic. To date, five formulations have been approved as therapies [51].

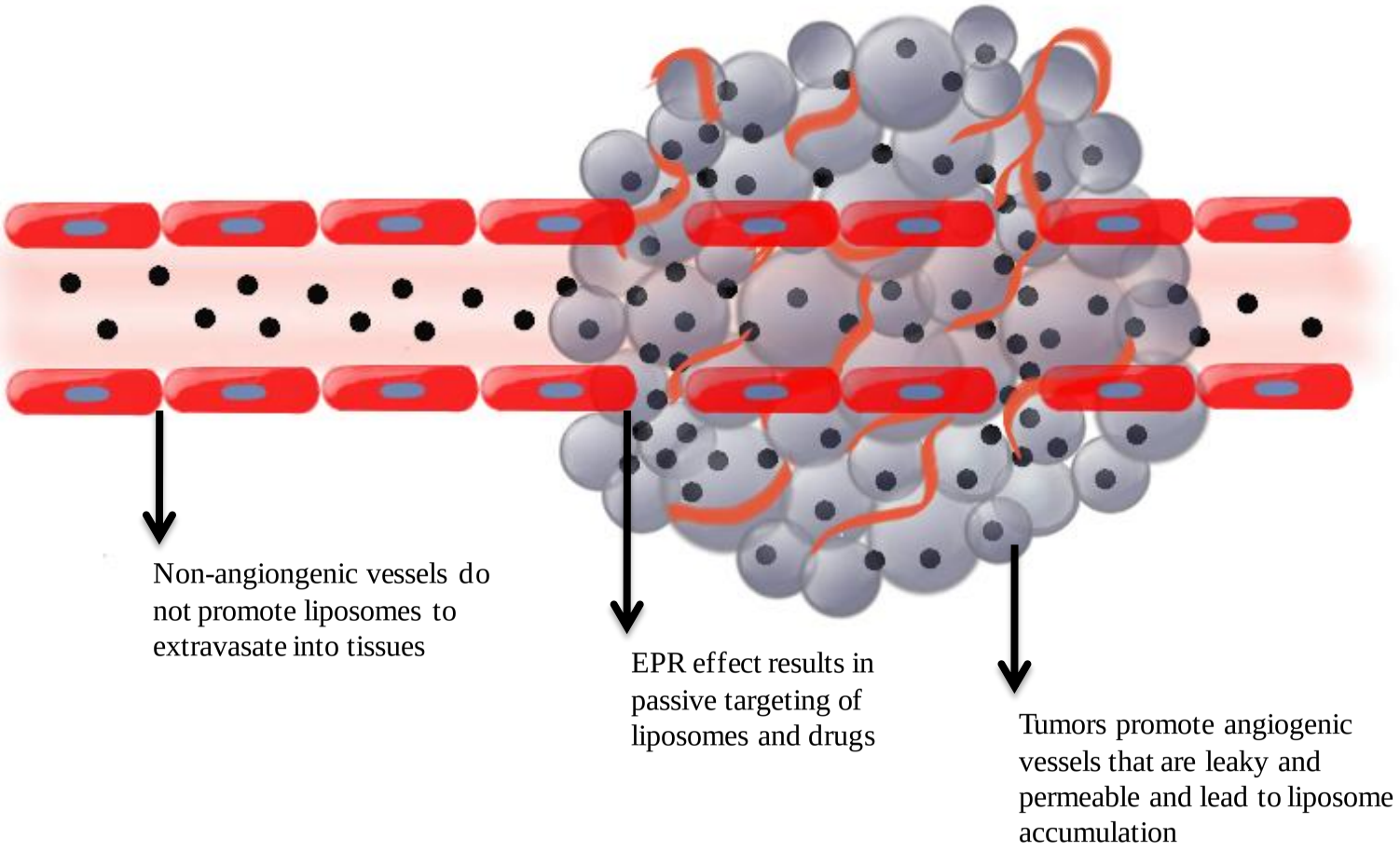

Figure 1.2: Schematic Illustration of EPR-Mediated Passive Targeting. Passive targeting relies on tissue extravasation as a mechanism for site accumulation. The leaky vasculature of tumors promotes the increased site accumulation of nanocarriers through the enhanced permeability and retention effect. The rate of drug release from the carrier dictates the bioavailability and the drug exposure to the surrounding cells.

1.5 Active Targeting

The ability to precisely target tissues by exploiting tissue-specific characteristics is known as active targeting. As an example, active targeting can be achieved by the direct conjugation of drugs to targeting antibodies or by the conjugation of antibodies to liposomes. This ligand to receptor paradigm has been widely used to target liposomes and other nanoparticulates to tumor sites as illustrated in Figure 1.3. In essence, it is a strategy that exploits the use of molecular zip codes.

Active targeting strategies are typically designed for receptors over expressed in diseased tissue and under expressed in other body sites. For instance, many solid tumors over express the membrane-bound receptor CD44 and are enriched in hyaluronan [52]. Hyaluronic acid (HA) oligosaccharides in the 6-8 saccharide range have been reported to inhibit the growth of tumor cells over expressing CD44 [53]. Liposomes modified with HA oligosaccharides were effective against CD44-over expressing tumor cells [54]. Hence, active targeting strategies that interfere with receptor-ligand interactions and deliver drug payloads could effectively treat tumors.

Active targeting moieties can include: antibodies and their fragments, peptides, lectins, hormones, small molecules, monosaccharides, oligosaccaharides, polysaccharides, and peptoids [9]. The choice of targeting moiety is dependent upon the ligand-receptor interaction. Ligand incorporation can be done before or after liposome formation and can be conjugated using different chemical modifications including thioether, disulfide, and amide covalent linkages [32]**.** To ensure proper exposure of the targeting ligand on the liposome surface and to improve receptor binding, ligands are typically attached to PEG, which provides a flexible linker and increases the distance between the liposome and the ligand [9].

A number of factors influence the efficiency of active targeted liposomes. For instance, the degree of vascularization at the disease site is a critical parameter for successful targeted

therapy. Liposomes that target vascular components, such as the tumor endothelium, have a higher degree of accumulation than passive targeted liposomes. This was demonstrated using liposomes targeted to the VEGFR receptor [55]. An improved therapeutic efficacy was observed for targeted liposomes versus non-targeted liposomes. Nevertheless, liposomes targeted to surface receptors within solid tumors had no significant improvement in accumulation when compared to non-targeted liposomes [56-58]**.** This is because the rate limiting step for liposome accumulation in the tumor microenvironment is extravasation from circulation. However, an enhanced anti-tumor effect has been reported for targeted liposomes as a result of increased particle internalization [59]. Thus, targeting ligands can enhance the degree of internalization and site-specific intracellular delivery of drugs, which are critical factors for successful chemotherapeutics [60].

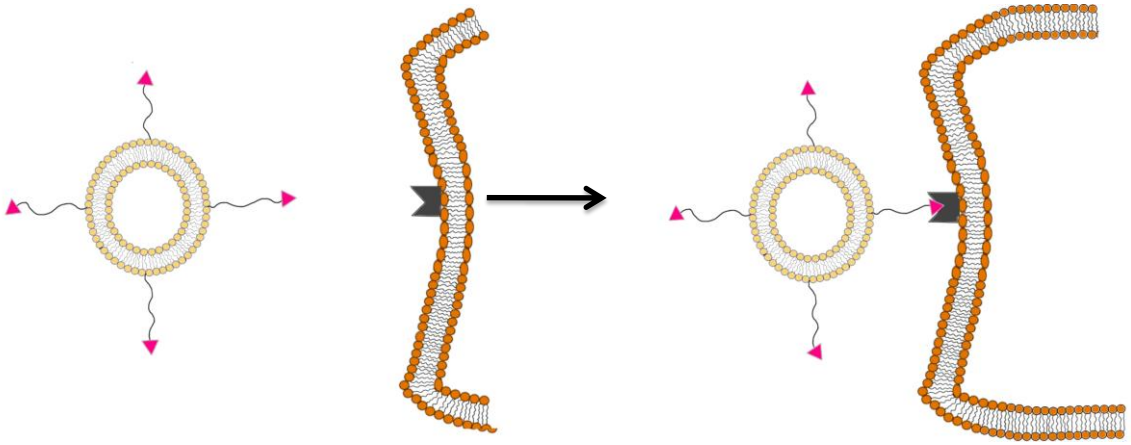

Figure: 1.3 Schematic Illustration of Active Targeting. Surface ligands (triangle) on liposomes allow the recognition of surface receptors on cells and enables site-specific accumulation.

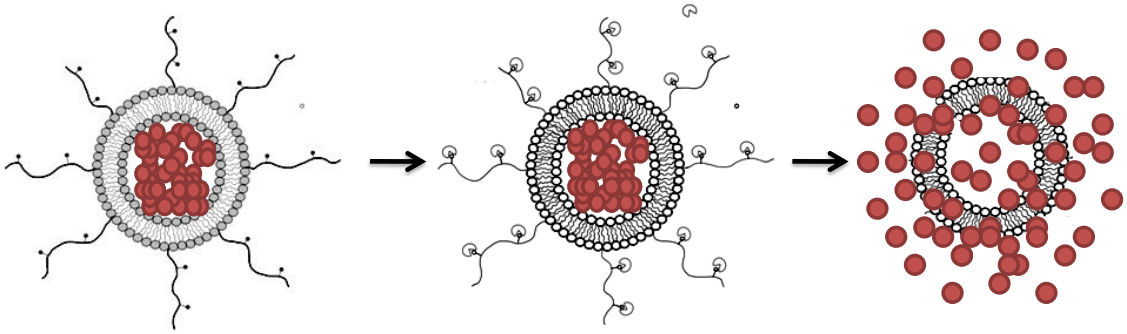

Figure: 1.4 Schematic Illustration of Enzyme-Induced Triggered Release. Enzymatically-active liposomes are designed to be stable in circulation until exposed to their specific enzyme. Trigger moieties attached to the surface of the liposomes provide a substrate for the enzyme. The enzyme acts on the substrates and cleaves the trigger moieties. This induces membrane fusion and/or drug release.

1.6 Triggered Release

Although passive and active targeting strategies mediate site-accumulation of liposomes, they do not offer control over drug release. Drug release is controlled by environmental triggers that disrupt the liposomes. Disruption of the contents of the liposomes is the most common mechanism of *in vivo* drug release. Thus, the composition of the lipid bilayer highly influences the kinetics of drug release. The charge, phase transition, hydrogen-bonding capacity, membrane rigidity, and trigger moieties are all parameters that affect drug retention and drug release [61]. Surface charges as well as charges at the membrane interface can modulate the release of drugs from liposomes. For example, DSPC/Chol liposomes that contained a negatively charged PEG-DSPE had reduced formulation stability and increased vincristine leakage rates in circulation [62]. Moreover, cationic lipids are used as electrostatic anchors and release mediators of nucleic acid in transfection reagents [10]. Strategically placed charges can also be used to enhance the permeability of ions and molecules to the bilayer. For instance, the anionic molecule carboxyfluorescein had an increased leakage rate from inverse phosphocholine liposomes as compared to zwitterionic phosphocholine liposomes [63]. This was attributed to the increased permeability of the anionic molecule to the membrane as a result of the head group inversion that positioned the quaternary amine adjacent to the bilayer.

The stimuli to induce release can be divided into physiological relevant microenvironment cues and externally applied stimulus [64]. Changes in redox potential [21], pH [8], enzyme concentrations [22], temperature [23, 24], light [25, 26], magnetic fields [27], and electrical fields [28] have been successfully used as triggers for drug release. For most cases, triggering results in changes in the physico-chemical state of the liposome and leads to efficient cytosolic or extracellular drug release.

The engineering of triggerable systems can be divided into a few simple strategies that include charge conversion, shape conversion, and substrate masking. Liposomes can be

engineered with one or more of these strategies to achieve triggered release. Charge conversion relies on changes of the surface membrane potential as a result of stimulus. These local changes in membrane potential can be used for triggering membrane fusion with neighboring membranes or for triggering lipid packing changes in the bilayer that result in drug release. The type of liposomal formulation determines the physico-chemical properties of the system as well as the release kinetics and delivery mode. For instance, surface exposed phosphate groups, as described in Chapter 4, can mask positive charges from quaternary amines adjacent to the bilayers [63]. When enzymatically triggered, these head groups undergo local charge conversion increasing the surface potential from negative to positive, and inducing lipid mixing and content release.

Localized pH changes that occur during endocytosis can also be used as triggers for charge conversion [8]**.** Ionizable lipids have been designed to undergo charge conversion as a result of head group protonation and mediate fusion and endosomal release [8]. Furthermore, charge conversion strategies have been incorporated into ionizable surface ligands for endosomal escape. For example, the GALA peptide was used to mediate pH-triggered endosomal escape of a targeted transferring liposomal formulation [65]. Thus, trigger moieties that promote charge conversion can be incorporated into lipid head groups and surface ligands in order to mediate endosomal release and drug delivery.

Shape conversion relies on the ability of triggers to induce structural changes in the architecture of the bilayer. One of the classical examples consists of liposomes made from the anionic cholesterol derivative, CHEMS, and the polymorphic lipid, DOPE. At neutral pH, the system is fairly stable with both lipids having cylindrical shape. Upon acidification, CHEMS becomes protonated, promoting a shape conversion that results in a cone shape. This in turn promotes the hexagonal phase transition of DOPE and destabilizes the liposome [66-70]. Shape conversion and substrate masking has also been incorporated into ligand design strategies of triggerable systems. For instance, Harris et al. demonstrated how the use of cleavable protease

linkers within sterically protective polymers can be used as a trigger strategy. They reported that in the presence of protease, the surface area of the sterically protective polymers was reduced, exposing a magnetofluorescent particle [71]. Although many trigger strategies have been pursued for physiological release, there is still a need for designing disease-specific triggers.

1.6.1 Enzyme Triggering

Enzymes are designed to be specific for their substrates. As a result, enzymatic triggering can provide an additional degree of target specificity for a liposome as illustrated in Figure 1.4. Successful enzyme triggering relies on disease-specific over expression of enzymes [22, 72]. When enzymes are over expressed in disease, they provide a disease-specific marker that can be exploited for trigger release. For instance, elevated levels of alkaline phosphatases are highly correlated with prostate cancer metastasis [73]. Thus, drug delivery systems that can take advantage of the local increase in phosphatase concentration could be useful for site-specific trigger release.

The spatial localization and time-dependent concentration of the enzyme impacts the efficacy of drug delivery. Liposomes can be designed to fuse at the cell membrane if a high concentration of membrane-bound enzyme is present. However, if the concentration of membrane-bound enzyme is lower than the concentration of enzyme in the extracellular matrix, then liposomes will be triggered extracellularly.

Enzyme-activated systems have been most commonly developed for triggered drug release to tumor microenvironments [72]. The most common approach involves designing liposomes that can be triggered by secreted enzymes such as phospholipases ($sPLA_2$) [74-77], matrix metalloproteinases (MMP) [71, 78-81], and elastases [82]. Nevertheless, these systems are

triggered in the extracellular matrix and are thus impractical for the intracellular delivery of proteins, nucleic acids and siRNA.

Phosphatases, which are commonly over expressed in tumor microenvironments [73], are an attractive enzyme for designing triggerable systems. They can facilitate triggering at the cell membrane or within intracellular compartments, and potentially mediate cytosolic delivery. Few systems, however, have been designed for phosphatase triggering.

1.6.2 Phosphatase Triggering

Phosphatases are responsible for catalyzing the hydrolysis of phosphoric acid monoesters. They have enzymatic activity towards proteins, peptides, nucleotides, alkaloids, phospholipids, and lipopolysaccharides [83-88]. Although considered an ubiquitous and promiscuous enzyme, phosphatases confer specificity, selectivity, and regulation on their biological substrates [83]. For example, cellular serine/threonine phosphatases are assembled as multimeric enzymes combining few catalytic subunits and a number of regulatory subunits. Their unique molecular assembly results in biological machines with high precision and low promiscuity that can carefully control and regulate highly specific biological processes [83]. These biological processes include gene transcription, RNA splicing, signal transduction [89], biopolymer dynamics [90], and biochemical pathways [83, 91]. Protein phosphatases are classified by their substrate specificity as serine/threonine protein phosphatases [92], tyrosine phosphatases [93], and histidine phosphatases [94]. They can also be classified by their optimum working pH as alkaline [93] or acidic [95]. Despite sharing common functionality and substrate specificity, phosphatase isoenzymes have marked differences in molecular weight, sequence homology, isoelectric points, resistance to different inhibitors, and tissue expression profiles [95].

Given the wide range of phosphatases in the body and their selective over expression in diseased tissue, phosphatases can provide a triggering mechanism for appropriately engineered liposomes.

Phosphatases have been used for decades to trigger pro-drugs and convert inactive phosphate derivatives into active compounds [96]. For example, amifostine is a clinically used drug that is activated by membrane bound phosphatases and has been used as a radical scavenger during chemotherapies [97]. Furthermore, alkaline phosphatase immunoconjugates have been designed as targeted triggers for pro-drugs [98]. In this approach, monoclonal antibodies were used to target alkaline phosphatases to diseased tissue, and subsequently catalyze the activation of systemically administered prodrugs at the site of disease. This strategy was successfully applied for the triggered delivery of etoposide phosphate [98], mytomicin C phosphate [99], a prodrug of p-[N,N-bis(2-chloroethyl)amino]phenol [100], and N-(4-phosphonooxy)phenylacetyl)-doxorubicin [101].

Phosphatases have also been used to trigger content release of liposomes containing cholesterol phosphate derivatives [88]. In this approach, Davis and colleagues designed a family of cholesteryl phosphate derivatives, which were used as substrate masks and stabilizers of phosphatidylethanolamine (PE) bilayers. The derivatives were shown to be a substrate for both alkaline and acidic phosphatases. Their dephosphorylation led to the charge conversion at the interface and promoted the hexagonal-phase of DOPE. This drove the collapse of the bilayer and prompted content release [88]. In another example, Cho and colleagues used phosphatases to trigger synthetic supramolecular systems and model the effects of phosphoryl transfers in molecular recognition [102]. They accomplished this by encapsulating cationic aromatic molecules in β-cyclodextrin-6A-phosphate scaffolds that triggered content release in the presence of phosphatases. Previous phosphatase triggerable systems, however, suffer from divalent cation induced aggregation as a result of their highly negative surface charge.

1.7 Conclusion

The versatility of liposomes offer engineers a unique platform for designing drug delivery systems with passive targeting, active targeting, and/or triggered release capabilities. Passive and active targeting strategies are efficient accumulating at the site of disease but offer no control over drug release nor prevent the premature leakage of drugs in circulation. Liposomes designed with trigger moieties have an additional layer of control and can release drugs upon site accumulation. Triggered release strategies use microenvironment cues or externally applied stimulus to induce drug release from liposomes. Triggerable release strategies include: charge conversion, shape conversion, and substrate masking. Enzymatically-active systems can be designed with these strategies in mind to take advantage of disease-specific triggers and provide greater control over drug release. Systems designed for MMP, elastase, phospholipase, or phosphatase triggering have exemplified the use of enzymes as triggers. Although a promiscuous enzyme, phosphatases can provide an enzymatic trigger for appropriately engineered liposomes. In this thesis, I extend the use of phosphatases as triggers for drug delivery systems by engineering systems for which phosphatases can trigger charge conversion and polarity reversal and induce drug release.

Chapter 2: The Engineering of Triggerable Fusogenic Phosphopeptides: Gaining Control over Membrane Fusion

2.1 Abstract

Phosphopeptides have been designed as triggerable components for drug delivery systems to mediate membrane fusion upon phosphatase catalyzed dephosphorylation. It was hypothesized that phosphates could be used as substrate masks for hydroxylated amino residues within fusion peptides. Strategically placed phosphates could inactivate the membrane destabilizing properties of the fusion peptides. Phosphatase catalyzed dephosphorylation would regenerate the hydrophobicity of the peptide, and trigger membrane fusion and content release from adjacent liposomes. To test this idea, the gp41 fusion peptide was selected as a template for phosphopeptide engineering and synthesis. Phosphate moieties were found to be effective at inactivating the membrane destabilizing properties of the fusion peptides. The decrease in activity was correlated to the number and position of phosphate groups, with a minimum of two phosphates needed for inactivation. Phosphatase catalyzed dephosphorylation regenerated the ability of the peptides to destabilize membranes and induced lipid mixing and content release of liposomes. To further investigate the specificity of the phosphatase trigger, the phosphate groups were replaced with sulfonates. The sulfonated peptide did not induce membrane fusion nor was the fusion activity regenerated in the presence of phosphatase. This robust trigger mechanism could be valuable as a component of a drug delivery system. The design and engineering considerations for the synthesis of triggerable fusogenic phosphopeptides as well as experimental evidence demonstrating the practicality of phosphatase triggering are presented in this chapter.

2.2. Introduction to Membrane Fusion and Fusion Peptides

2.2.1 Membrane Fusion

Membrane fusion of biological systems plays an important role in many cell-cell and cell-compartment interactions, as well as in intracellular trafficking and viral infection [103-105]. In order for membranes to fuse, they must be first brought together. This requires complete dehydration of the water layer that separates lipid bilayers [106]. In non-biological membranes, this distance ranges between 2-3 nm [107], whereas in biological membranes the distance ranges between 10-20 nm.

Membrane fusion is a complex process driven by enthalpy and opposed by entropy [108, 109]. At the interbilayer gap, there is an entropic (hydrophobic forces) and enthalpic (hydration forces) cost that needs to be overcome for fusion to start. A number of intermolecular forces, such as electrostatics, hydrogen bonding, and van der Waals forces, must act in concert to orchestrate each fusion event. Although there are high kinetic and thermodynamic barriers, once started, fusion of two bilayers is thermodynamically favorable [110].

Many fusogens are known to facilitate membrane fusion. For example, viral fusion proteins and fusion peptides are known to lower the kinetic barrier of fusion between two membranes [110]. The energy liberated as part of conformational changes during the activation of fusion proteins is used to drive the insertion of fusion peptides into the bilayer of adjacent membranes, bridging the interbilayer gap, and bringing both membranes into close proximity [108, 109]. Thermodynamic studies of the hemagglutinin fusion peptide-membrane interactions reported that the gain in Gibbs Free Energy as a result of peptide insertion into bilayers was -7.6 kcal/mol and was primarily driven by enthalpy [109]. The use of fusion peptides as a component of a drug delivery system could result in a carrier with enhanced lipid mixing and cytosolic delivery capabilities as a result of enthalpic gains provided by the fusion peptide.

The mechanism of membrane fusion is thought to occur via a stalk structure [111]. The stalk hypothesis proposes that membrane fusion occurs after two lipid bilayers come in close contact with one another at the angstrom level (Figure 2.1). Dehydration of the contact site promotes local membrane bending that disrupts the bilayer and initiates lipid mixing of the outer leaflet. This creates a fusion stalk, which expands into a hemifusion diaphragm where inner leaflet mixing occurs. Upon successful mixing, a fusion pore is formed that facilitates content transfer [108]. It is important to note that not every hemifusion event leads to pore formation.

Hemifusion might be restricted by limited lipid mixing and/or diffusion [108] and is observed only for specific lipid composition [106]. Lipids that promote positive membrane curvature of the outer leaflet, such as inverted-cone shaped lysophospholipids (LP), inhibit stalk formation and fusion. On the other hand, lipids that promote negative membrane curvature of the outer leaflet, such as cone-shaped phosphatidylethanolamines (PE), promote hemifusion [105]. Also, because of the drastic structural rearrangements that occur at the membrane interface, energy input is a requirement for fusion [105]. Events that trigger conformational changes in bilayer structure, such as the docking of viral fusion proteins, or lipid charge conversion at membrane interfaces, can provide enough energy for membrane association. In this chapter, the focus is on viral fusion peptides that provide “fusion energy” by partitioning into membranes to form hemifusion stalks [104, 105, 108]. These peptides are engineered with phosphatase-dependent trigger moieties that control their membrane destabilizing properties.

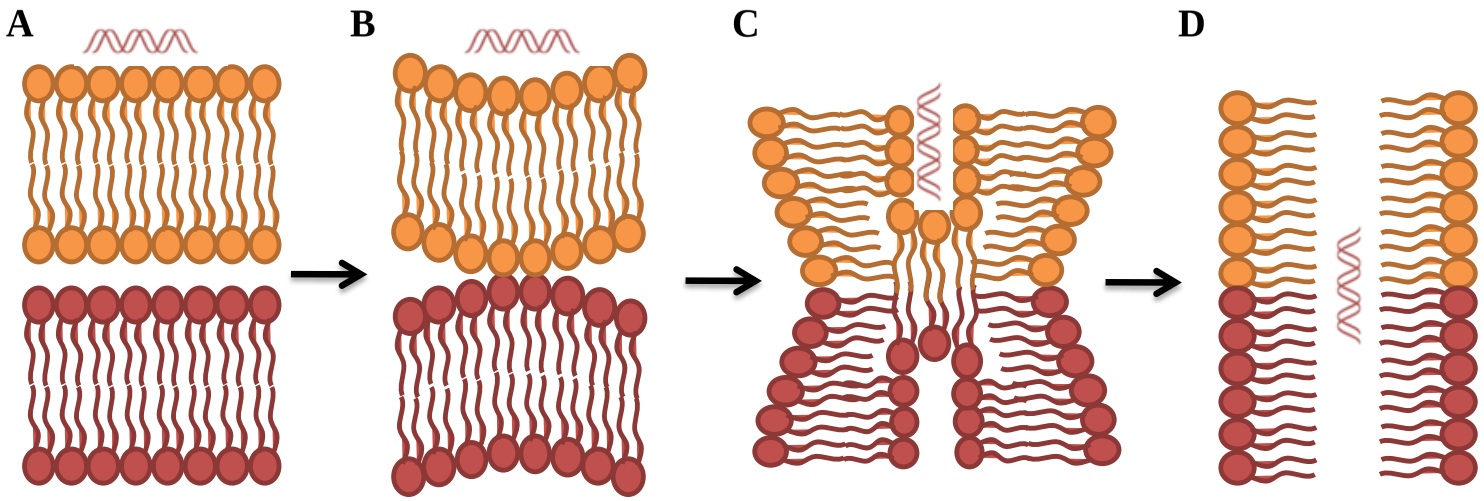

Figure 2.1: Schematic Illustration of Hemifusion-Mediated Membrane Fusion. A) Membrane fusion requires two bilayers to come in close contact and bridge the interbilayer gap that separates them. Intermolecular interactions, such as electrostatics, hydrogen bonding, van der Waals forces, and hydration and hydrophobic forces are responsible for mediating the process. Fusion proteins, peptides, small molecules, and other fusogens can facilitate this initial interaction. B) After membrane dehydration, the proximal leaflets come in close contact and form a fusion stalk, initiating lipid mixing. C) The fusion stalk expands into a hemifusion diaphragm in which the inner leaflets can mix. D) The break of the hemifusion can then lead to the formation of a fusion pore that facilitates content transfer, such as DNA, between membranes [106, 111]

2.2.2 gp41 Fusion Protein and Peptide

Membrane fusion between viral and cellular membranes is a requirement for HIV cell entry. The fusion machinery of HIV is composed of a glycoprotein envelope made of 2 non-covalently associated subunits, gp120 and gp41, both of which are organized as trimers [112]. These subunits precisely orchestrate a series of molecular events that culminate with membrane fusion and infection. The fusion process starts with gp120 binding to the CD4 receptor on target cells [113]. This event catalyzes a structural reorganization of the fusion machinery and releases the gp41 fusion protein from its metastable constraints leading to its activation [114]. Further conformational changes within the gp41 fusion protein result in a pre-hairpin intermediate that bridges the viral and cellular membranes via the insertion of the N-terminus fusion peptide [115]. Mutagenesis experiments indicate that the insertion of the fusion peptide into the cell membrane is a key requirement for fusion and viral content exchange [116, 117]. Collapse of the pre-hairpin intermediate provides sufficient energy to bring the viral and cellular membranes together and promote fusion.

The gp41 fusion peptide is composed of 16 hydrophobic amino acids at the N-terminus, AVGIGALFLGFLGAAG. This highly conserved stretch of hydrophobic amino acids has a high content of alanine and glycine residues. Because of its hydrophobic nature, the fusion peptide preferentially partitions and inserts into cellular membranes. By doing so, it decreases the bending energy at the membrane interface and promotes curved fusion intermediates [118]. Although 16 amino acids insert into target membranes, it has been shown that the minimum fusion peptide can consist of only 12 amino acids [119]. Several studies indicate that the peptide adopts alpha-helical structure upon membrane insertion and micellization [120], as illustrated in Figure 2.2. This interesting fact is useful for the design of fusogenic peptides.

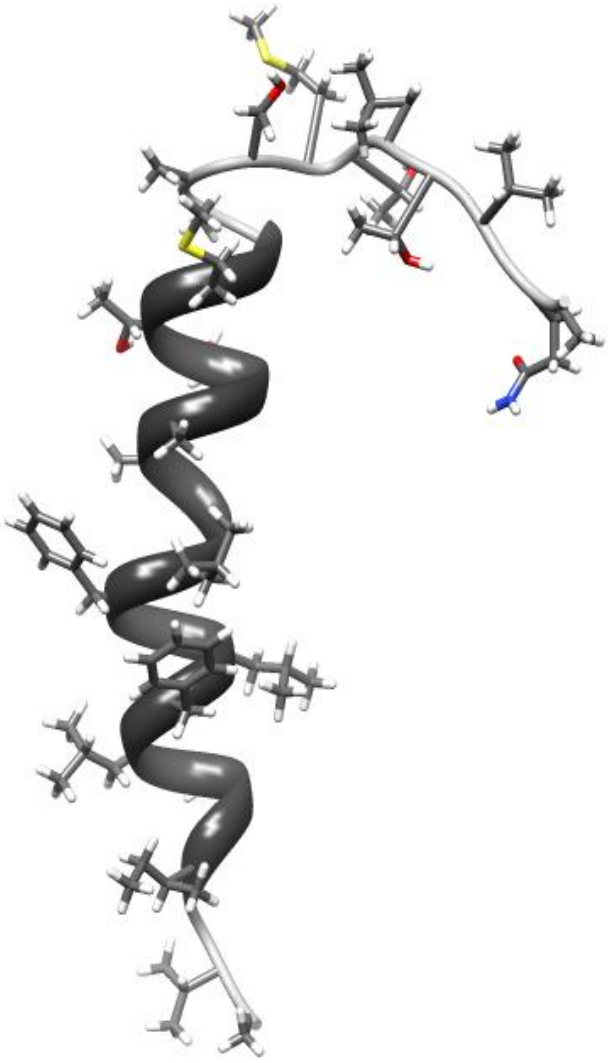

Figure 2.2: Crystal Structure of a 23-mer gp41 Fusion Peptide in a Micelle [120]. The figure depicts PDB structure #2ARI, which is the structure of the N-terminus fusion peptide, AVGIGALFLGFLGAAGSTMGAAS, in a micelle solution. The first 16 amino residues are represented as a ribbon diagram (charcoal), with side chain atoms shown in gray and colored by heteroatom. The 16 amino acids exhibit high alpha helical content in a micelle solution. The figure was prepared using UCSF Chimera.

2.3. Results and Discussion

2.3.1 Engineering Triggerable Fusion Peptides

The gp41 fusion peptide, AVGIGALFLGFLGAAG, has membrane perturbing properties that can accelerate the rate of lipid mixing [121-123], and assist in fusion and infection of target cells [114]. Bioactive ligands that can mimic viral site-activation would be useful for the delivery of small molecules and genetic material. Since the gp41 N-terminus fusion peptide has been well characterized [121, 123-125], it was chosen as a template for designing triggerable fusogenic phosphopeptides. It was hypothesized that the membrane destabilizing properties of the gp41 fusion peptide could be inactivated by properly placed phosphates. Phosphatase catalyzed dephosphorylation would then regenerate the fusion peptide and restore its membrane destabilizing properties.

When designing triggerable fusogenic phosphopeptides, one must first identify the critical residues of the fusion peptide involved in membrane insertion and carefully evaluate the impact of amino acid substitutions. For instance, the first 16 amino acids at the N-terminus of gp41 are known to insert into target membranes, although 12 amino acids are required for fusion [119]. The gp41 fusion peptide contains a conserved five residue sequence at positions 8 through 12, FLGFL, which is essential for fusion [126], and must not be modified. Extended residues at position 17 through 23 are considered to be part of a flanking region that aid in membrane insertion but can be modified. The presence of six glycines suggests a high degree of flexibility within the peptide structure.

Mutations within the membrane inserting domain of the gp41 fusion peptide have been reported to significantly affect membrane fusion [116, 117, 127]. Replacement of the highly conserved Gly residues with Val [127] or deletion of short amino acid sequences at the N-terminus greatly reduces fusion [128] and should also be avoided. Mutations at position 2 and 9 with polar residues, such as V2E and L9R, reduce the fusogenic activity of the peptide [116, 117,

127], and indicate that polar substitutions within the membrane insertion region can decrease the fusogenicity of the peptide. Therefore, cleavable modifications that produce local increases in polarity while conserving the flexibility of the region would be suitable for the design of triggerable phosphopeptides. Figure 2.3 illustrates major modifications that can affect the activity of the gp41 fusion peptide.

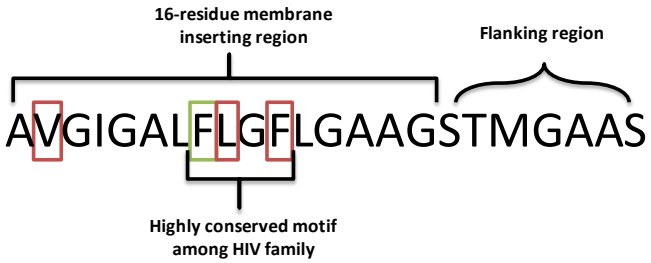

Figure 2.3 Known Modifications that Inactivate the Membrane Destabilizing Properties of the gp41 Fusion Peptide. Substitution of the following conserved residues would lead to loss of activity: 5-residue motif FLGLF in the middle of the membrane inserting region, the valine at position 2, and all glycine residues within the 16-residue membrane inserting region

The design of fusogenic phosphopeptides is constrained by the following design parameters: 1) the number of phosphorylatable residues in the wild type sequence, 2) the number of residues that can be substituted for a phosphorylated residue without loss of activity, and 3) the number of commercially available phospho amino acids. For instance, the wild-type fusion peptide has 3 residues that can be phosphorylated; however they are all in the flanking region. Conserved residues in the peptide sequence limit the number of modifications that can be introduced without loss of activity. These include: a 5-residue motif FLGLF in the middle of the membrane inserting region, the valine at position 2, and all glycine residues within the 16-residue membrane inserting region. Hence, modifications can only be introduced at the 1, 4, 6, 14, and 15 positions. The C-terminus flanking region, however, has fewer restrictions and allows for a greater number of modifications. Finally, we are restricted to phospho residues that are commercially available. These included: serine, threonine, and tyrosine phospho residues.

Since the N-terminus of the peptide inserts first into the membrane, a polar mutation must be introduced near the N-terminus to disrupt membrane insertion. The isoleucine residue at position 4 was selected for modification given its proximity to the N-terminus valine. Phosphorylation sites within the flanking region were also selected for modification since they could provide increased sequence polarity and perhaps greater trigger control. As a result, seven gp41 fusion peptides were designed to evaluate the effect of hydrophilic phosphate groups on fusion and lysis activity.

Phosphopeptides (FP-1PT, FP-2PT, FP-2PY) and their fusogenic counterparts (FP, FP-T, FP-Y) were synthesized to determine the number of phospho residues required to significantly reduce their membrane destabilizing activity as well as to evaluate how phosphoresidue selection can affect triggering and peptide alpha-helical structure [129, 130]. A sulfonated peptide (FP-2Sul), that is not a substrate for phosphatase, was also synthesized to investigate the specificity of the phosphatase trigger. Table 2.1 summarizes the sequences of these peptides. The peptides were synthesized using solid phase synthesis and purified by reverse phase HPLC on a C_{18} column using an acetonitrile linear gradient. As expected, the addition of phosphate groups to the fusion peptides resulted in earlier elution times. Depending on the number of phosphates or sulfates, peptides eluted between 45-55% acetonitrile. The doubly phosphorylated peptides eluted earlier at 45%.

Nomenclature	Sequence
FP	AVGIGALFLGFLGAAGSTWGAK
FP-T	- - - T- - - - - - - - - - - - - - - - - -
FP-Y	- - - Y- - - - - - - - - - - - - - - - - -
FP-1PT	- - - T - - - - - - - - - - - pT - - - - -
FP-2PT	- - - pT- - - - - - - - - - -pT - - - - -
FP-2PY	- - - pY- - - - - - - - - - -pY - - - - -
FP-2Sul	- - -sul- - - - - - - - - - -sul - - - - -

Table 2.1: Peptide Nomenclatures and Sequences. Abbreviations: FP: gp41 fusion peptide (C-terminus lysine); FP-T: gp41 fusion peptide with 2 substituted threonine; FP-Y: gp41 fusion peptide with 2 substituted tyrosine; FP-1PT: gp41 fusion peptide with 1 substituted threonine phosphoamino acid residue near C-terminus; FP-2PT: gp41 fusion peptide with 2 substituted threonine phosphoamino acid residues; FP-2PY: gp41 fusion peptide with 2 substituted tyrosine phosphoamino acid residues; FP-2Sul: gp41 fusion peptide with 2 substituted cysteic acids. Dashes indicate positions that are conserved within the synthesized peptides.

FP

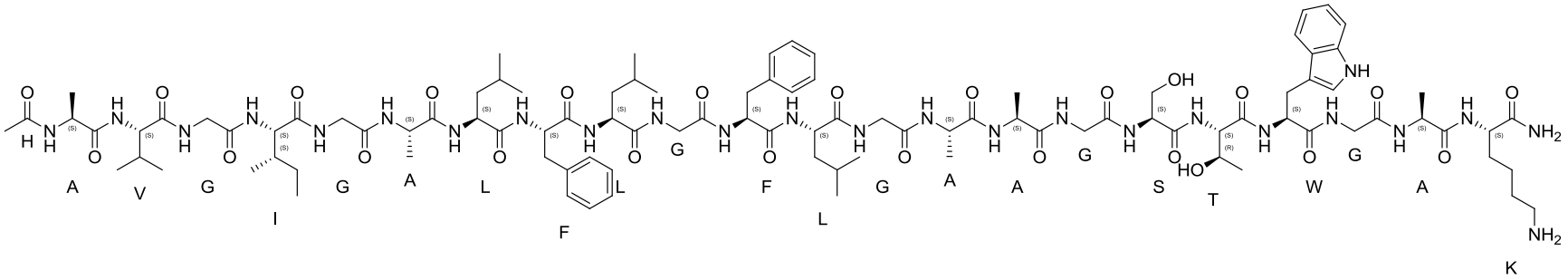

Sequence: AVGIGALFLGFLGAAGSTWGAK

Chemical Formula: $C_{100}H_{153}N_{25}O_{25}$

Exact Mass: 2104.15

Calculated Molecular Weight: 2105.44

Observed Molecular Mass by MALDI-TOF: 2104.89

Figure 2.4: Structure and Properties of FP

FP-T

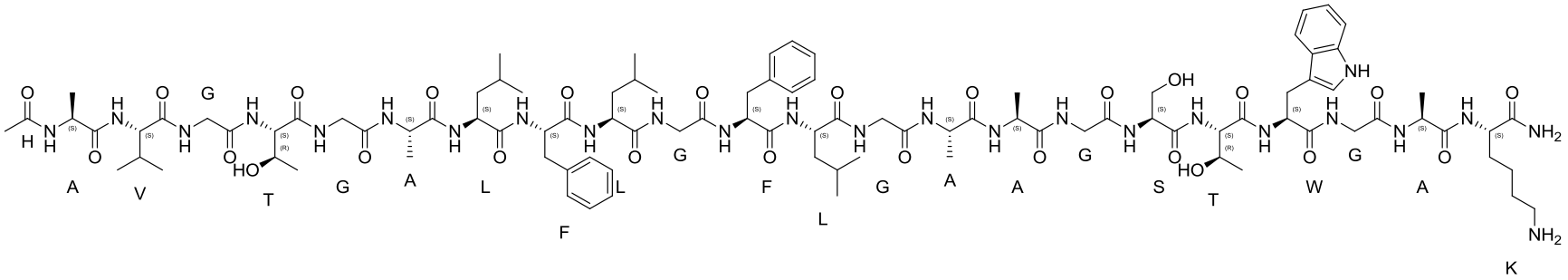

Sequence: AVGTGALFLGFLGAAGSTWGAK

Chemical Formula: $C_{98}H_{149}N_{25}O_{26}$

Exact Mass: 2092.11

Calculated Molecular Weight: 2093.39

Observed Molecular Mass by MALDI-TOF: 2092.67

Figure 2.5: Structure and Properties of FP-T

FP-Y

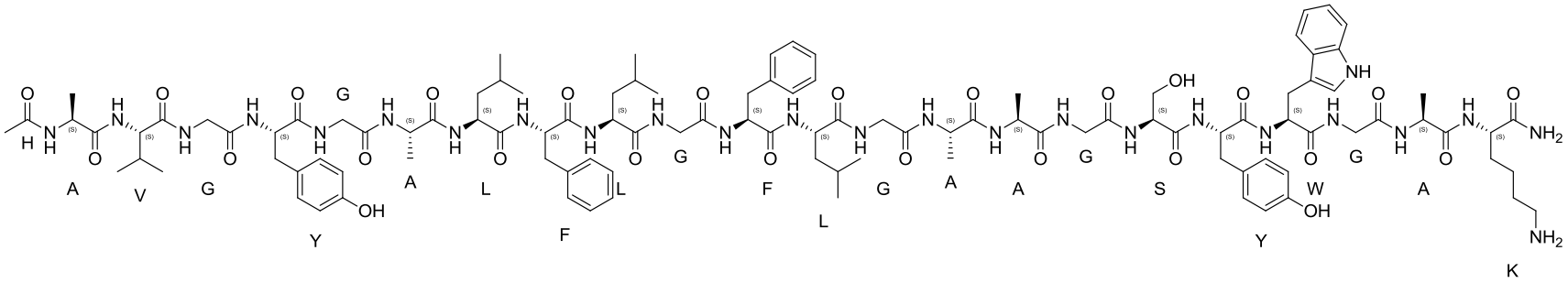

Sequence: AVGYGALFLGFLGAAGSYWGAK

Chemical Formula: $C_{108}H_{153}N_{25}O_{26}$

Exact Mass: 2216.14

Calculated Molecular Weight: 2217.52

Observed Molecular Mass by MALDI-TOF: 2240.16 [$M+Na^{+}$]

Figure 2.6: Structure and Properties of FP-Y

FP-1PT

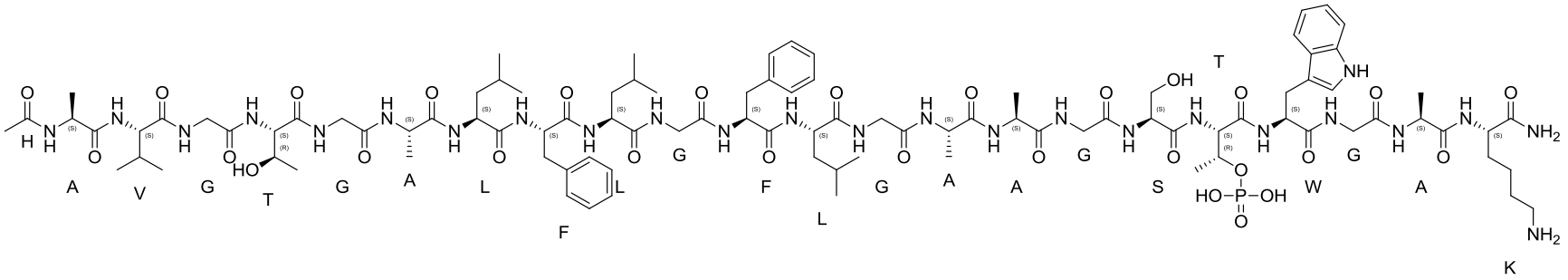

Sequence: AVGTGALFLGFLGAAGSpTWGAK

Chemical Formula: $C_{98}H_{150}N_{25}O_{29}P$

Exact Mass: 2172.08

Calculated Molecular Weight: 2173.36

Observed Molecular Mass by MALDI-TOF: 2173.04

Figure 2.7: Structure and Properties of FP-1PT

FP-2PT

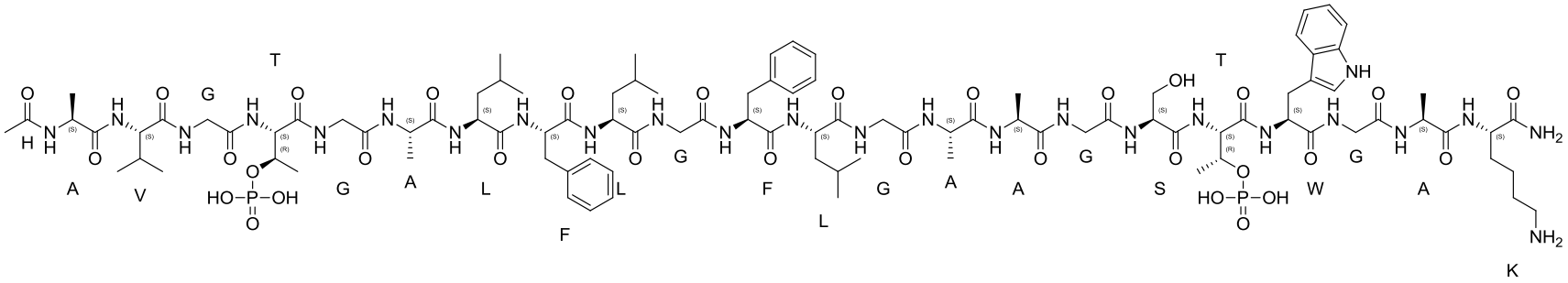

Sequence: AVGpTGALFLGFLGAAGSpTWGAK

Chemical Formula: $C_{98}H_{151}N_{25}O_{32}P_2$

Exact Mass: 2252.04

Calculated Molecular Weight: 2253.34

Observed Molecular Mass by MALDI-TOF: 2276.20 [M + Na^+]

Figure 2.8: Structure and Properties of FP-2PT

FP-2PY

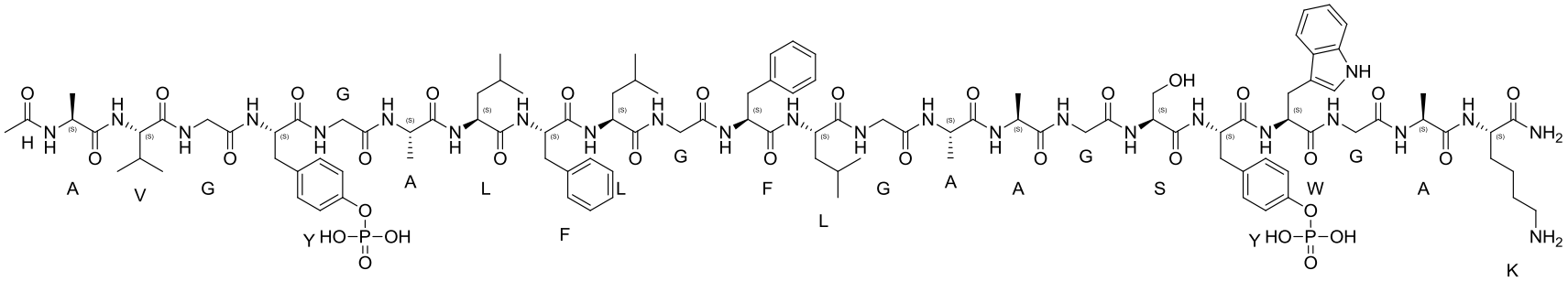

Sequence: AVGpYGALFLGFLGAAGSpYWGAK

Chemical Formula: $C_{108}H_{155}N_{25}O_{32}P_2$

Exact Mass: 2376.06

Calculated Molecular Weight: 2377.48

Observed Molecular Mass by MALDI-TOF: 2378.00

Figure 2.9 Structure and Properties of FP-2PY

FP-2Sul

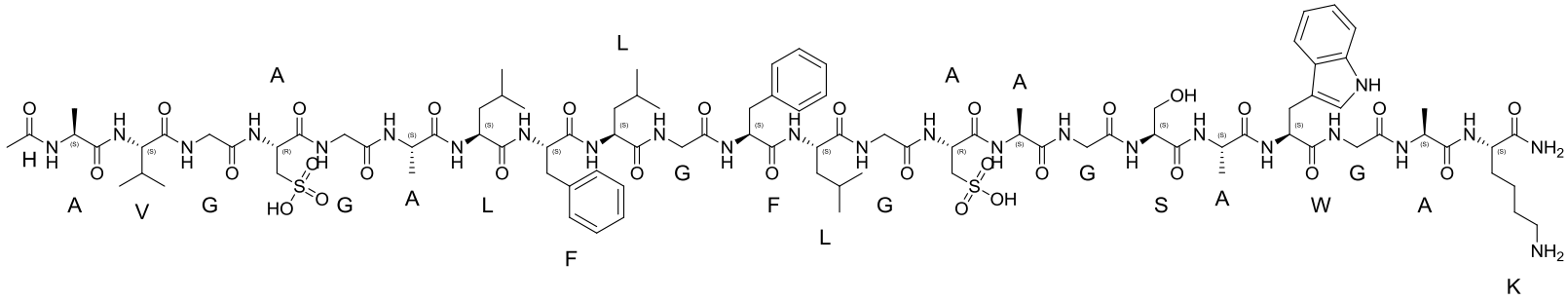

Sequence: AVG(sul)GALFLGFLGAAGS(sul)WGAK

Chemical Formula: $C_{96}H_{145}N_{25}O_{30}S_2$

Exact Mass: 2192.00

Calculated Molecular Weight: 2193.46

Observed Molecular Mass by MALDI-TOF: 2193.81

Figure 2.10: Structure and Properties of FP-2Sul

2.3.2 Effect of Phosphates on the Lytic and Lipid Mixing Properties of gp41 Fusion Peptide

To study the effect of hydrophilic phosphate masking, fluorescence leakage and lipid mixing assays were performed in a FluoroLog-3 spectrofluorometer (Horiba Jobin Yvon, Edison, NJ). The release of carboxyfluorescein (CF) from the liposomes was quantified by the increase in fluorescence intensity at 517 nm for 20 minutes and was normalized to the maximum intensity after the liposomes were lysed with $C_{12}E_{10}$ surfactant. Lipid mixing was measured by fluorescence energy transfer [131] using a mixture of unlabeled and labeled palmitoyloleoylphosphatidylcholine (POPC) vesicles at a 9:1 molar ratio. Fluorescence intensity changes were normalized to the maximum fluorescence observed after surfactant lysis.

The addition of phosphates to the fusion peptide sequence significantly reduced both leakage and lipid mixing. This is consistent with reports claiming that polar substitutions within the membrane inserting region led to a decrease in fusogenic activity [116, 117, 127]. The addition of two phosphates led to an 8-fold decrease in leakage, and a complete loss of lipid mixing. Interestingly, the degree of inactivation was dependent on the number of phosphate groups as illustrated on Figure 2.11. A single phosphate group (FP-1PT) placed in the flanking region was not sufficient to inactivate the fusion peptide. Although the extent of leakage was reduced compared to the wild-type fusion peptide, FP-1PT was fairly active in the absence of phosphatase (Figure 2.11a).

The addition of a second phosphate group to the membrane inserting region provided enough polarity to inactivate the peptide and inhibit leakage (Figure 2.11b) and lipid mixing (Figure 2.12b). Both FP-2PT and FP-2PY induced minimal leakage and lipid mixing even at high peptide concentrations. At a 10:1 lipid to peptide (L/P) ratio, the maximum leakage rate observed for FP-2PT and FP-2PY, after background subtraction, was 7% and 15% compared to the 45% leakage rate of FP-1PT. At a 10:1 L/P ratio, the doubly phosphorylated peptides showed no

apparent lipid mixing as illustrated in Figure 2.12. Moreover, fusion activity could not be regained in the presence of inactive phosphatases. These findings suggest that two phosphates groups, one in the membrane inserting region and another in the flanking region, are required to significantly reduce the fusogenic properties of these peptides. It is possible, however, that a single phosphate within the membrane inserting region of the gp41 fusion peptide could inactivate the sequence. Further experimentation is required to find such an optimal sequence.

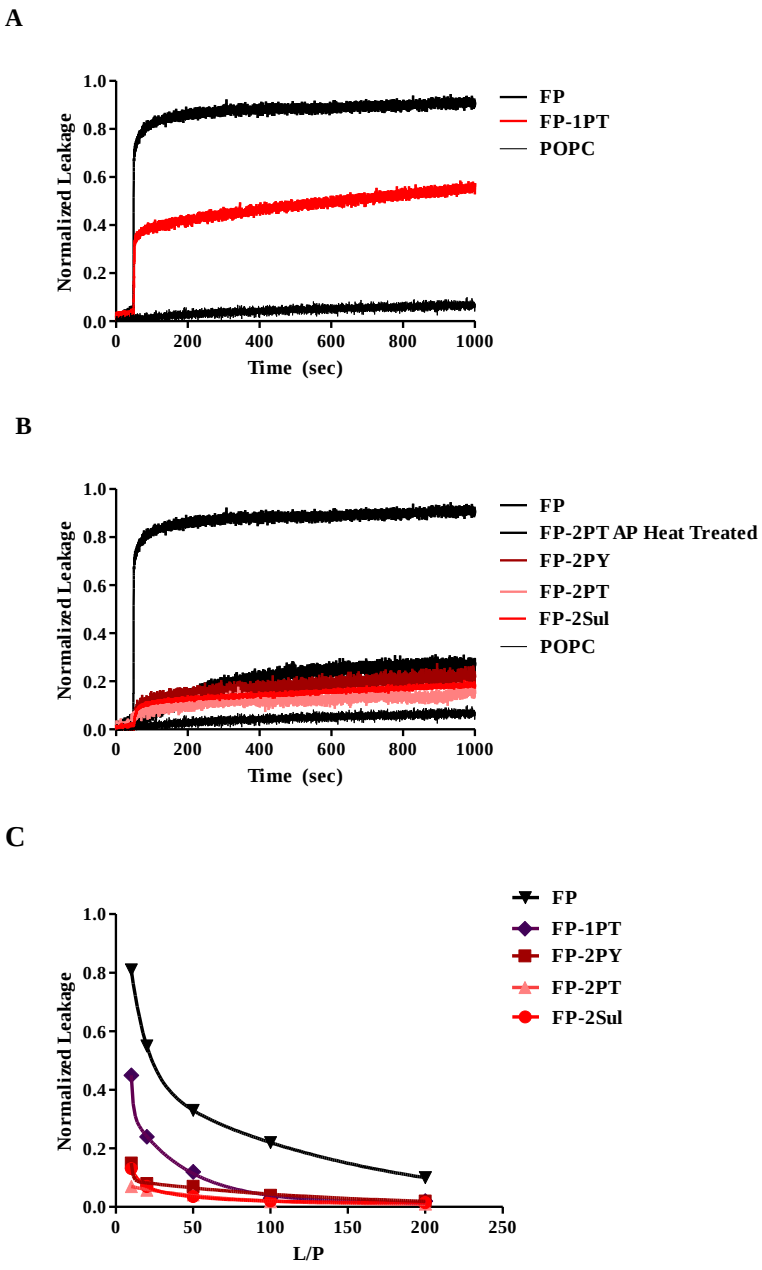

Figure 2.11: Effect of Phosphate Substitutions on Lysis Potential of Fusion Peptides. A) A single phosphate does not inactivate lysis of liposomes by fusion peptides. At a 10:1 L/P ratio, FP-1PT induced significant content release of POPC liposomes loaded with CF. B) The addition of two phosphates inactivated the peptides. At a 10:1 L/P ratio, FP-2PT, FP-2PY and FP-2Sul induced minimal content release of POPC liposomes loaded with CF. C) Peptides with two phosphoresidue did not induce contents leakage over the entire range of L/P ratios tested. Results are representative of the average of at least three runs. All runs were performed at 37 ^{o}C in a Hepes buffered solution (145 mM NaCl, 5 mM Hepes, pH 7.4).

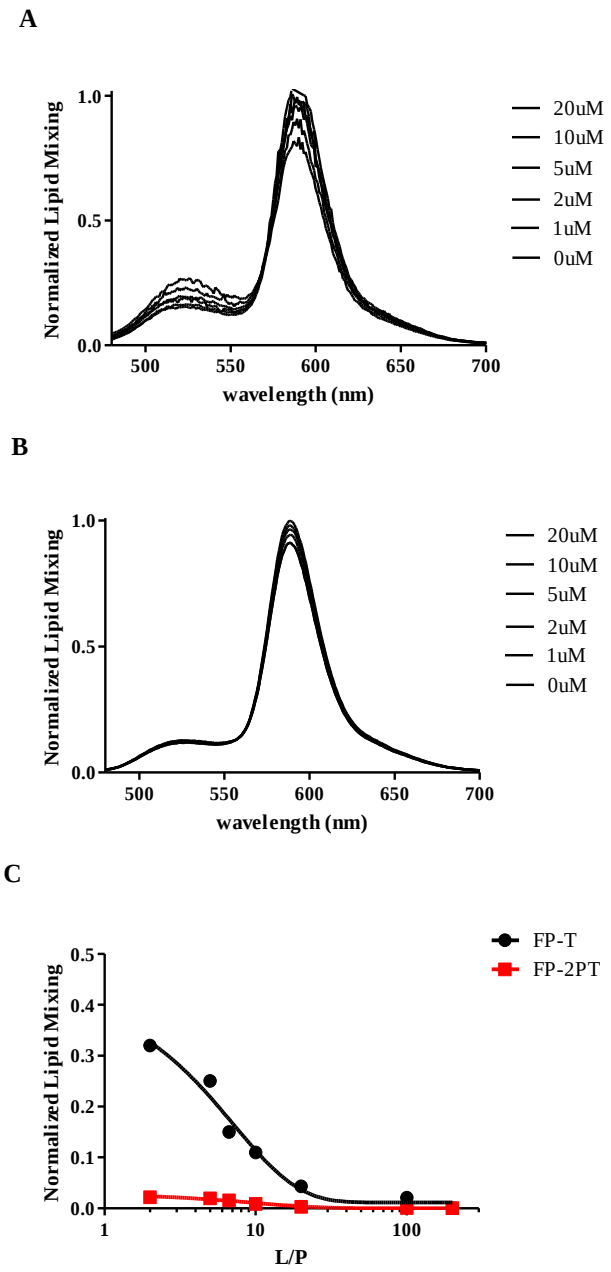

Figure 2.12: Effect of Phosphate Substitution on Lipid Mixing Potential of Fusion Peptides. A) Incremental addition of FP increased lipid mixing of POPC liposomes containing 1 mol% of NBD-PE and Rho-PE. B) Lipid mixing is attenuated in fusion phosphopeptides such as FP-2PT. Increasing the concentration of FP-2PT did not have a significant effect on lipid mixing even at 5:1 L/P ratios. C) No significant increase in lipid mixing is observed over the entire range of L/P ratios tested. Results are representative of the average of at least three runs. All runs were performed at 37 ^{o}C in a Hepes buffered solution (145 mM NaCl, 5 mM Hepes, pH 7.4).

2.3.3 Effect of Phosphates on the Structural Properties of gp41 Fusion Peptides

Phosphorylated peptides and proteins have been reported to have altered secondary structures as compared to their wild-type form [132, 133]. Thus, it was hypothesized that the addition of phosphate groups to the gp41 fusion peptide would lead to an altered secondary structure and an increase in random coil content. Circular dichroism (CD) studies were performed to investigate the role of phosphate addition on secondary structure. The peptides and phosphopeptides were re-suspended in a hydrophobic aqueous solution that mimicked the lipid bilayer and the CD spectrum was recorded from 187.5 nm to 300 nm.

Significant differences in secondary structures were observed between the phosphorylated and non-phosphorylated fusion peptides. FP, FP-T, and FP-Y had alpha-helical secondary structures as has been previously reported [129, 130]. Spectra for FP, FP-T, and FP-Y were predominantly alpha helical with a double negative peak: one at 220 nm and another at 208 nm (Figure 2.13a). Phosphorylated peptides, FP-2PT and FP-2PY, had altered secondary structures (Figure 2.13b). The spectra of FP-2PT and FP-2PY had reduced alpha helical content, with local minima at 220 nm, and a predominant random coil structure dominated by a negative peak at 195 nm. The effect of polar substitutions on secondary structure was further assessed with a sulfonated peptide. The CD spectra of FP-2Sul also had a high content of random coil structure. The data indicates that polar substitutions within the fusion peptide result in a loss of helical content and an increase in random coil content. Although membrane insertion can be modulated by changing the hydrophilicity of the fusion peptide with phosphate groups, conformational changes in the peptide structure can also impact fusion. Thus, the decreased activity of the phosphopeptide can be partially attributed to its altered secondary structure. Figure 2.13 depicts the spectra of the fusion peptides.

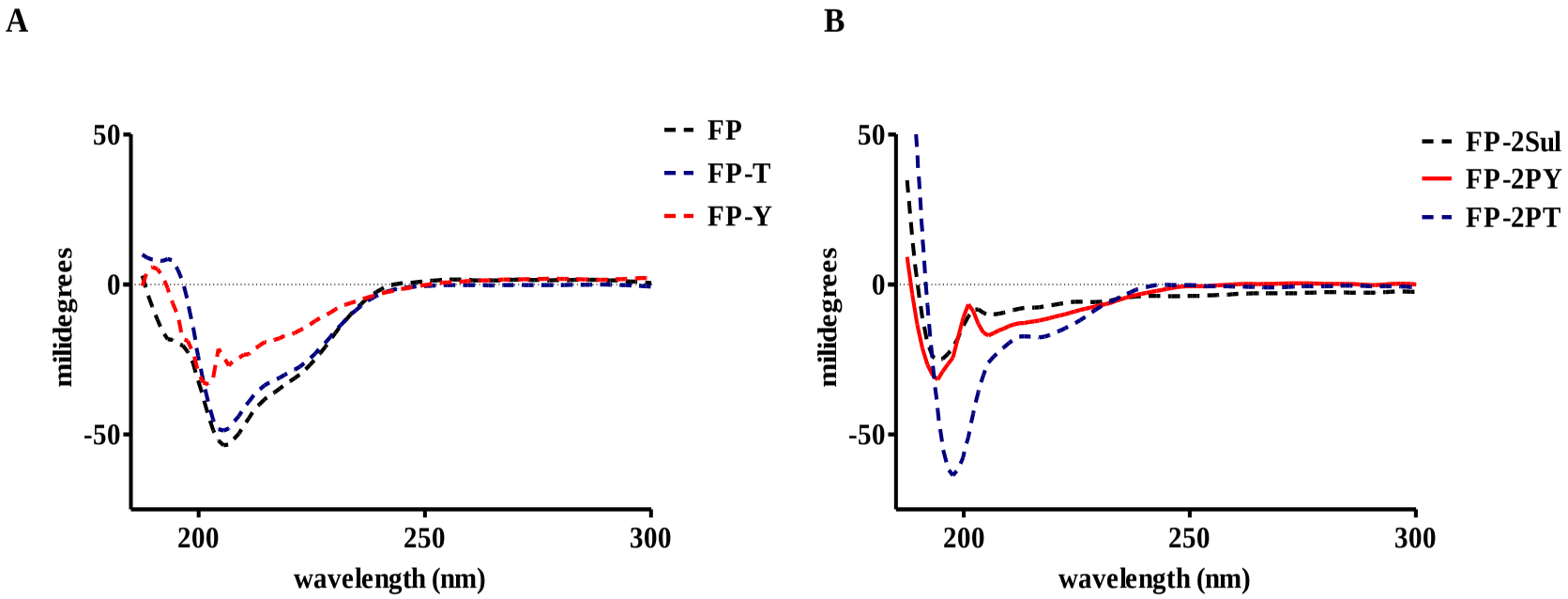

Figure 2.13: Effect of Phosphate Substitution on Secondary Structure. A) FP, FP-T, and FP-Y exhibit a predominant alpha helical structure. B) Addition of phosphate groups alters the helical structure of fusion peptides, increasing their random coil content. Sulfonate groups also exhibited an altered secondary structure (FP-2Sul). CD spectra are representative of 20 µM solutions of peptide in 80% TFE, 20% 5 mM Hepes buffer (pH 7.4) at 37 ^{o}C.

2.3.4 Triggering of Phosphorylated Fusion Peptides by Phosphatase

Phosphatases are known to catalyze the dephosphorylation of phosphate containing proteins and peptides [83, 93]. Thus, it was hypothesized that fusogenic phosphopeptides could serve as substrate for phosphatases. Moreover, phosphatase catalyzed dephosphorylation would lead to a polarity reversal that exposes the hydrophobic segments of the fusion peptide and re-establishes lysis and fusion. This in turn leads to triggered release and/or lipid mixing. To study the effect of phosphatase triggering, fluorescence leakage and lipid mixing assays were performed in a FluoroLog-3 spectrofluorometer (Horiba Jobin Yvon, Edison, NJ) as described before in section 2.3.2.

Leakage assays in the presence of alkaline phosphatase (AP) (Calf Intestinal Alkaline Phosphatase (CIP), New England Biolabs, Ipswich, MA) restored lysis potential of all phosphopeptides and demonstrated that phosphopeptides are substrates for phosphatases (Figure 2.14). Triggering of FP-2PY with AP resulted in nearly identical leakage profiles to FP-Y (P-value>0.05; 0.85). Triggering of FP-1PT and FP-2PT with AP resulted in statistically similar leakage profiles to FP-T (P-value>0.05; 0.93, P-value>0.05; 0.476 respectively). However, a reduced leakage rate as compared to FP-T was observed for FP-2PT with increasing peptide concentration. This can be attributed in part to the lower catalytic activity of alkaline phosphatases towards serine/threonine residues [93]. A temperature dependent effect of triggered CF-release was observed when the reaction was run at 25 ^{o}C as compared to 37 ^{o}C. This can be attributed to the increase in membrane fluidity and enhanced catalytic activity of alkaline phosphatase at 37 ^{o}C as illustrated in Figure 2.15.

Lipid mixing assays also confirmed the phosphatase dependent triggering, as illustrated in Figure 2.16. Phosphopeptides had minimal lipid mixing activity in the absence of phosphatase as discussed in section 2.3.2, even at high peptide concentrations where the maximum lipid mixing observed was 2.2% at a 2:1 lipid to peptide (L/P) ratio. Addition of phosphatase restored

lipid mixing (Figure 2.16b), with FP-2PT having a 10-fold increase in lipid mixing (Figure 2.16c). Sulfonated peptides, which cannot be activated by phosphatases, induced minimal leakage and lipid mixing even in the presence of phosphatase. This supports the notion that the phosphatases are responsible for triggering the phosphorylated fusion peptides and restoring their membrane destabilizing properties.

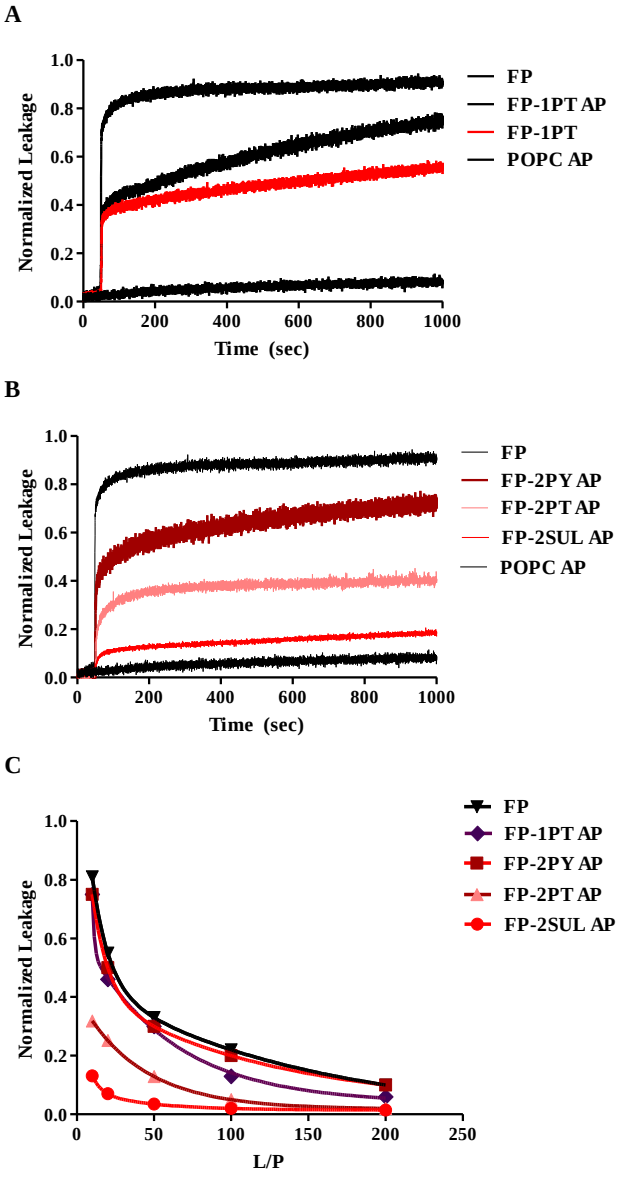

Figure 2.14: Effect of Phosphatase Triggering on Lysis Potential of Fusion Peptides. A) At a 10:1 L/P ratio, addition of alkaline phosphatase triggered FP-1PT causing enhanced leakage of POPC liposomes loaded with CF. Nevertheless, the activation effect is small compared to doubly phosphorylated peptides. B) At a 10:1 L/P ratio, addition of alkaline phosphatase triggered FP-2PT and FP-2PY and induced significant content leakage. Triggering is not observed in sulfonated peptides as they are not substrates for alkaline phosphatase. C) Triggering is observed across all phosphorylated peptides over the entire range of L/P ratios tested. Results are representative of the average of at least three runs. All runs were performed at 37 ^{o}C in a Hepes buffered solution (145 mM NaCl, 5 mM Hepes, pH 7.4).

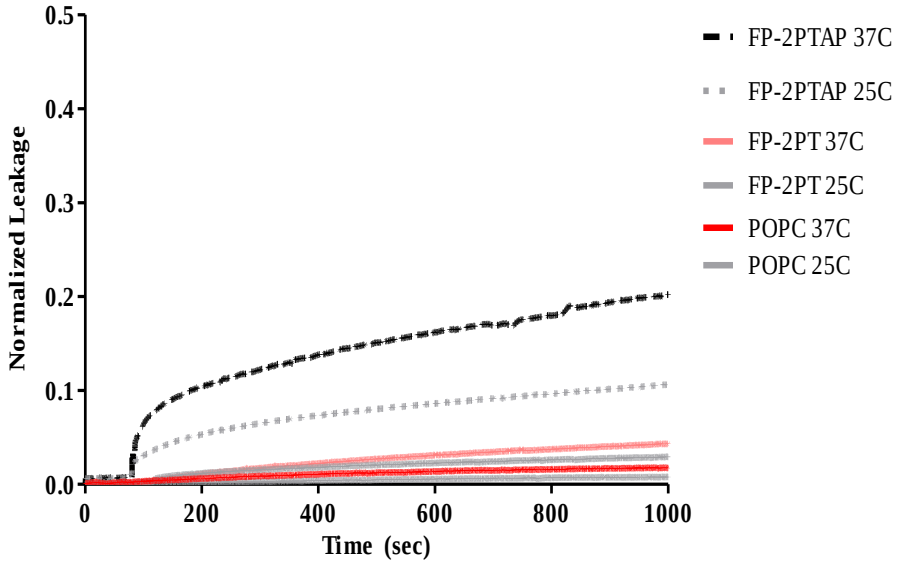

Figure 2.15: Effect of Temperature on Phosphatase Induced Triggered Leakage of POPC-CF Vesicles. Leakage traces shown are representative of triggered leakage of POPC-CF liposomes by 5 μM FP-2PT at 25 ^{o}C and 37 ^{o}C. FP-2PT triggering is enhanced at 37 ^{o}C. All runs were performed in a Hepes buffered solution (145 mM NaCl, 5 mM Hepes, pH 7.4).

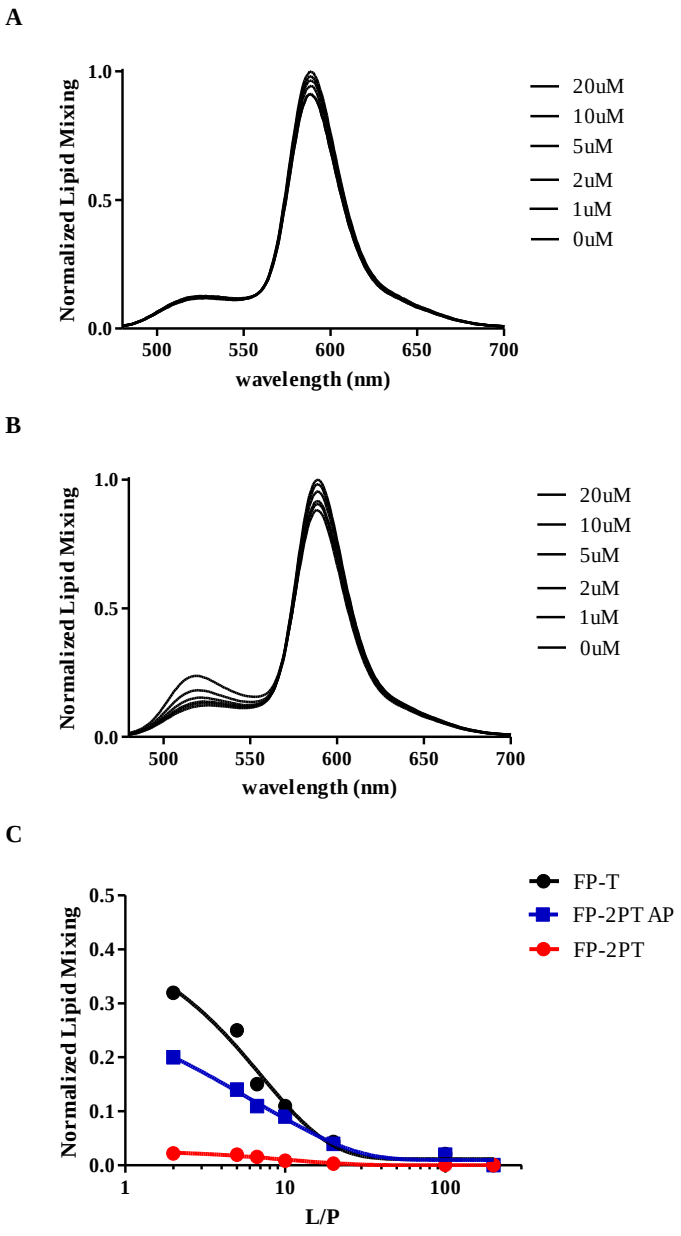

Figure 2.16: Triggered Lipid Mixing of FP-2PT by Alkaline Phosphatase. A) Spectra of POPC liposomes containing 1% mol of NBD-PE and Rho-PE in the presence of FP-2PT. Increasing the concentration of FP-2PT in the medium did not have a significant effect on lipid mixing. B) Spectra of POPC liposomes containing 1% mol of NBD-PE and Rho-PE in the presence of FP-2PT and alkaline phosphatase. Lipid mixing is observed in the presence of alkaline phosphatase. Increasing the concentration of phosphopeptide led to an increase in lipid mixing. The increase in NBD fluorescence is observed at 520 nm. C) FP-2PT is fairly inactive over a broad range of lipid/peptide (L/P) ratios. Addition of phosphatase restored lipid mixing activity. Results are representative of the average of at least three runs. All runs were performed at 37 ^{o}C in a Hepes buffered solution (145 mM NaCl, 5 mM Hepes, pH 7.4).

2.4 Conclusion

In this chapter, the engineering of triggerable phosphopeptides was demonstrated through the use of substrate masking. The addition of polar hydrophilic phosphate groups to the gp41 fusion peptide resulted in a reduction of its membrane destabilizing properties. The degree of inactivation of the phosphopeptide was dependent on the number of phosphates added to the membrane inserting and flanking regions. Interestingly, the addition of phosphates altered the secondary structure of the fusion peptides by reducing helicity and increasing random coil content. Phosphatase catalyzed dephosphorylation of the phosphopeptides was effective at restoring both fusion and lysis potential. These findings suggest that phosphorylated fusion peptides could be used as design components for phosphatase triggerable liposomes. The results in this chapter have practical applications for the fields of peptide design, membrane biophysics, virology, and drug delivery.

2.5 Materials and Methods

2.5.1 Reagents

1-palmitoyl-2-oleyl-sn-glycero-3-phosphocholine (POPC), 1,2-dipalmitoyl-*sn*-glycero-3-phosphoethanolamine-N-(7-nitro-2-1,3-benzoxadiazol-4-yl) (ammonium salt) (NBD-PE), and 1,2-dipalmitoyl-*sn*-glycero-3-phosphoethanolamine-N-(lissamine rhodamine B sulfonyl) (ammonium salt) (Rho-PE) were obtained from Avanti Polar Lipids Inc. (Alabaster, Alabama). Amino acid building blocks, resins, and coupling agents were obtained from Novabiochem (Darmstadt, Germany), Anaspec (San Jose, CA), or ChemPep (Miami, FL). 5-FAM (carboxyfluorescein) was obtained from Anaspec (San Jose, CA). 3β-Hydroxy-5-cholestene (CHOL), 3β-Hydroxy-5-cholestene 3-hemisuccinate (CHEMS), *N*-hydroxysuccinimide (NHS), and dicyclohexylcarbodiimide (DCC) Sigma-Aldrich (St. Louis, MO). All reagents and solvents

used were of analytical or HPLC grade. All buffers were made with MilliQ water and subsequently filtered through 0.1 µM filters.

2.5.2 Peptide Synthesis

Peptides were synthesized on Rink Amide MBHA resin using automated solid phase synthesizers (ABI 433A, Applied Biosystems, Foster City, CA or Prelude 6 Channel Peptide Synthesizer, Protein Technologies, Tucson, AZ) with standard FMOC/HBTU/HOBT (Fluorenylmethyloxycarbonyl/o -benzotriazole- N,N,N,N- tetramethyl -uronium -hexafluoro-phosphate/n-hydroxybenzotriazole) protocols. Phosphopeptides and sulfopeptides were synthesized on NovaPeg resin. An orthogonally protected lysine (Fmoc-Lys(1-(4,4-dimethyl-2,6-dioxo-cyclohexylidene)-3-methyl-butyl)-OH; Fmoc-Lys(ivDde)-OH) was incorporated at the C-terminus. All synthesized peptides were acetylated at the N-terminus using acetic anhydride. Following acetylation, the resin was washed with dimethylformamide (DMF) and dichloromethane (DCM), dried under vacuum, and stored under argon at -20 ^{o}C.

Prior to resin cleavage, the ivDde group was removed by 3 × 20 minutes treatments of the peptidyl resin with 2% hydrazine hydrate in DMF (10 mL per g resin). The removal of ivDde was monitored spectrophotometrically by absorption of the resulting indazole at 300 nm. The resin was then washed in DMF (3 × 10 mL) and DCM (3 × 10 mL) and dried under vacuum. Peptides were cleaved from the resin by treatment with a trifluoroacetic acid (TFA) cleavage solution containing 94% TFA, 2.5% water, 2.5% ethanedithiol, and 1% triisopropylsilane for 4 hours under argon. Phosphopeptides and sulfopeptides were cleaved from the resin using similar acidic conditions, but with a reduced incubation time of 2 hours. Cleaved peptides were separated from the resin by filtration and precipitated into cold ethyl ether. The precipitate was pelleted by centrifugation at 3000 rpm (CR412, Jouan, Winchester, VA) and washed once with cold ethyl

ether. The ether was decanted and the pellet was re-dissolved in trifluoroethanol (TFE), transferred to a flask, and dried by rotary evaporation under reduced pressure and high vacuum.

Purification was carried out by reverse phase HPLC on a Dionex HPLC equipped with a Dynamax C_{18} column. Peptides, phosphopeptides, and sulfopeptides were eluted with a linear gradient of acetonitrile containing 0.1% trifluoroacetic acid and collected using an automated fraction collector. The addition of phosphate groups to the fusion peptides resulted in earlier elution times. Depending on the number of phosphates or sulfates, peptides eluted between 45-55% acetonitrile, with doubly phosphorylated peptides eluting earlier at 45%. Peptide fractions were identified by MALDI-MS in 2,5-dihydroxybenzoic acid matrix, pooled, lyophilized, and stored under argon at -20 ^{o}C. Peptide properties are summarized in Table 2.2.

Name	Sequence	Expected MW	Observed Mass by MALDI-TOF		MeCN Elution (%)	CD Major Structure
FP	AVGI GALFLGFLGAAGSTWGAK	2105.44	2104.89		55	Helical
FP-T	AVGTGALFLGFLGAAGSTWGAK	2093.39	2092.67		55	Helical
FP-Y	AVGYGALFLGFLGAAGSYWGAK	2217.52	2240.16	[M + Na^+]	55	Helical
FP-1PT	AVGTGALFLGFLGAAGSpTWGAK	2173.36	2173.04		48	Not Evaluated
FP-2PT	AVGpTGALFLGFLGAAGSpTWGAK	2253.34	2276.20	[M + Na^+]	45	Random
FP-2PY	AVGpYGALFLGFLGAAGSpYWGAK	2377.48	2378.00		45	Random
FP-2Sul	AVG(sul)GALFLGFLGAAGS(sul)WGAK	2193.46	2193.81		42	Random

Table 2.2: Properties of Fusion Peptides and Phosphopeptides. The table summarizes the name, sequence, calculated and observed molecular weights, HPLC elution profiles and observed major secondary structure of the peptides studied. Abbreviations: FP: gp41 fusion peptide (C-terminus lysine); FP-T : gp41 fusion peptide with 2 substituted threonine; FP-Y: gp41 fusion peptide with 2 substituted tyrosine; FP-1P: gp41 fusion peptide with 1 substituted threonine phosphoamino acid residue near C-terminus; FP-2PT: gp41 fusion peptide with 2 substituted threonine phosphoamino acid residues; FP-2PY: gp41 fusion peptide with 2 substituted tyrosine phosphoamino acid residues; FP-2Sul: gp41 fusion peptide with 2 substituted cysteic acids.

2.5.3 Circular Dichroism

CD spectra were measured on an OLIS DMS10 spectrometer (Olis, Bogart, GA) equipped with a Peltier temperature control stage and flushed with nitrogen gas to enable measurements of CD spectra below 200 nm. Peptide solutions (20 μM) were prepared in an 80:20 mixture of TFE and 5 mM Hepes buffer (pH 7.4). Hepes buffer was necessary to hydrate the phosphates and solubilize the phospho and sulfo peptides. The monochromator was set to record from 187.5 nm to 300 nm (1200 lines/mm), with an integration time of 5 seconds and the temperature set to 37 ^{o}C. Spectra were recorded using a cell with an optical path length of 1 mm. Recorded spectra were averaged by a minimum of 3 runs in Matlab, baseline subtracted, and processed using a Savitsky-Golay smoothing algorithm [134].

2.5.4 Vesicle Preparation for Leakage and Lipid Mixing

Lipid stock solutions were prepared in chloroform ($CHCl_3$). Prior to use, glassware was rinsed in methanol (MeOH) and $CHCl_3$ and dried. Liposomes were prepared by combining chloroform solutions of POPC in borosilicate glass tubes and drying them under reduced pressure using rotary evaporation. Residual solvent was removed overnight under high vacuum. Lipid films were hydrated in buffer, containing 145 mM NaCl and 5 mM Hepes (pH 7.4), by intermittent vortexing and sonicated for 10 minutes under argon. Defined diameter liposomes were then formed by extruding 10 times through 100 nm polycarbonate membranes using a hand-held extruder (Avestin, Ottawa, Canada). Labeled liposomes for lipid mixing contained 1 mol % of NBD-PE and Rho-PE and were also prepared in buffer 145 mM NaCl, 5 mM Hepes, pH 7.4. Liposomes containing CF were prepared as previously described [135]. Lipid formulations of POPC were dried from chloroform stock solutions in a test tube to form a thin film. The thin film was rehydrated in a 100 mM CF solution containing 5 mM Tris-HCl buffer, pH 7.4. The solution was then sonicated for 10 minutes under argon, and the liposomes were extruded through

polycarbonate membranes with 100 nm pores. Free CF was removed by size exclusion chromatography (PD-10 sephadex column; GE Healthcare, Piscataway, New Jersey). The mobile phase for separation consisted of a 5 mM Hepes buffer with 145 mM NaCl (pH 7.4). The encapsulated CF liposomes were capped with argon following separation. All liposome preparations were sized using a Malvern dynamic light scattering (Zetasizer NanoZS, Malvern Instruments, Worcestershire, UK).

2.5.5 Fluorescence Measurements

Fluorescence assays of lipid mixing and leakage were performed in a FluoroLog-3 spectrofluorometer (Horiba Jobin Yvon, Edison, NJ) equipped with a temperature controlled stage (LFI-3751) and a magnetic stirrer. A 450-W xenon light source was used for all recordings. Data acquisition was done through FluorEssence software (Horiba Scientific, Kyoto, Japan) and analyzed using MATLAB. In general, small aliquots of peptides were added to stirred suspensions of 100 μM lipid to begin each experiment, unless otherwise stated. Leakage was monitored for 20 minutes with data collected in intervals of 0.1 seconds. Lipid mixing spectrums were collected in triplicates with detergent added to record maximum lipid mixing.

2.5.6 FRET Lipid Mixing

Membrane fusion was measured by changes in fluorescence intensity resulting from fluorescence resonance energy transfer between the head group labeled probes NBD-PE and Rho-PE as previously described [136] using a Fluorolog-3 spectrofluorometer (Horiba Jobin Yvon, Edison, NJ). Liposomes were prepared as follows: unlabelled POPC liposomes and labeled POPC liposomes with 1 mol% NBD-PE and Rho-PE. A mixture of unlabeled and labeled liposomes at a 9:1 molar ratio of 100 μM lipids were suspended in 2 mL buffer containing 145 mM NaCl, 5 mM

Hepes, and 1 mM $MgCl_2$ (pH 7.4). For peptide-induced lipid mixing, small aliquots of peptides were added to the stirred suspensions in the presence or absence of phosphatases. Samples were incubated at 37 ^oC and fluorescence intensities of the samples were measured. Emission spectra were obtained from 490 nm to 700 nm using an excitation wavelength of 467 nm. Intensity changes were monitored at 520 nm (near the emission maximum of NBD-PE) and at 590 nm (near the emission maximum of Rho-PE). Lipid mixing was evidenced by an increase in fluorescence intensity at 520 nm, due to relief of energy transfer, and a decrease in 590 nm intensity. Changes in the fluorescence intensity ratio of NBD to Rho were normalized and quantified as follows:

$$Lipid\ Mixing(\nabla) = \frac{NBDintensity(\nabla) - background(\nabla)}{detergent(\nabla) - background(\nabla)}\ where\ \nabla \text{ represents } emission\ wavelength$$

Background fluorescence from vesicles containing 1 mol % of NBD-PE and Rho-PE in a 1:9 mixture with non-probe-containing vesicles was set to 0% lipid mixing and the maximum intensity recorded from detergent lysis was set to 100% lipid mixing. The addition of peptide did not alter the fluorescence of the probes.

2.5.7 Carboxyfluorescein Release (CF)

100 nanomoles of POPC-CF liposomes were re-suspended in 2 mL buffer containing 145 mM NaCl, 5 mM Hepes, and 1 mM $MgCl_2$ (pH 7.4), and stirred at 37 ^oC in the presence or absence of phosphatase. For peptide-induced CF release, small aliquots of peptides were added to the stirred suspensions. The release of CF from the liposomes was monitored by the increase in fluorescence intensity as measured by excitation and emission wavelengths of 492 nm and 517 nm, respectively. CF release was monitored for 20 minutes with data collected in intervals of 0.1 seconds. The assays were carried out in a FluoroLog-3 spectrofluorometer (Horiba Jobin Yvon,

Edison, NJ) equipped with a temperature controlled stage (LFI-3751) and a magnetic stirrer. A 450-W xenon light source was used for all recordings. Data acquisition was done through FluorEssence software (Horiba Scientific, Kyoto, Japan) and analyzed using MATLAB. Each peptide concentration was done in triplicates and the results are representative of the mean. The release of CF from the liposomes was monitored, with the excitation and emission wavelengths set to 485 nm and 520 nm respectively. Data analysis was performed in Matlab. For all experiments, percent CF leakage values were calculated by measuring the total CF released, and normalized to the maximum intensity after the liposomes were lysed with $C_{12}E_{10}$ surfactant, and adjusted for background fluorescence as follows:

$$CF(\nabla) = \frac{CFintensity(\nabla) - background(\nabla)}{detergent(\nabla) - background(\nabla)}$$ *where ∇ represents emission wavelength.*

Chapter 3: The Engineering of FTP: Fusogenic & Triggerable Phosphopeptide Displaying Liposomes

3.1 Abstract

A fusogenic and triggerable liposome (FTP(s)) can be designed by displaying phosphopeptides on the surface of liposomes. The concept is that phosphatase catalyzed dephosphorylation activates the fusogenic phosphopeptides on the surface of FTP, and leads to membrane fusion with adjacent bilayers. To test this idea, a doubly phosphorylated fusogenic lipopeptide (FP-2PT-Chems) was prepared by conjugating cholesteryl hemisuccinate (CHEMS) to the C-terminus of FP-2PT. Anchoring of 5 mol% of FP-2PT-Chems in liposomes resulted in a FTP with enhanced membrane destabilizing properties compared to the non-lipidated peptide. FTP containing 2 mol% FP-2PT-Chems had improved cellular uptake as compared to control liposomes and mediated cytosolic delivery of low molecular weights fluorophores and macromolecules in cultured mammalian cells. Phosphatase inhibitors reduced the cellular uptake and cytoplasmic delivery efficiency of FTP. Liposomes modified with sulfonated lipopeptides exhibited reduced uptake and cytosolic delivery as compared to FTP, which indicates that FTP mediates cytosolic delivery through the dephosphorylation of the displayed phosphopeptides. FTP are a prime example of the utility of phosphate groups to mask the hydrophobicity of surface displayed fusion peptides, and provides proof-of-principle that phosphate substrate masking can be used for engineering triggerable liposomes. In this chapter, the biophysical and cellular data supporting the trigger mechanism of FTP is reported.

3.2 Introduction

Triggerable systems are usually stable under physiological conditions and release their contents or fuse with membranes upon stimuli [72]. Triggerable nanocarriers have been designed to react to changes in redox potential and pH, and to external stimuli such as light, ultrasound, and magnetic fields [8, 21, 25-27, 72, 74, 88, 137]. Although these systems have validated the utility of triggers as a method for site-activated content release, many are unable to transport drugs through cell membranes and into cells [72]. Enzymatic systems that trigger membrane fusion offer a unique strategy to overcome these barriers.

Enzyme-activated systems have been developed for triggered drug release [72]. One approach involves the design of nanoparticles activated by secreted enzymes in tumor microenvironments. This strategy has generated several trigger systems that react to phospholipases ($sPLA_2$) [74-77], matrix metalloproteinases (MMP) [71, 78-81], or elastases [82]. These examples are activated in the extracellular matrix and are thus impractical for intracellular delivery of macromolecules.

Phosphatases, which are over expressed in certain tumor microenvironments [73], are an attractive enzyme family since they can facilitate triggering at cellular membranes or intracellular compartments. Phosphatases are responsible for catalyzing the hydrolysis of phosphoric acid monoesters and show selectivity for phosphorylated proteins, peptides, nucleotides, alkaloids, phospholipids, and lipopolysaccharides [83-88]. Although an ubiquitous and promiscuous enzyme, phosphatases confer a high degree of specificity, selectivity, and regulation on their biological substrates [83].

A number of diseases are characterized by an over expression of phosphatase. Acid phosphatases are a biomarker for prostate cancer [138], with the highest level of acid phosphatases found in metastasized prostate tumors. Moreover, high levels of alkaline

phosphatase are correlated with the spread of prostate cancer into bones [73]. Acid phosphatases are also over expressed in cervical cancer and serve as a serum biomarker for the disease [139]. High levels of phosphatase expression have also been implicated in Alzheimer's [140], heart failure [141], and arthritis [142].

Phosphatases have been used for decades as a trigger mechanism for the local activation of pro-drugs since attachment of a phosphate to a drug increases its water solubility [96, 143]. In addition, nanocarriers have also been designed with phosphate moieties that are substrates for phosphatases [88, 102]. Of particular interest are liposomes composed of cholesteryl phosphate derivatives, since they set the precedence for this work [88]. One of the intrinsic limitations of the cholesteryl phosphate liposomes is their high anionic surface charge that results in their aggregation at physiological levels of calcium and/or other divalent cations. Strategies that can reduce the number of phosphate groups on the surface of liposomes and still induce triggering could greatly improve the use of phosphatases as triggers for multivalent drug carriers.

The engineering and optimization of phosphatase triggerable liposomes (FTP) displaying phosphorylated fusion peptides is described in this chapter. FTP were designed to be substrates for acid, alkaline, and protein phosphatases and were engineered to fuse membranes upon phosphatase triggering as illustrated in Figure 3.1. The design of FTP reduces the density of phosphate groups on the surface of liposomes. This prevents aggregation effects from calcium and other divalent cations, which was a limitation of the earlier phosphatase activated liposomes [88].

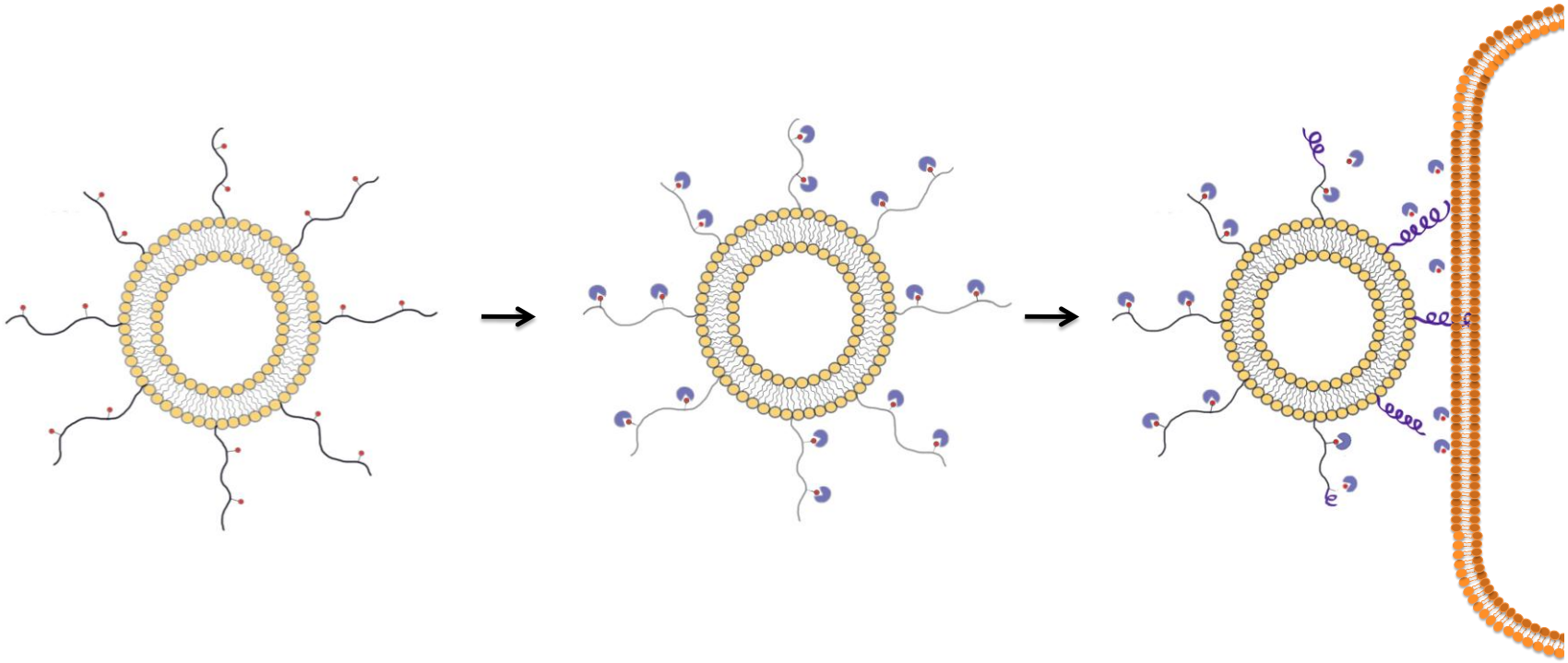

Figure 3.1 Schematic Illustration of Phosphatase Catalyzed Triggering of FTP. FTP are designed with triggerable fusogenic phosphopeptides ligands. Two phosphate groups are used as enzymatic triggers (left). Phosphatases act on the phosphopeptides, dephosphorylating them and exposing hydrophobic fusion peptides that can insert into adjacent membranes (middle). Peptide insertion into adjacent bilayers leads to lipid mixing and contents release (right).

3.3 Results and Discussion

3.3.1 Effect of Lipopeptide Density on the Diameter and Zeta Potential of FTP

FTP were engineered using the phosphorylated fusion peptides designed in Chapter 2. Lipopeptides, FP-2PT-Chems and FP-2Sul-Chems, were synthesized via C-terminus lysine conjugation of NHS-Chems and then incorporated into liposomes by brief sonication of the lipid mixture followed by extrusion through polycarbonate membranes with 100 nm pores. Interestingly, vesicle formation was not possible if unphosphorylated fusogenic lipopeptides were used instead. This supports the notion that phosphate groups prevent the lipopeptide from inserting into the FTP membrane.

The sonication and extrusion process produced consistent FTP with an average hydrodynamic diameter of 100 nm (94.1 ± 6.7 nm), and an average PDI of 0.233. No significant change in particle diameter was observed by increasing the surface density of lipopeptides. FTP were slightly anionic, but had significantly reduced zeta potential as compared to phosphate-containing lipids [63, 88]. For instance, FTP containing 2 mol% FP-2PT-Chems had a zeta potential of -17 ± 3 mV at physiological pH, whereas the inverse phosphocholine DOCP, which has a phosphate extending into the aqueous phase, has a zeta potential of -60 mV [63]. The zeta potential could be easily modulated by changing the phosphopeptide surface density. Decreasing the density to 0.5 mol% of FP-2PT-Chems reduced the zeta potential to neutral. Thus, changes in the surface density of the lipopeptide correlated well with changes in zeta potential. An increase in zeta potential was also observed upon dephosphorylation. Incubation of FTP containing 2 mol% FP-2PT-Chems with phosphatase led to an increase in zeta potential, with FTP having a zeta potential of -7.5 ± 1 mV.

3.3.2 Effect of Membrane Anchoring on the Secondary Structure of Phosphorylated Fusion Peptides

Anchoring of gp41 peptide epitopes to liposomes enhanced their secondary structure [144]. Therefore, it was hypothesized that lipidation and anchoring of fusogenic phosphopeptides to FTP should partially restore secondary structure and decrease random coil content. To test this idea, circular dichroism measurements were undertaken to examine the effect of lipidation and membrane anchoring on the secondary structure of phosphopeptides displayed on FTP. Spectras for FTP containing 2 mol% FP-2PT-Chems were scanned at wavelengths of 180 nm to 300 nm and were background adjusted by subtracting the spectrum of peptide-free FTP. When formulated in FTP, the secondary structure of the phosphorylated lipopeptide was greatly altered (Figure 3.2a). The recorded spectrum had a minimum at 220 nm, characteristic of a beta-sheet, and a reduced content of a random coil. The decrease in random coil content and increase in secondary structure can be attributed to the C-terminus lipidation of the phosphopeptide and its incorporation into FTP.

3.3.3 Phosphatase Specificity of Phosphopeptides Displayed on FTP

An increase in secondary structure could greatly benefit the fusion potential of FTP only if the displayed phosphopeptide is still a substrate for phosphatase. To determine this, phosphatase catalyzed dephosphorylation of FTP was monitored using a highly sensitive phosphate-binding fluorescent protein sensor that can measure nanomolar phosphate concentrations [145] (Phosphate Sensor, Life Technologies, Carlsbad, CA). The sensor is a purified form of a recombinant E. coli phosphate binding protein that has been modified with the coumarin fluorophores *N*-[2-(1-maleimidyl)ethyl]-7-(diethylamino) coumarin-3-carboxamide (MDCC). The binding of phosphate is rapid and tight (Kd ~ 0.1 μM) and results in increased

fluorescence that can be readily measured in a FluoroLog-3 spectrofluorometer (Horiba Jobin Yvon, Edison, NJ).

Exposure of FTP to alkaline phosphatase resulted in rapid dephosphorylation of the phosphopeptides, with 72±15% of the phosphates cleaved in a period of 10 minutes. The enzymatic progress curve is characterized by an initial lag phase followed by a linear phase (Figure 3.2b). Interestingly, dephosphorylation plateaus after 10 minutes with an estimated 30% of the phosphate groups uncleaved. This can be explained by a number of factors. For instance, the phosphorylated lipopeptide is incorporated into FTP by sonication and extrusion, rather than by micelle transfer techniques. As a result, a percentage of the phosphopeptides end up facing the enclosed aqueous compartment and are inaccessible to the phosphatases. Also, as the FTP are dephosphorylated they can undergo fusion with neighboring liposomes, which reduces the fraction of phosphate groups accessible to the phosphatase. Nevertheless, the substantial dephosphorylation measured by the assay suggests that the phosphopeptides displayed on FTP are substrates for phosphatases.

Formulation	Z-ave (nm)	Std.	PDI	Std.	Zeta (mV)	Std.
FP-2PT-Chems 5 mol%	86.0	10.1	0.3	0.1	n.d.	n.d.
FP-2PT-Chems 2 mol%	96.0	14.1	0.2	0.1	-17.4	2.9
FP-2PT-Chems 0.5 mol%	104.8	13.2	0.2	0.1	-5.0	2.5
FP-2Sul-Chems 2 mol%	96.7	8.1	0.2	0.1	-9.2	1.5
FP-2Sul-Chems 0.5 mol%	91.9	6.1	0.2	0.1	n.d.	n.d.

Table 3.1: Diameter and Zeta Potential of FTP Formulations. The surface density of phosphopeptide did not affect the diameter of FTP. A negative surface charge is observed for most FTP formulations, and is correlated to the phosphopeptide surface density. The zeta potential could be modulated by the surface density of the phosphopeptides.

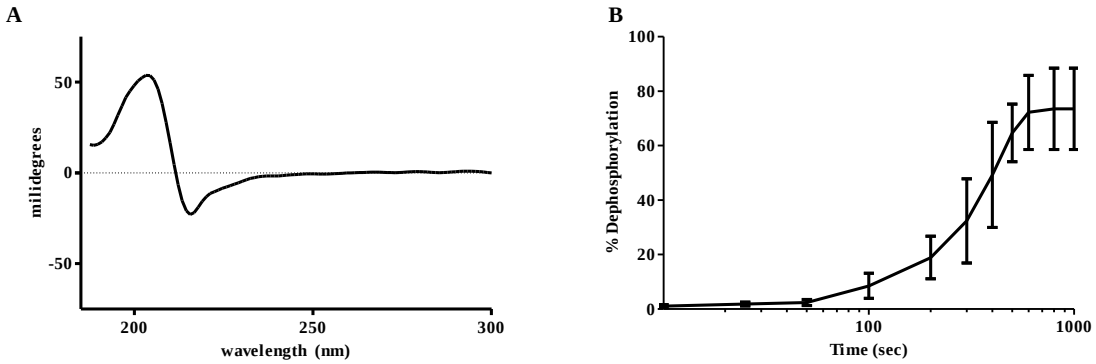

Figure 3.2: Secondary Structure and Dephosphorylation Time Course of Phosphopeptides Displayed on FTP. A) Circular Dichroism spectra of 2 mol% FP-2PT-Chems on the surface of FTP exhibits reduced random coil content. B) The dephosphorylation of phosphorylated lipopeptides displayed on FTP proceeds through a lag phase followed by a linear phase.

3.3.4 Effect of Phosphatase on the Leakage and Lipid Mixing Properties of FTP

FTP are engineered to destabilize membranes and induce membrane fusion upon dephosphorylation by phosphatases. It was hypothesized that dephosphorylation of the surface displayed phosphopeptides would lead to enhanced lipid mixing and content release of adjacent membranes. In order to investigate this mechanism, content release and lipid mixing assays with target membranes were performed.

Content release assays were performed by monitoring the release of CF from peptide-free POPC liposomes upon exposure to FTP. POPC-CF liposomes were mixed with FTP containing 2 mol% FP-2PT-Chems in a 1:1 ratio and incubated at 37 ^{o}C in the presence or absence of phosphatase. The release of CF was then followed by measuring the changes in fluorescence intensity. Upon dephosphorylation by alkaline phosphatase, FTP containing 2 mol% FP-2PT-Chems induced significant content release (60±10%) of POPC liposomes encapsulating CF as compared to the 20±5% release rate observed in the absence of phosphatase (Figure 3.3a). As expected, an accelerated rate of release was observed when FTP were triggered by highly specific serine/threonine phosphatases. Exposure of FTP to ser/thr protein phosphatases (PP1) resulted in nearly complete content release (85±10%) of POPC liposomes encapsulating CF (Figure 3.3b).

Anchoring of the phosphopeptide to the bilayer also led to efficient lipid mixing with neighboring liposomes. Lipid mixing was measured by changes in fluorescence intensity resulting from fluorescence resonance energy transfer between the head group labeled probes NBD-PE and Rho-PE as previously described [136]. Two set of liposomes were prepared: unlabeled FTP with FP-2PT-Chems liposomes and labeled POPC liposomes with 1 mol% NBD-PE and Rho-PE. A mixture of unlabeled FTP to labeled liposomes at a 9:1 molar ratio of 100 μM total lipids was prepared in 2 mL buffer containing 145 mM NaCl, 5 mM Hepes and 1 mM $MgCl_2$ (pH 7.4). Samples were incubated at 37 ^{o}C and fluorescence intensities of the samples were measured. Phosphatase triggering of FTP containing 2 mol% of FP-2PT-Chems induced 30±10% lipid

mixing as compared to 5% lipid mixing for the free peptide (Figure 3.3c). Increasing the surface density of phosphopeptide to 5% resulted in enhanced triggered lipid mixing (50±15%) (Figure 3.3d). This suggested that the surface density of the phosphopeptide influences the degree of lipid mixing.

Although triggered lipid mixing and content release was greatly enhanced in FTP, the basal leakage and lipid mixing in the absence of phosphatases was surprisingly higher than expected. The increase in basal activity can be attributed to a higher local concentration of peptides as a result of membrane anchoring [65]. Perhaps increasing the number of phosphate groups could further reduce the observed basal activity and results in a more stable system. The original design of FTP called for a phosphopeptide with four phosphates. We synthesized and tested this peptide for lipid mixing and content release. Although the phosphopeptide had minimal leakage and lipid mixing, phosphatases failed to regenerate its activity. This was surprising but it exposed the limitation of the gp41 fusion peptide as a platform for trigger phosphopeptide design. Thus, selecting or designing a fusion peptide that allows for a greater number of phosphate modifications would be important when designing a third generation of FTP.

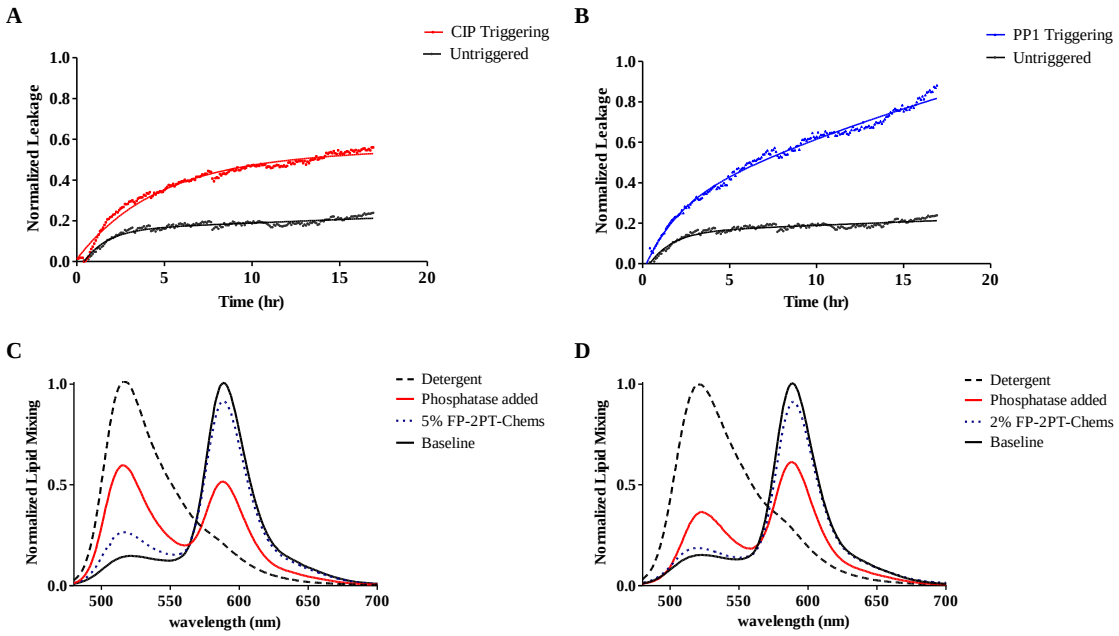

Figure 3.3 Triggered Content Release and Lipid Mixing of FTP by Alkaline Phosphatase. A) FTP containing 2 mol% FP-2PT-Chems induced content release of POPC-CF liposomes in the presence of alkaline phosphatase. B) FTP containing 2 mol% FP-2PT-Chems liposomes had accelerated content release when triggered with a phosphatase (ser/thr protein phosphatase PP1) that is more specific to its substrate. C) FTP containing 2 mol% FP-2PT-Chems exhibited modest lipid mixing with POPC liposomes containing 1 mol% NBD-PE and Rho-PE upon phosphatase triggering. D) Increasing the surface density of phosphopeptides led to an increase in triggered lipid mixing as was observed in FTP containing 5 mol% FP-2PT-Chems.

3.3.5 Cytotoxic Effects of FTP

To be effective drug carriers, FTP must be biocompatible and have acceptable toxicity. MTT assays were performed over a broad range of lipid concentrations to test the cytotoxicity of FTP formulations (Figure 3.6c). No significant difference in cell toxicity, as compared to POPC, was observed with FP-2Sul-Chems and FP-2PT-Chems liposomes at concentrations (10 μM) relevant for cellular uptake studies. Increasing the concentrations by 10-fold reduced the cell viability by 30±5% in cells treated with FP-2PT-Chems liposomes as compared to 18±5% reduction for cells treated with FP-2Sul-Chems and 12±5% for POPC liposomes. The lower viability of cells treated with FP-2PT-Chems liposomes can be attributed to the surfactant-like membrane disturbing properties of the displayed fusogenic phosphopeptides.

3.3.6 Uptake of FTP and Control Liposomes in Cultured Cells

The cellular association of FTP was measured in phosphatase expressing cells. The metastatic B16F10 cell line was selected for the assay because of their phosphatase expression and their previous use to evaluate the cytotoxic effects of phosphate pro-drugs [146-148]. B16F10 cells (0.5×10^5) were seeded in glass bottom dishes and grown to 70% confluency. Fluorescently-labeled FTP, containing 1 mol% Rho-PE, were incubated with B16F10 cells for 0.5, 1, 2, 4, 6, and 12 hours and the cell association was monitored by fluorescence microscopy. Cellular association was observed within the first hour for FTP containing 2 mol% FP-2PT-Chems, with a high percentage of FTP localized to the cell membrane (Figure 3.4 and 3.5). Cellular accumulation and internalization was greatly enhanced at later time points (Figure 3.4b-c and 3.5e-f). Lower uptake and internalization was observed in cells treated with controlled liposomes containing 2 mol% FP-2Sul-Chems (Figure 3.4d-f). This suggests that the anchored phosphopeptide on the FTP was dephosphorylated, which resulted in greater cellular accumulation. Furthermore, the significant reduction in uptake and accumulation of liposomes

containing FP-2Sul-Chems provides further evidence that dephosphorylation is a requirement for FTP internalization (Figure 3.4d-f).

3.3.7 FACS analysis of FTP Uptake in Cultured Cells

To quantify the extent of uptake between FTP and control liposomes, flow cytometry studies were performed on a FACSarray system (Becton Dickinson, CA). B16F10 cells were incubated with fluorescently labeled FTP for fixed periods of time, as described above. After removal of unbound liposomes, the cells were detached from cell culture plates using calcium and magnesium free HBSS media and analyzed by FACS analysis. Cells were gated on FSC/SCC (forward scatter/ side scatter) to remove debris. The fluorescence from FTP containing Rho-PE was then measured using the mCherry emission channel. FACS analysis confirmed the time-dependent uptake of FTP (Figure 3.6a), as well as their enhanced cellular association relative to control liposomes. A gradual increase in fluorescence was observed over time, with a five-fold higher uptake of FTP compared to control liposomes at 6 hours. Uptake of liposomes containing FP-2Sul-Chems was at background level, and no statistically significant difference was observed between the control liposomes.

To quantify the extent of cell-associated FTP as a function of lipopeptide surface density, B16F10 cells were incubated with FTP modified with various surface densities of phosphopeptides. After a 4 hour incubation period, the uptake was quantified by FACS as described above. FACS analysis confirmed the effect of the phosphopeptide surface density on the uptake of FTP. FTP containing 2 mol% FP-2PT-Chems displayed a 3-fold increase in uptake as compared to FTP containing 0.2 mol% FP-2PT-Chems (Figure 3.6b). However, increasing the surface density to 5 mol% did not increase cell association. These results were further confirmed by fluorescence microscopy studies (Figure 3.7). The cell association of control liposomes

modified with FP-2Sul-Chems was low and did not increase when the surface density was increased (Figure 3.6a-b).

3.3.8 Effect of Phosphatase Inhibitors on FTP uptake

Uptake studies were performed in the presence of inhibitors and under energy depletion conditions to further test the hypothesis that active phosphatases are necessary for uptake. Inhibition of phosphatase activity by phosphatase inhibitors (1 μM okadaic acid, a serine/threonine phosphatase inhibitor and/or 0.1 mM sodium orthovanadate, a tyrosine phosphatase inhibitor [92, 149]) resulted in differences in uptake. Uptake was marginally affected by inhibition of tyrosine phosphatases, but greatly reduced by inhibition of threonine phosphatases as expected. Cells treated with an inhibitor cocktail of both inhibitors exhibited no significant uptake. Incubation of fusogenic phospholiposomes under energy depletion conditions (4^{o}C, serum-free medium) exhibited significantly reduced uptake and internalization of FTP, implying that uptake is a temperature and energy dependent process [150]. These findings support the hypothesis that the uptake of FTP is mediated by active phosphatases that catalyze the dephosphorylation and membrane insertion of the fusogenic phosphopeptides.

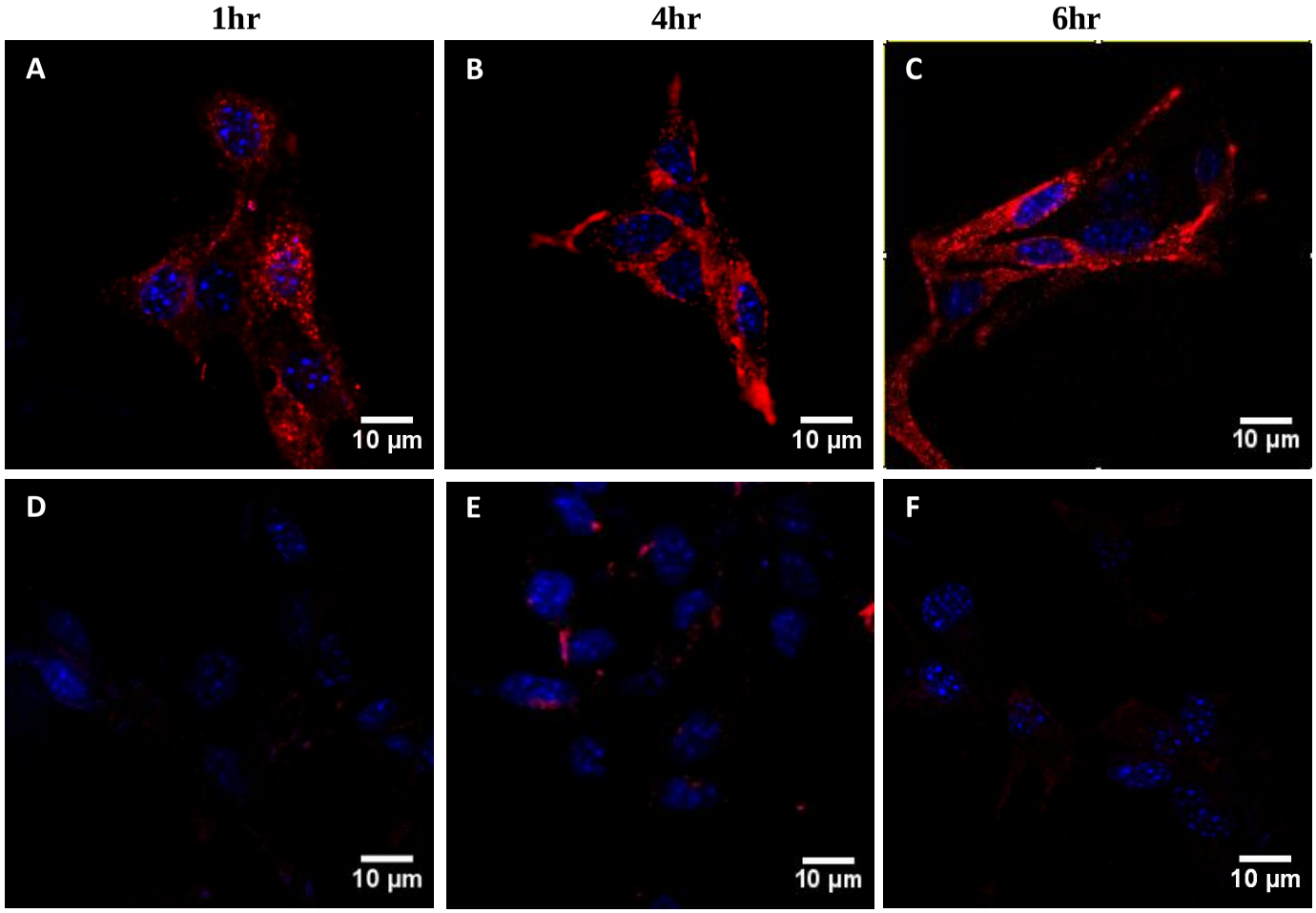

Figure 3.4 Confocal Images of Time Dependent Uptake of FTP. Confocal images show time dependent uptake in B16F10 of FTP containing 2 mol% FP-2PT-Chems (top a-c) as compared to liposomes containing 2 mol% FP-2Sul-Chems (bottom, d-f) with Rho-PE. Uptake of FP-2PT-Chems FTP was significantly greater than FP-2Sul-Chems liposomes. Nuclei were stained with dapi (blue).

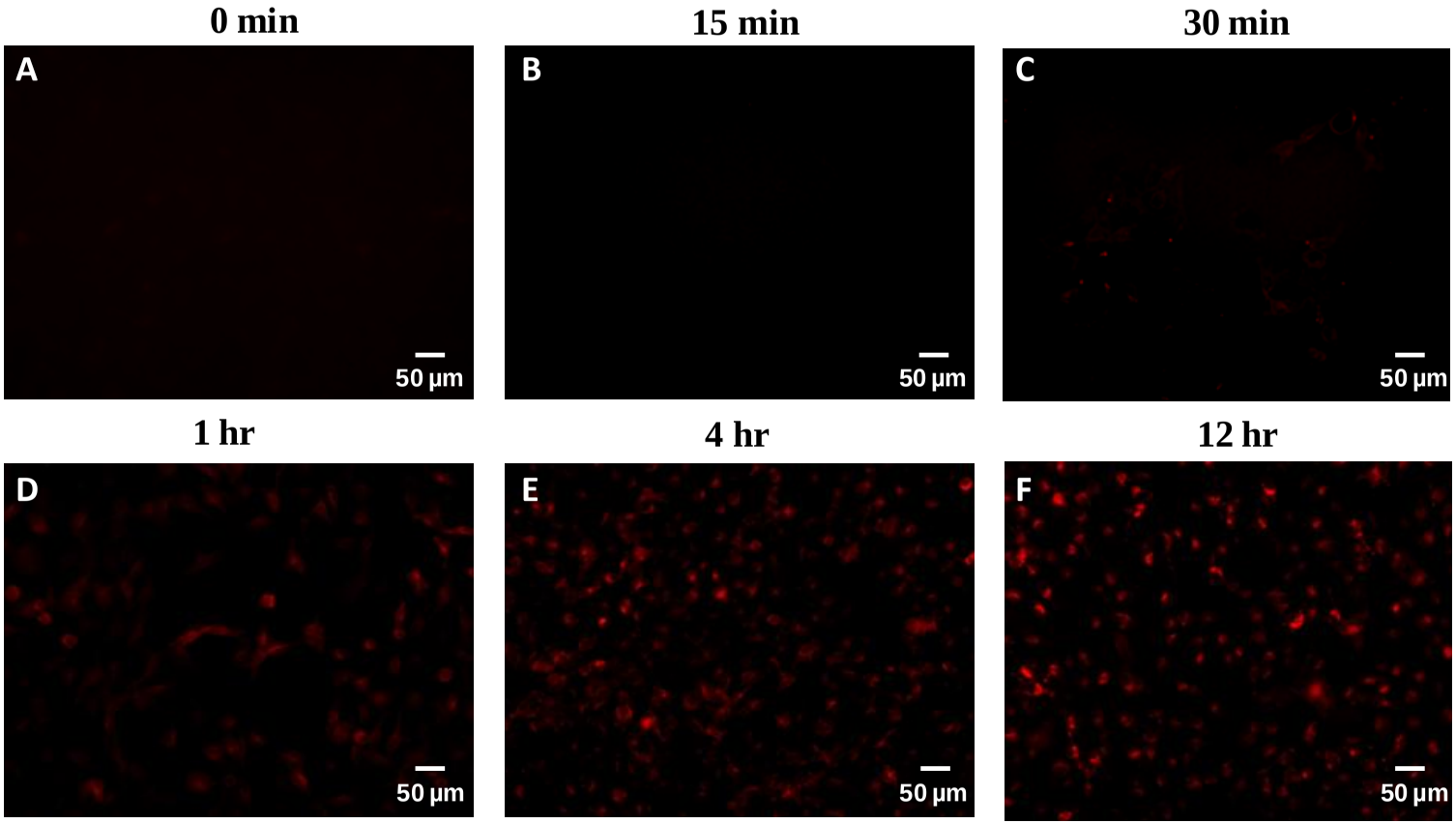

Figure 3.5: Time Dependent Uptake of FTP Containing 2 mol% FP-2PT-Chems. B16F10 cells (0.5×10^5) were plated in Fluorodish glass bottom dishes and grown to 70% confluency at 37 ^{o}C and 5% CO_2 in medium (RPMI 1640 with 10% (v/v) FBS). The cell monolayer was rinsed with FBS-free medium and then medium containing 10 µM of liposomes was added. Cells were incubated with 10 nanomoles of FTP for 0.25, 0.5, 1, 4, and 12 hours at 37 ^{o}C and 5% CO_2. At the end of the incubation, the medium was removed and the cells were washed three times with 1 mL HBSS (HBSS). FTP association and uptake is observed within 30 minutes and increases over time.

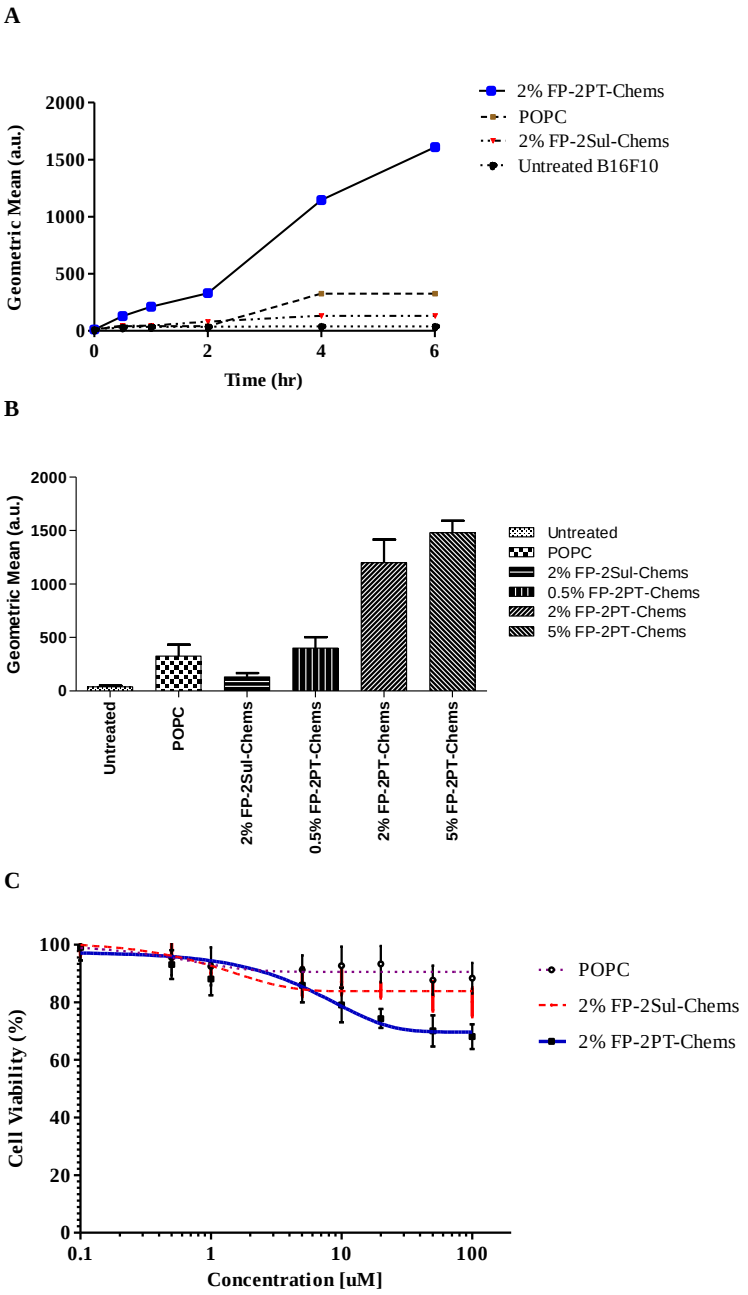

Figure 3.6: Quantification of Uptake and Cell Toxicity of FTP in Cultured Cells. A) FACS analysis showed that FTP with 2 mol% FP-2PT-Chems liposomes had greater time-dependent uptake than peptide-free liposomes or liposomes with 2 mol% FP-2Sul-Chems. B) At 6 hours, FTP containing FP-2PT-Chems exhibited enhanced uptake relative to control liposomes. Increasing the surface density of FP-2PT-Chems from 0.5% to 5% led to a higher cellular uptake of FTP. C) FP-2PT-Chems FTP showed concentration dependent cytotoxicity as revealed by MTT assay.

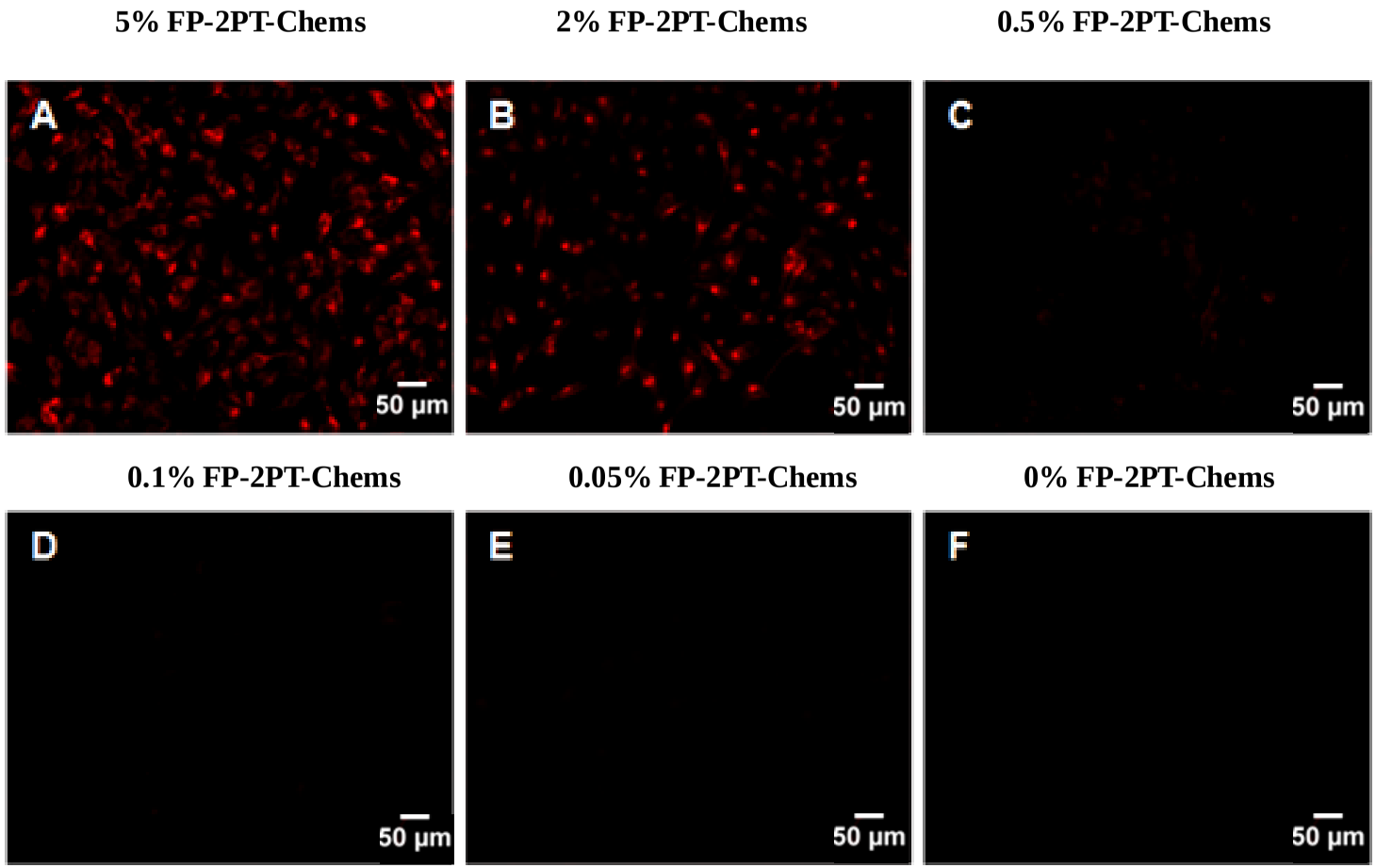

Figure 3.7: Effect of Lipopeptide Surface Density on FTP Uptake at 4 Hours. B16F10 cells (0.5 x 10^5) were plated and grown to 70% confluency at 37 ^oC and 5% CO_2 in medium (RPMI 1640 with 10% (v/v) FBS). The cell monolayer was rinsed with FBS-free medium and then medium containing 10 µM of FTP was added. Cells were incubated for 4 hours at 37 ^oC and 5% CO_2. At the end of the incubation, the medium was removed and the cells were washed three times with 1 mL HBSS (HBSS). Reduced uptake is observed with decreasing FP-2PT-Chems concentration.

3.3.9 FTP Delivery of Low-Molecular Weight Fluorophores and Fluorescent Macromolecules into the Cytosol of Cultured Cells

To be effective drug carriers, FTP must be able to encapsulate and retain a cargo, and mediate cytosolic delivery. To test this, FTP encapsulating carboxyfluorescein (CF), FITC-Dextran, or propidium iodide (PPI) were prepared by sonication and extrusion, followed by size exclusion chromatography. The encapsulation process did not have a significant effect on the hydrodynamic diameter of FTP, with loaded FTP having an average size of 100 nm.

FTP were efficient at delivering fluorophores to the cytosol of B16F10 cells. Cytosolic delivery of either CF or PPI was visible in over 50% of the cells. Delivery of CF was confirmed within 2 hours (Figure 3.8a-c). Confocal images indicated cytoplasmic delivery of CF, as well as co-localization of FTP containing Rho-PE probes near the perinuclear space of B16F10 cells (Figure 3.8b). The delivery of PPI also resulted in time-dependent delivery of the fluorophore, as well as in perinuclear accumulation of FTP (Figure 3.8d-f).

When propidium iodide is delivered into the cytosol it must diffuse through the cytosol and into the nucleus where it can intercalate between the bases of DNA. This leads to a 20-30 fold increase in fluorescence that can be used as a surrogate marker for cytosolic delivery. B16F10 cells incubated with FTP loaded with PPI showed cytosolic delivery within 4 hours, indicative that PPI was able to diffuse through the cytosol and into the nucleus and bind to DNA (Figure 3.8d). In some instances, the cells also showed a diffused red fluorescence, which occurs when PPI complexes with RNA in the cytosol.

The cytosolic delivery of macromolecules was also possible but to a lesser extent. When FITC-Dextran is delivered to the cytosol, a diffuse fluorescence is observed throughout the cytoplasm of the cell. The fluorescence can be easily differentiated from staining of membranes or intracellular compartments such as vacuoles [67]. Incubation of FTP encapsulating FITC-

Dextran demonstrated cytosolic delivery within 4 hours. Significant particle accumulation around the perinuclear space was also observed (Figure 3.8g-i). However, compared to low molecular weight fluorophores, the degree of delivery was reduced. Only 30% of the cells exhibited distinct cytoplasmic fluorescence at 4 hours (Figure 3.8h) even though significant FTP accumulation was observed in all cells. Control liposomes containing FP-2Sul-Chems were unable to mediate cytosolic delivery of the fluorophores (Figure 3.9).

Inefficiencies in the passive encapsulation of FITC-Dextran can account for the reduced cytoplasmic delivery observed. Also, FTP could be triggered extracellularly and lose substantial amounts of cargo prior to being internalized. Thus, further optimization of the formulations is required to improve the cytosolic delivery of macromolecules by FTP.

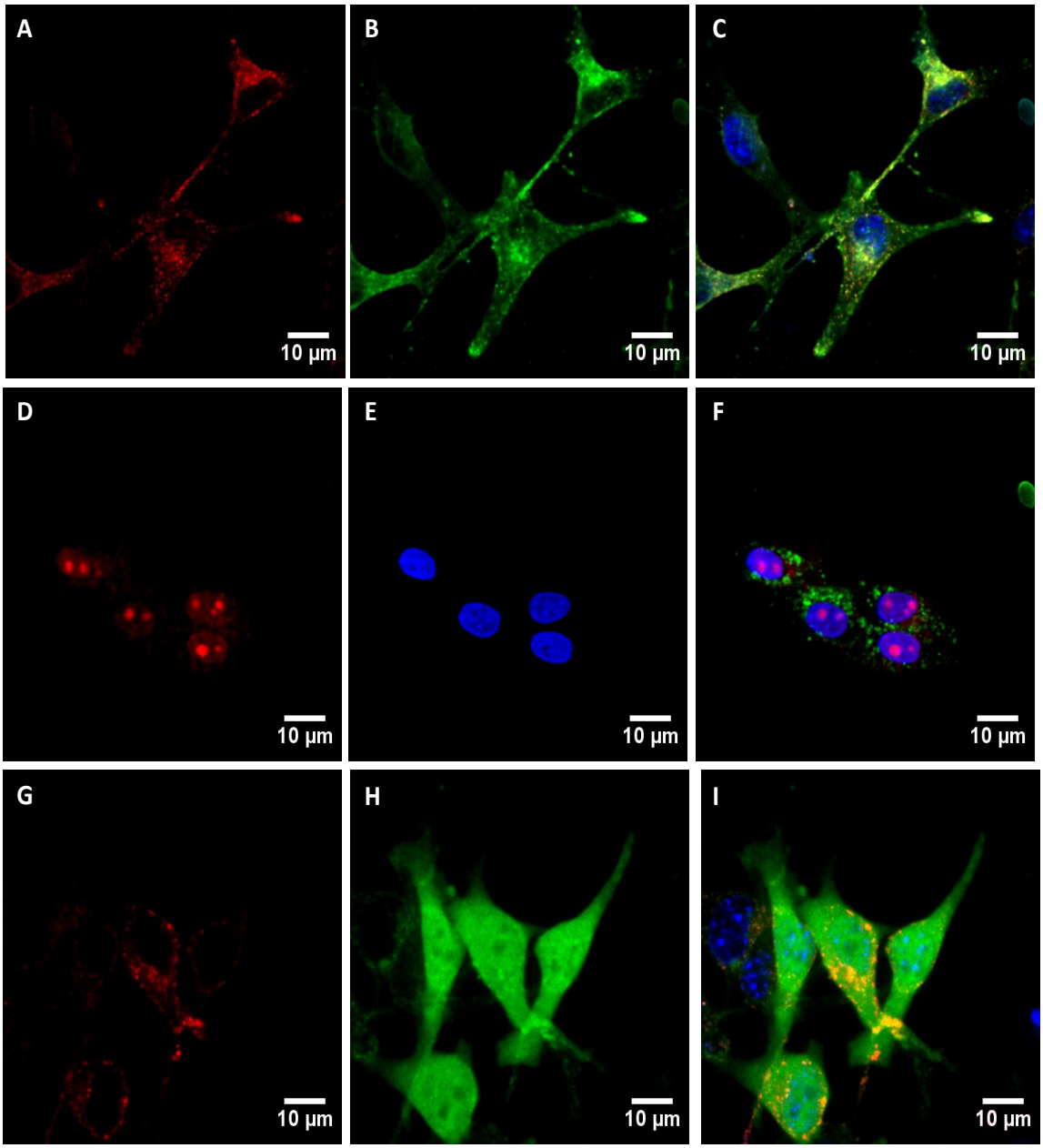

Figure 3.8: Cytosolic Delivery of Low-Molecular Weight Fluorophores and Fluorescent Macromolecules in Cultured Cells by FTP Modified with FP-2PT-Chems. Confocal images show uptake of FTP and cytoplasmic delivery of small molecules (carboxyfluorescein), intercalating agents (propidium iodide) and macromolecules (FITC-Dextran). (A-C) B16F10 cells were incubated for 2 hours with FTP encapsulating 100 mM of carboxyfluorescein. (D-F) B16F10 cells were incubated for 2 hours with FTP encapsulating 1 mM of propidium iodide. (G-I) B16F10 cells were incubated for 4 hours with FTP encapsulating 1 mM FITC-Dextran (10kd). After 2 hours, FTP formulations were visible in the perinuclear space of the cells (A, D, G). All formulations exhibited both a punctuate staining and a more uniform staining of the cell interior indicative of cytoplasmic delivery of the encapsulated fluorophores. FTP formulations were prepared with 2 mol% FP-2PT-Chems and contained the fluorescent lipids Rho-PE (A, G) or NBD-PE (F). Dapi was used to stain the nuclei of the cells (C, E, F, I).

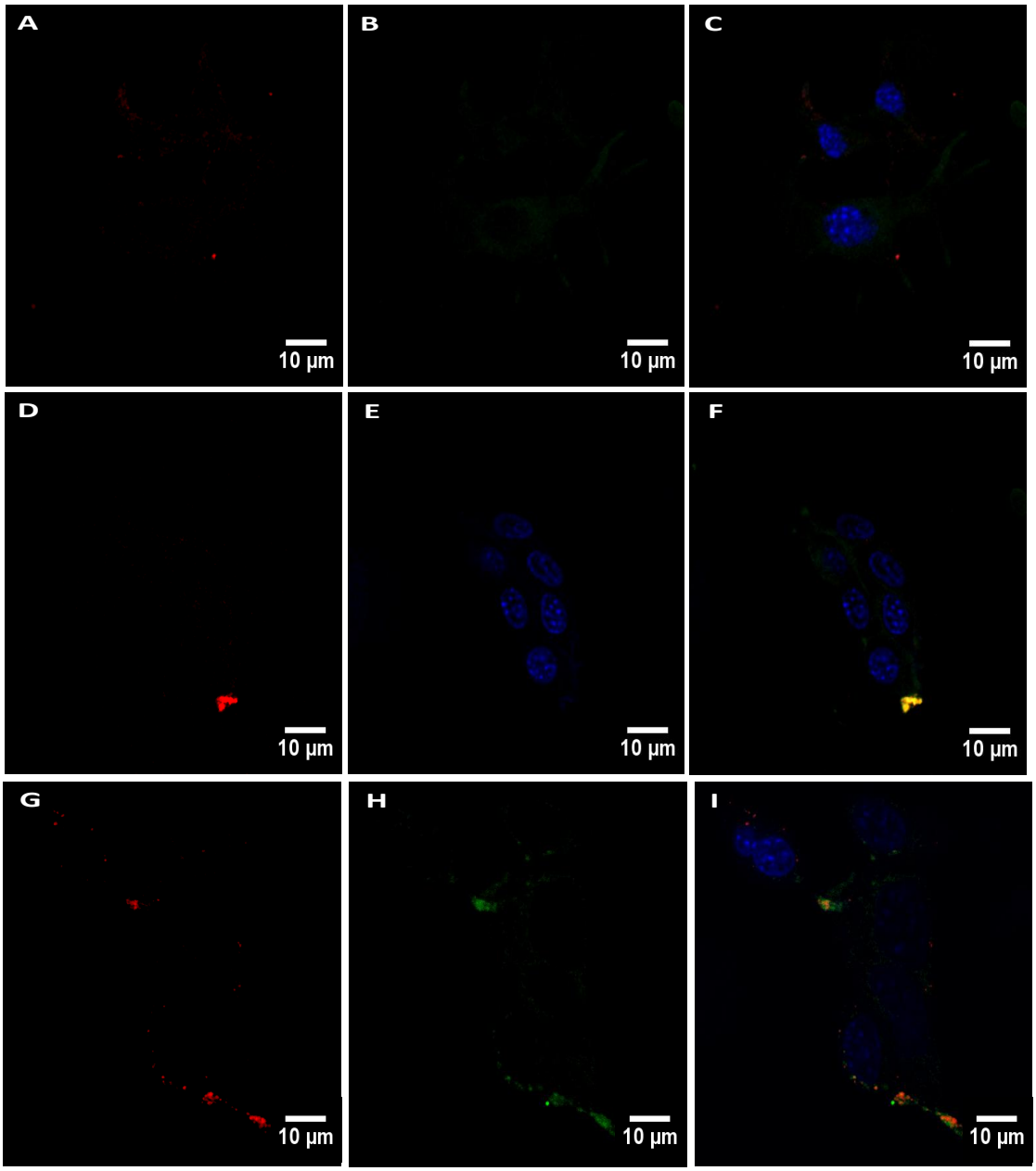

Figure 3.9: Low Uptake and Cytosolic Delivery of Low-Molecular Weight Fluorophores and Fluorescent Macromolecules in Cultured Cells by Control Liposomes Modified with FP-2Sul-Chems. Low uptake of FP-2Sul-Chems modified liposomes was observed after 2 hours in cells treated with FP-2Sul-Chems modified liposomes (A, D, G). Cytosolic delivery, however, was not observed. No cytosolic delivery of CF was observed after 2 hours in B16F10 cells treated with liposomes encapsulating 100 mM of CF (A-C). No cytosolic delivery of PPI was observed after 2 hours in B16F10 cells treated with liposomes encapsulating 1 mM of propidium iodide (D-F). No cytosolic delivery of FITC-Dextran was observed in B16F10 cells treated with liposomes encapsulating 1 mM FITC-Dextran (10kd) (G-I). FTP formulations were prepared with 2 mol% FP-2Sul-Chems and contained the fluorescent lipids Rho-PE (A, G) or NBD-PE (F). Dapi was used to stain the nuclei of the cells (C, E, F, I).

3.4 Conclusion

Triggerable fusogenic liposomes can be engineered to bind to cells and deliver their contents by means of phosphorylated fusion lipopeptides anchored to the bilayer. Phosphorylated lipopeptides on FTP remained active substrates for phosphatases, and mediated triggered membrane fusion efficiently. The membrane destabilizing potential of FTP could be readily modulated by changing the surface density of the lipopeptide, as well as by the type of phosphatase catalyzing dephosphorylation.

These findings have implications for the design of triggered release systems. First, the engineering of FTP provides a blueprint for designing phosphatase triggerable systems. Substrate masking by hydrophilic phosphate groups was proven to be a valuable technique for displaying and controlling the membrane destabilizing properties of fusion peptides. The use of phosphopeptides as trigger moieties also enables the design of phosphatase triggerable liposomes with reduced negative surface charge. This is a direct result of the enthalpic gain that fusion peptides provide upon membrane insertion into adjacent bilayers.

Since a low percentage of phosphorylated lipopeptides are required for membrane fusion, a low negative surface charge can be achieved. This enables the use of FTP as triggerable liposomes and circumvents the cation-induced aggregation effect that plagued earlier phosphatase triggerable liposomes [88]. Finally, it is important to note that phosphatase triggerable systems such as FTP can be substrates for different types of phosphatases. The *in vivo* consequences can be profound, since phosphatases are expressed in many parts of the body during disease. In prostate cancer, for instance, over expression of phosphatase in the tumor tissue also leads to an over expression of phosphatase in circulation [138]. This is problematic since a high percentage of FTP could be triggered in circulation before reaching the tumor site. It is possible that premature triggered release can be overcome by the use of sterically protective polymers that limit substrate accessibility, as has been reported for other enzymatically active systems [71].

However, the use of protective polymers could shield the fusion peptide and limit the functionality of FTP. Perhaps advanced protective polymers with trigger functionality, such as pH-sensitivity [151] or enzymatic cleavable groups [79], could serve as complementary components of third generation FTP. We must also not overlook the potential immunogenic response that FTP modified with gp41 fusion phosphopeptides could elicit in circulation, since liposomes displaying peptide sequences from the membrane proximal region of gp41 are known to elicit an immune response [144]. Nevertheless, the potential of FTP to mediate cytosolic release of cell impermeable molecules, proteins, and nucleic acid is apparent and could lead the way for new drugs and therapeutics against cancer and other disorders in which phosphatases are over expressed.

3.5 Materials and Methods

3.5.1 Reagents

1-palmitoyl-2-oleyl-sn-glycero-3-phosphocholine (POPC), 1,2-dipalmitoyl-*sn*-glycero-3-phosphoethanolamine-N-(7-nitro-2-1,3-benzoxadiazol-4-yl) (ammonium salt) (NBD-PE), and 1,2-dipalmitoyl-*sn*-glycero-3-phosphoethanolamine-N-(lissamine rhodamine B sulfonyl) (ammonium salt) (Rho-PE) were obtained from Avanti Polar Lipids Inc. (Alabaster, Alabama). Amino acid building blocks, resins, and coupling agents were obtained from Novabiochem (Darmstadt, Germany), Anaspec (San Jose, CA), or ChemPep (Miami, FL). 5-FAM (carboxyfluorescein) was obtained from Anaspec (San Jose, CA). 3β-Hydroxy-5-cholestene (CHOL), 3β-Hydroxy-5-cholestene 3-hemisuccinate (CHEMS), fluorescein isothiocyanate-dextran (FITC-Dextran, MW 10,000), *N*-hydroxysuccinimide (NHS), dicyclohexylcarbodiimide (DCC), sodium orthovanadate, okadaic acid, and propidium iodide were obtained from Sigma-Aldrich (St. Louis, MO). All reagents and solvents used were of analytical or HPLC grade. All buffers were made with MilliQ water and subsequently filtered through 0.1 μM filters.

3.5.2 Lipopeptide Synthesis

Lipopeptide samples were synthesized via conjugation of NHS-Chems to a C-terminal positioned lysine. NHS-Chems was synthesized as previously described [152]. Briefly, 2.5 mmol of NHS was dissolved in 25 mL of DCM and 10 mL of ethyl acetate and was left stirring for 5 minutes. 2.5 mmol of Chems was then added to the reaction followed by 2.5 mmol of DCC in 10 mL of DCM. The reaction was left stirring at room temperature for 4 hours. The product was then filtered, flask dried by rotary evaporation under pressure, and placed overnight under high vacuum. The final product was then purified by methanol recrystallization.

NHS-Chems was then reacted with pure peptide in a 1.2:1 molar ratio under neat conditions in a 2:1 mixture of DMSO:DCM. The reaction was left stirring overnight at 30 ºC. The product was then precipitated in cold ethyl ether. The precipitate was pelleted by centrifugation at 3000 rpm (CR412, Jouan, Winchester, VA), the supernatant containing excess unreacted cholesterol was decanted, and the pellet was washed again with cold ethyl ether. After a second centrifugation, the solvents were decanted and the pellet was re-suspended in TFE, transferred to a flask and dried by rotary evaporation under reduced pressure and high vacuum. Reaction yield was 80-85% product. Quantification was determined as the percent of peptide to cholesterol in the purified sample. Peptide concentration was determined using a Nanodrop ND-1000 spectrophotometer (Thermo Fisher Scientific, Wilmington, DE), and cholesterol concentration was quantified with ferric acid chloride as previously described [153]. The final products were confirmed by MALDI-MS (FP-2PT-Chems Expected Molecular Weight: 2722.05, Observed Molecular Weight: 2721.88; FP-2Sul-Chems Expected Molecular Weight: 2662.47, Observed: 2662.79). Lipopeptides were lyophilized and stored under argon in -20 ^{o}C. FP-2PT-Chems and FP-2Sul-Chems lipopeptide stock solutions were prepared in trifluoroethanol (TFE) and used for formulating liposomes.

3.5.3 Circular Dichroism

CD spectra were measured on an OLIS DMS10 spectrometer (Olis, Bogart, GA) equipped with a Peltier temperature control stage and a nitrogen flush system. 100 μM solutions of POPC liposomes containing 2 mol% FP-2PT-Chems were prepared in a buffered solution consisting of 145 mM NaCl and 5 mM Hepes (pH 7.4). The monochromator was setup to record from 187.5 nm to 300 nm (1200 lines/mm), with an integration time of 5 seconds and the temperature set to 37 ^{o}C. Spectra were recorded using a cell with an optical path length of 1 mm. The spectra of POPC liposomes containing 2 mol% cholesterol was also recorded for background subtraction. Recorded spectra were averaged by a minimum of 3 runs. The secondary structure of the peptide was then determined by subtracting the spectra of POPC liposomes containing 2 mol% cholesterol.

3.5.4 Fluorescence Measurements

Fluorescence assays of lipid mixing and dephosphorylation were performed in a FluoroLog-3 spectrofluorometer (Horiba Jobin Yvon, Edison, NJ) equipped with a temperature controlled stage (LFI-3751) and a magnetic stirrer. A 450-W xenon light source was used for all recordings. Data acquisition was done through FluorEssence software (Horiba Scientific, Kyoto, Japan) and analyzed using MATLAB.

3.5.5 Quantification of FTP Dephosphorylation by Phosphate Sensor

Phosphatase catalyzed dephosphorylation of FTP was monitored using a highly sensitive phosphate-binding fluorescent protein sensor that can measure nanomolar phosphate concentrations [145] (Phosphate Sensor, Life Technologies, Carlsbad, CA). FTP containing 2 mol% FP-2PT-Chems was incubated with 10 nanomoles of phosphate sensor in the presence of

alkaline phosphatase (CIP). The release of phosphate from the liposomes was monitored using a FluoroLog-3 spectrofluorometer (Horiba Jobin Yvon, Edison, NJ), with the excitation and emission wavelengths set to 430 nm and 450 nm respectively. The assay was run at 37 ^{o}C in a buffered solution containing 145 mM NaCl, 5 mM Hepes and 1 mM $MgCl_2$ (pH 7.4). Runs were done in triplicate and data was analyzed in Matlab. For all experiments, percent of dephosphorylation were calculated by measuring the total phosphate released, and normalized to the maximum intensity after the liposomes were lysed with $C_{12}E_{10}$ surfactant, and adjusted for background fluorescence.

3.5.6 FTP Content Release Assay

For FTP induced CF release, POPC-CF liposomes were mixed at with FTP containing 2 mol% FP-2PT-Chems in a 1:1 ratio and incubated at 37 ^{o}C in the presence or absence of phosphatase (CIP or Protein Phosphatase I (PPI)) in buffer containing 145 mM NaCl, 5 mM Hepes and 1 mM $MgCl_2$ (pH 7.4). The release of CF from the liposomes was monitored, with the excitation and emission wavelengths set to 485 nm and 520 nm respectively. Runs were done in triplicate and data was analyzed in Matlab. For all experiments, percent CF leakage values were calculated by measuring the total CF released, and normalized to the maximum intensity after the liposomes were lysed with $C_{12}E_{10}$ surfactant and adjusted for background fluorescence as follows:

$$CF(\nabla) = \frac{CFintensity(\nabla) - background(\nabla)}{detergent(\nabla) - background(\nabla)}$$ *where ∇ represents emission wavelength.*

3.5.6 FTP Lipid Mixing

Membrane fusion was measured by changes in fluorescence intensity resulting from fluorescence resonance energy transfer between the head group labeled probes NBD-PE and Rho-PE as previously described [136] using a Fluorolog-3 spectrofluorometer (Horiba Jobin Yvon, Edison, NJ). Two set of liposomes were prepared: unlabelled FTP with FP-2PT-Chems liposomes and labeled POPC liposomes with 1 mol% NBD-PE and Rho-PE. A mixture of unlabeled FTP to labeled liposomes at a 9:1 molar ratio of 100 μM total lipid concentration were suspended in 2 mL buffer containing 145 mM NaCl, 5 mM $MgCl_2$ (pH 7.4). Samples were incubated at 37 ^oC and fluorescence intensities of the samples were measured. Emission spectra were obtained from 490 nm to 700 nm using an excitation wavelength of 467 nm. Intensity changes were monitored at 520 nm (near the emission maximum of NBD-PE) and at 590 nm (near the emission maximum of Rho-PE. Lipid mixing was evidenced by an increase in fluorescence intensity at 520 nm due to relief of energy transfer, and a decrease in 590 nm intensity. Changes in the fluorescence intensity ratio of NBD to Rho were normalized and quantified as follows:

$$Lipid\ Mixing(\nabla) = \frac{NBDintensity(\nabla) - background(\nabla)}{detergent(\nabla) - background(\nabla)}\ where\ \nabla \text{ represents } emission\ wavelength$$

Background fluorescence from vesicles containing 1 mol% of NBD-PE and Rho-PE in a 1:9 mixture with non-probe-containing vesicles was set to 0% lipid mixing and 100% lipid mixing was set to 100% lipid mixing.

3.5.7 Cell Culture

B16F10 murine melanoma cell line was obtained from the UCSF Cell Culture Facility. B16F10 cells were maintained in RPMI 1640 medium containing 10% (v/v) CultraPure fetal bovine serum (Axenia Biologix, Dixon, CA), 25 mM Hepes, and 1% penicillin-streptomycin.

Cells were cultured with complete medium at 37 ^{o}C in a humidified atmosphere of 5% CO_2 in air. Media was filtered through a 0.1 µM filter prior to use. Experiments were performed with cells harvested from subconfluent cultures using 0.05% trypsin and re-suspended in complete medium prior to plating.

3.5.8 Microscopy

Fluorescence microscopy was performed using a Nikon Eclipse TS100 fluorescence microscope (Nikon, Tokyo, Japan), using the following filters: FITC (Excitation: 460 nm, Emission: 510 nm) and Texas Red (Excitation: 532 nm, Emission: 605 nm). Images were captured with a Spot RT MonoChrome digital camera using a 20X objective. Spot software (Diagnostic Instruments, Sterling Heights, MI) was used for data capture and Image J was used for post processing overlays and pseudo coloring.

Spinning disk confocal images were acquired using a Zeiss Axiovert 200 M microscope with a 40x/1.3 NA oil objective or a 63x/1.4 NA oil objective, Andor iXon 887 EMCCD Camera, Prior Proscan III stage, Yokogawa CSU-10 spinning disk with 488 nm and 561 nm laser lines modulated by a Neos AOTF (Solamere Technology Group, Salt Lake City, Utah). Cells were kept at 37 ^{o}C using a Zeiss objective and sample heater. Metamorph (Molecular Devices, Sunnyvale, CA) was used to control the microscope, as well as for image acquisition and processing. Imaris (Bitplane Scientific Software, Zurich, Switzerland) was used for three dimensional reconstruction and rendering.

3.5.9 FACS Analysis

Flow cytometric analysis (FACS analysis) for liposome fluorescence was performed using a FACSArray BioAnalyzer system (Becton Dickinson, CA). B16F10 cells were incubated

with fluorescently labeled FTP with 1 mol% Rho-PE for defined periods of time. Three washing steps were performed to remove any unbound liposomes. The cells were then detached from cell culture plates using calcium and magnesium free HBSS media and analyzed by FACS analysis. Cells were gated on FSC/SCC (forward scatter/ side scatter) to remove debris. A minimum of 10,000 events were collected by list-mode data that consisted of side scatter, forward scatter and fluorescence (green, yellow, mCherry, DsRed) emission. Data was analyzed using FlowJo software (Ashland, OR). The fluorescence from the FTP containing 1 mol% Rho-PE was measured using the mCherry emission channel. The geometric mean of mCherry emission was used to quantify the amount of liposome uptake.

3.5.10 FTP Uptake in Cultured Cells

B16F10 cells (0.5×10^5) were plated in Fluorodish glass bottom dishes (World Precision Instruments, Sarasota, FL) and grown to 70% confluency at 37 ^oC and 5% CO_2 in medium (RPMI 1640 with 10% (v/v) FBS). The cell monolayer was rinsed with FBS-free medium and then medium containing 10 μM of liposomes was added. Cells were incubated for 0, 0.25, 0.5, 1, 2, 4, 6, and 12 hours at 37 ^oC and 5% CO_2. At the end of the incubation, the medium was removed and the cells were washed three times with 1 mL of Hank's Buffered Saline Solution (HBSS). To determine whether the uptake of FTP liposomes was energy-dependent or cell-function dependent, B16F10 cells were incubated with FTP under cold conditions and in the presence of phosphatase inhibitors. For energy-dependent studies, B16F10 were rinsed with cold FBS-free medium and incubated at 4 ^oC for 1 hour prior to addition of liposomes. A 10 μM solution of liposomes was added to the cells and the mixture was incubated for 1 hour at 4 ^oC. After the incubation period, the medium was removed and the cells were washed three times with cold HBSS and imaged by fluorescence microscopy.

For uptake studies in the presence of inhibitors, B16F10 were rinsed with FBS-free medium and pre-incubated for 1 hour with either 1 μM okadaic acid, 0.5 mM sodium orthovanadate, or an inhibitor cocktail of 1 μM okadaic acid and 0.5 mM sodium orthovanadate. Liposomes were then added to the cells and incubated for 2 hours, after which the cells were rinsed three times with HBSS. Confocal and fluorescence microscopy as described above were then used to image the wells.

3.5.11 Cytotoxicity Assay

Cytotoxicity of liposomes was determined by the MTT assay (Sigma, St. Louis, USA). B16F10 cells were seeded into 96-well plates at a density of 9,000 cells per well and cultured for 24 hours. After 24 hours the cell culture medium was replaced and the cells were incubated with increasing liposome concentration in 100 μL cell culture medium. After a 4 hours incubation, the medium was replaced by RPMI1640 containing 0.5 mg/mL MTT (3-(4,5-dimethylthiazol-2-yl)-2,5-diphenyl tetrazolium bromide) (Sigma, St. Louis, USA). After 4 hours incubation at 37 °C, the medium was aspirated and formazane crystals were dissolved in 200 μL DMSO per well. Measurement was performed using a microplate reader at a wavelength of 570 nm, with a background correction at 690 nm. Relative viability was calculated using 0% (wells without cells) and 100% (wells with untreated cells) controls, and data is presented as an average of four measurements.

3.5.12 FTP Cytosolic Delivery Assay

FP-2PT-Chems and FP-2Sul-Chems lipopeptide stocks solutions were prepared in trifluoroethanol (TFE) and used for formulating liposomes. Liposomes were prepared by combining chloroform solutions of POPC with 2% mol TFE solutions of FP-2PT-Chems or FP-

2Sul-Chems peptide: lipid ratio. Lipids were dried by a combination of rotary evaporation and high vacuum, and hydrated in buffer containing CF, propidium iodide, or FITC-Dextran by intermitted vortexing. Liposomes encapsulating CF were prepared by thin film rehydration of a 100 mM CF solution containing 5 mM Tris-HCl (pH 7.4). Liposomes encapsulating propidium iodide were rehydrated in 1 mL of 10 mg/mL solution of propidium iodide as previously described [154]. Liposomes encapsulating FITC-Dextran were prepared as previously described [67] and rehydrated in 1 mL of 50 mM solution of FITC-Dextran (10kd MW) containing 145mM NaCl, 5mM Hepes (pH 7.4). All solutions were sonicated for 10 minutes under argon, and the liposomes were extruded through polycarbonate membranes with 100 nm pores. Free CF and propidium iodide were removed by size exclusion chromatography (Sephadex G25 column; PD-10GE Healthcare, Piscataway, New Jersey). Free FITC-Dextran was removed by Sephadex G-75 (1 x 20 cm) gel filtration. The mobile phase for separation consisted of a 5 mM Hepes buffer with 145 mM NaCl (pH 7.4). The encapsulated liposomes were capped with argon and stored at 4 ^{o}C.

B16F10 cells (0.5 x 10^5) were plated in Fluorodish glass bottom dishes (World Precision Instruments, Sarasota, FL) and grown to 70% confluency at 37 ^{o}C and 5% CO_2 in medium (RPMI 1640 with 10% (v/v) FBS). The cell monolayer was rinsed with FBS-free medium and medium containing 10 μM of liposomes was added. Cells treated with liposomes containing CF, propidium iodide and FITC-Dextran were incubated for 0.5, 1, 2, and 4 hours at 37 ^{o}C and 5% CO_2. At the end of the incubation, the medium was removed and the cells were washed three times with 1 mL HBSS. The cells were then counterstained with DAPI. Confocal and fluorescence microscopy was then used to image the wells.

3.5.13 Statistical Analysis

Statistical analysis was assessed by analysis of variance and two-tailed student's t-test using Prism 5. Significance was attributed to groups with p values less than 0.05.

Chapter 4: The Engineering of Surface Charge Converters (SCC): Charge Conversion via Phosphatase Triggering

4.1 Abstract

Surface charge converters (SCC) were engineered as liposomes that convert their negative surface charges into positive surface charges by the action of a phosphatase. SCC exploit the chemical structure of dioleoylcholinephosphate (DOCP), which is a newly synthesized lipid that has a quaternary amine at the hydrophobic interface and a phosphate extending into the aqueous phase [63]. This lipid is a substrate for phosphatases. It was hypothesized that dephosphorylation of the extended phosphate could trigger charge conversion at the membrane interface, converting the anionic head group into a cationic head group. The surface charge conversion in an appropriate lipid composition will modulate lipid packing changes in the bilayer. In the presence of anionic membranes, the generation of a cationic surface charge would trigger membrane mixing, content release, and cytosolic delivery. Phosphatase catalyzed dephosphorylation transformed the anionic DOCP into a cationic lipid with a concomitant dramatic increase in zeta potential. Surface charge converters formulated with phosphatidylethanolamine and cholesterol induced significant lipid mixing and content release upon exposure to phosphatase. Triggered content release was efficient in physiological pH, while lipid mixing was enhanced in acidic conditions by acid phosphatases. Incorporation of PEG-lipids into the liposome composition reduced the trigger effect of the phosphatase. This tactic provides a substantial level of cytosolic delivery of the liposome cargo into cells in culture. This observation provides encouragement that the SCC will have applications in drug delivery.

4.2 Introduction

Surface charge converting liposomes, termed SCC, refer to liposomes composed of inverted phosphocholine lipids, such as DOCP, whose surface charge can be dramatically altered from negative to positive. DOCP is a lipid characterized by an inversion of the classical zwitterionic head group structure, with the quaternary amine positioned next to the bilayer and the phosphate group extended towards the aqueous phase (Figure 4.1) [63]. This geometric inversion transforms some of the biophysical properties of the lipid, producing an anionic head group whose electrical properties are governed by the protonation state of its extended phosphate. The extended phosphate of DOCP is readily cleaved by phosphatases, and its dephosphorylation leads to the generation of a cationic lipid. This lipid is analogous to the cationic lipid DORI, which has been reported to be an effective mediator of gene delivery [155, 156]. Further understanding the consequences of this charge conversion as well as the cellular and physiological impact would help elucidate the requirements of phosphatase-active liposomes with a relatively simple liposome composition.

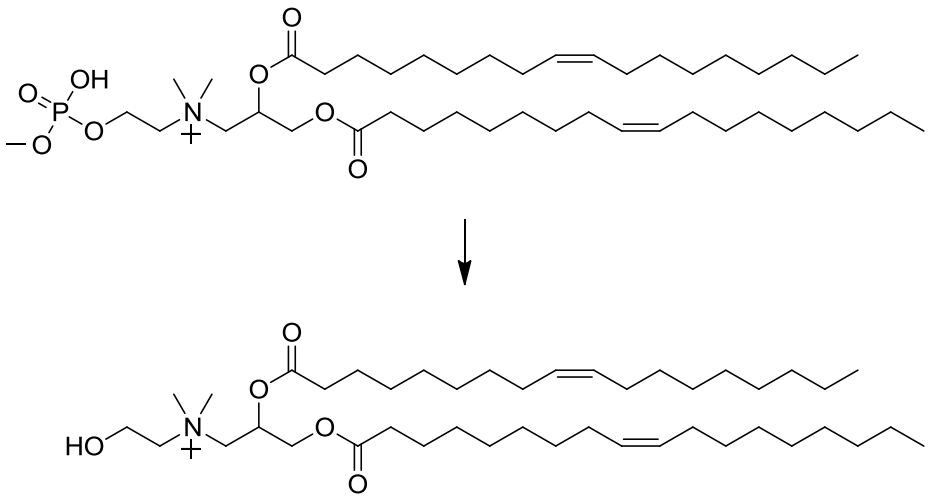

Figure 4.1 Structural Change in the DOCP Head Group as a Result of Dephosphorylation. DOCP has a quaternary amine positioned next to the bilayer and a phosphate group extended towards the aqueous phase. Phosphatase catalyzed dephosphorylation of DOCP generates a cationic lipid.

4.3 Results and Discussion

4.3.1 Charge Conversion Mediated by Phosphatase Triggering

The zwitterionic DOCP has a negative surface charge across a wide range of pH. This is a result of the head group inversion that positions the phosphate into the aqueous phase [63]. The charge on the phosphate is modulated by the pH of the aqueous environment and is affected by ionic interactions at the bilayer interface. In a buffered solution of 25 mM NaCl and 5 mM Tris-HCl (pH 8.5), DOCP liposomes have a negative surface charge of -60±10 mV. Hence, it is slightly more negative than the anionic phosphatidylglycerol (PG) (Figure 4.2). The zeta potential of DOCP is probably more negative than PG because it has a doubly negatively charged phosphate group extending into the aqueous phase and a singly positively charged quaternary amine, resulting in a head group that has a net charge of -1 Since DOCP is a substrate for phosphatase [63], dephosphorylation of the extended phosphate would expose the quaternary amine adjacent to the bilayer thereby transforming the lipid from anionic to cationic. This local increase in surface potential, from -1 to +1, results in a charge conversion of +2.

Charge conversion assays were designed to assess the effect of phosphatase triggering on charge conversion. Charge conversion was measured by two methods: (1) the time-dependent change in zeta potential of DOCP SCC in the absence and presence of phosphatase (Antarctic Phosphatase, New England Biolabs, Ipswich, MA), and (2) the time-dependent change in zeta potential of DOCP SCC treated with phosphatase as measured after lipid extraction and liposomal reconstitution. The extraction method was used to correct for the coating of the cationic liposome surface by the binding of the negatively charged phosphatase (pI 4.5) at pH 7.4. A tris-buffered saline solution (25 mM NaCl, 5 mM Tris, pH 7.4) without magnesium was used to minimize the interaction of divalent cations with phosphate groups at the bilayer interface. Divalent cations were present in the system only when alkaline phosphatase was added. To correct for this effect,

the zeta potential of the DOCP SCC was recorded in the presence of 0.1 mM of $MgCl_2$ and 0.01 mM of $ZnCl_2$. Under these conditions, no significant changes in zeta potential were measured.

Exposure of DOCP SCC to alkaline phosphatase resulted in a complete conversion of the surface charge of the liposomes. Triggered charge conversion proceeded through three surface charge states: anionic, neutral, and cationic (Figure 4.3), and followed first-order kinetics (Figure 4.4b). DOCP SCC started off with a negative zeta potential of -60 mV. Addition of phosphatase resulted in an initial lag phase with minimal charge conversion. Shortly after, an exponential increase in zeta potential was observed. This burst phase, in which the SCC transitioned from an anionic to a cationic liposome, exhibited the greatest charge conversion. The change in zeta potential was substantial, with vesicles prepared from extracted lipids having a net gain of 81±10 mV in 1 hour. The addition of a heat inactivated alkaline phosphatase produced no change in zeta potential, which also indicates that charge conversion proceeds through the exposure of the quaternary amine upon dephosphorylation of the exposed phosphate.

Charge conversion was also observed in the non-extracted DOCP SCC liposomes, but the net charge gain was lower (60±8 mV). This discrepancy is explained by the presence of alkaline phosphatase in the reaction mixture. As the surface of the SCC converts from negative to positive, the phosphatase will absorb to the newly created cationic head group and shield its charge. This hypothesis was confirmed upon addition of phosphatase to vesicles prepared from extracted lipids. A 15±5 mV decrease in zeta potential was observed. Furthermore, a decrease in zeta potential was also observed when alkaline phosphatase was added to cationic DOTAP liposomes, with the zeta potential decreasing from 60±5 mV to 35±5 mV. These observations indicate that the anionic phosphatase can interact with the newly formed cationic lipid. This results in a shielding of its positive charge, thereby decreasing the measured zeta potential.

The charge conversion properties of DOCP are analogous to a logic switch. In the absence of phosphatase, represented as an input of '0', the system does not undergo charge conversion and has an output of '0'. This is also true if the input is an inactive phosphatase, or a different enzyme such as phospholipase A_2. In the presence of phosphatase, represented as an input of '1', the system undergoes full charge conversion and has an output of '1'. The intriguing logic switch characteristics of DOCP SCC could be useful for designing novel drug delivery carriers. In the subsequent sections, I focused on understanding the characteristics of liposomes composed of the DOCP molecular switch and exploit their convertible potential to engineer triggerable liposomes that can collapse upon switch activation.

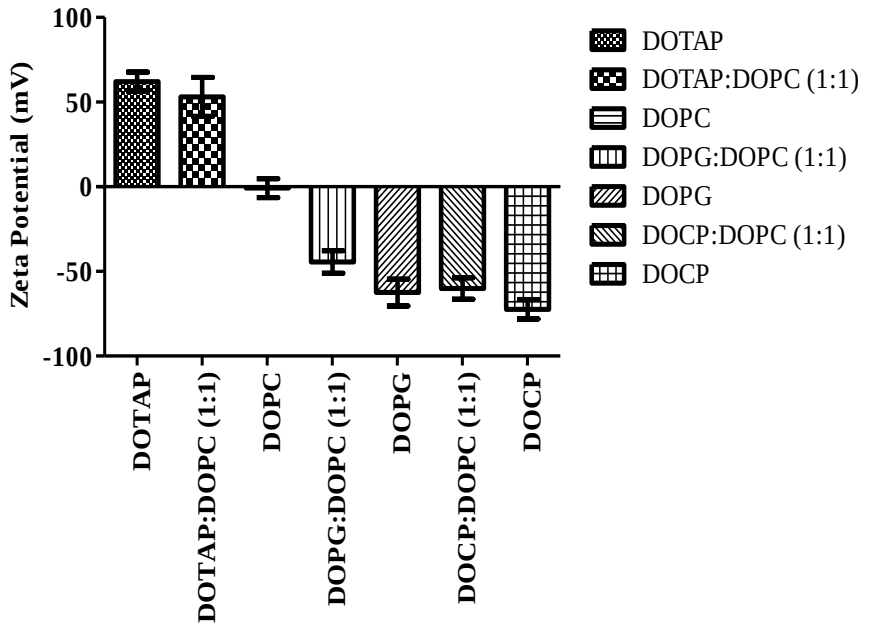

Figure 4.2 Zeta Potential of Cationic, Neutral and Anionic Formulations in Comparison to DOCP. In a 25 mM NaCl, 5 mM Tris (pH 8.5) solution, DOCP is anionic and has a zeta potential below -60±10 mV.

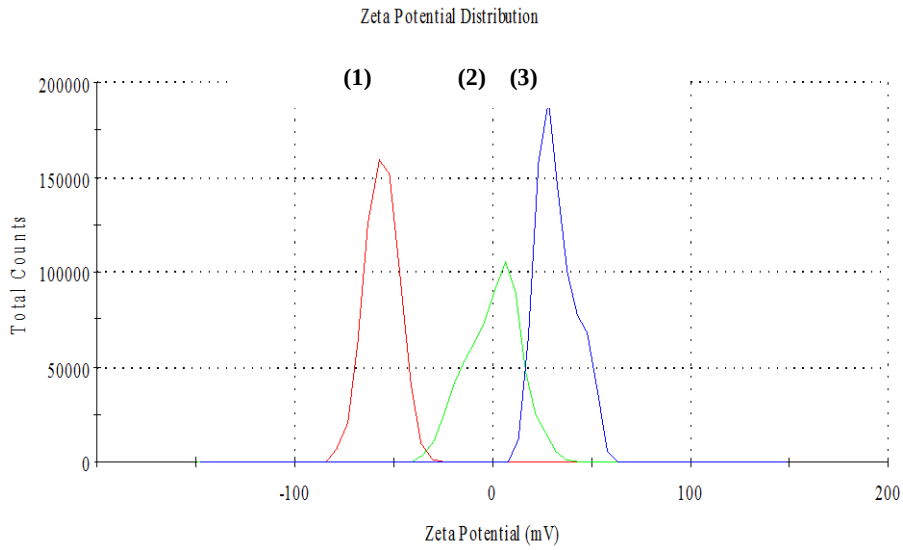

Figure 4.3 Surface Charge Transition of DOCP SCC by Alkaline Phosphatase. 100 nanomoles of DOCP SCC liposomes were incubated with 25 units of alkaline phosphatase at 37°C for 1 hour. Three surface charge states were observed as a result of charge conversion: anionic (1), neutral (2), and cationic (3). The zeta potential starts off negative (-60 mV). Within 30 minutes of phosphatase addition, the membrane converts first into a neutral membrane and then into positive membrane.

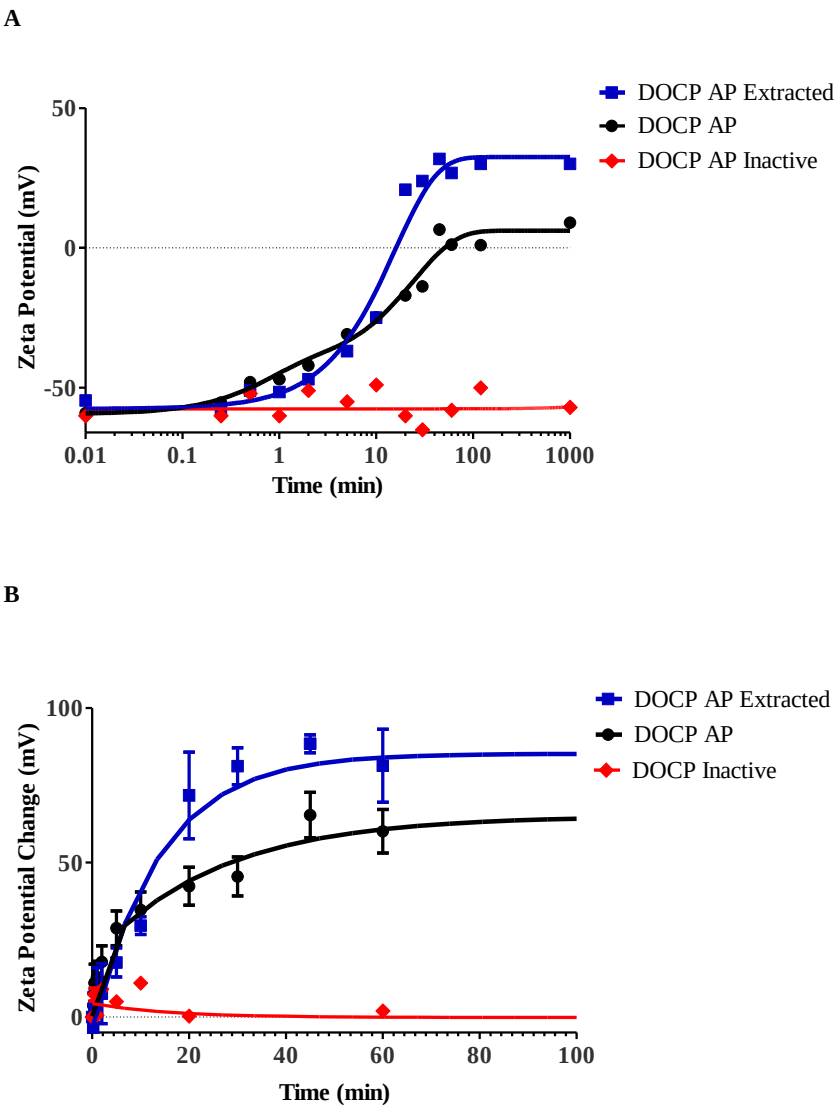

Figure 4.4.Charge Conversion Progress Curves of DOCP SCC by Alkaline Phosphatase. A) 100 nanomoles of DOCP SCC liposomes were incubated with 25 units of alkaline phosphatase at 37^{o}C in a Tris-buffered solution (pH 7.4) containing 25 mM NaCl and 5 mM Tris. The charge conversion progress curves show an initial lag phase, followed by a burst phase. The reaction plateaus after 30 minutes. A positive zeta potential was measured at the end of the reaction. The extraction method showed a greater charge conversion. B) The zeta potential change as a result of charge conversion is plotted. The change in zeta potential was substantial, with reconstituted membranes having a net gain of 81±10 mV in 1 hour. Charge conversion was also observed for non-extracted DOCP SCC, but the net charge gain was lower (60±8 mV).

4.3.2 Effect of Phosphatase Triggered Charge Conversion on Content Release

Since SCC display "switch-like behavior" due to their charge conversion, they are suited for engineering systems that can take advantage of lamellar to hexagonal phase transitions to trigger drug release. Changes in the lipid packing of the bilayer as a mechanism to induce lamellar to hexagonal phase transition has been successfully exploited in a number of pH triggered systems [8, 69, 88, 151, 157]. These systems make use of lipids such as phosphatidylethanolamine [68] and cholesterol [68, 158] to promote hexagonal phase transitions upon a pH-triggered structural transformation of the lipid head group. Drawing parallels from these well-studied pH systems, it was hypothesized that SCC containing phosphatidylethanolamine or cholesterol could be designed for charge-conversion mediated content release.

To design stable SCC, we first had to determine if they could encapsulate small molecules via self-assembly and passive encapsulation. We searched for formulations that had minimal content leakage at room temperature and at 37 ^{o}C. SCC formulated with just DOCP were found to be unsuitable for encapsulating small molecules like carboxyfluorescein (CF). The formulation was unstable, as it lost most of its contents when purified on a size exclusion column. This enhanced leakage effect can be partially attributed to the head group inversion of DOCP, where the quaternary amine adjacent to the bilayer greatly affects the permeability of encapsulated anionic solutions. In addition, DOCP is a racemic mixture of lipids, which can influence chain packing and the stability of the liposomes [63]. The use of helper lipids such as DOPE, POPE, and cholesterol is required to formulate stable SCC. SCC made from mixtures of DOCP, POPE, DOPE, or cholesterol were stable and formed vesicles with average hydrodynamic diameters of 85±10 nm.

To investigate if phosphatase triggering leads to triggered content release, SCC were formulated encapsulating CF with different helper lipids compositions, which included

DOCP:Chol (60:40 molar ratio), DOCP:POPE (60:40 molar ratio), and DOCP:POPE:Chol (50:30:20 molar ratio). The SCC were tested for their ability to trigger content release by monitoring the release of CF in the presence and absence of alkaline phosphatase (Calf Intestine Phosphatase or Antarctic Phosphatase, New England Biolabs, Ipswich, MA). The effect of phosphatase availability on SCC triggering was also investigated by varying the enzyme concentration in solution.

Although a limited set of SCC formulations were tested, it was apparent that content release could be modulated by the lipid composition as has been reported for many triggerable systems [8, 67, 69, 88]. For instance, cholesterol is known to reduce the permeability of ions and small polar molecules across bilayers and make liposomes less leaky [159]. Cholesterol also produces a decrease in electrical conductance and an increase in the electrical resistance and capacitance of phospholipid bilayers. This results in a "tighter" membrane and reduces the ability of a number of proteins to penetrate and increase disorder within the bilayer [160, 161]. The inclusion of cholesterol in SCC was expected to make this lipid composition more stable and less prone to triggered content release as a result of charge conversion. SCC formulated with cholesterol (DOCP:Chol SCC) were found to be least sensitive to phosphatase triggering as illustrated in Figure 4.5a. Although DOCP:Chol SCC was responsive to changes in cholesterol, the formulation exhibited the least content release. The leakage of DOCP:Chol SCC in the presence of phosphatase (2 units/nanomole of lipid) was measured at 20±2% after 2 hours.

SCC formulated with phosphatidylethanolamine were expected to have increased triggered content release given the preference of phosphatidylethanolamine for the hexagonal phase [68]. We hypothesized that the anionic DOCP would inhibit the hexagonal phase transition of POPE. Upon phosphatase triggering, the increase in positive surface charge, as well as the structural transformation of the head group into a more "cone-shape" structure would promote the transition of POPE into the hexagonal phase and induce trigger content release. DOCP:POPE

SCC had a 60% increase in content release relative to DOCP:Chol SCC (Figure 4.5b). After 2 hours, 55±5% of the content was released upon exposure to phosphatase (2 units/nanomole of lipid). Formulating SCC with both helper lipids was hypothesized to provide enhanced triggered content release since cholesterol is known to destabilize bilayer structures containing phosphatidylethanolamine by promoting the formation of a hexagonal phase [69, 162, 163]. As expected, DOCP:POPE:Chol SCC had the greatest trigger effect with over 68±10% of their contents released (Figure 4.5c).

The extent of content release from SCC was dependent on the concentration of phosphatase (Figures 4.5 and 4.6). The addition of phosphatase resulted in triggered leakage for all concentrations tested. SCC triggered with 0.2 units of phosphatase per lipid had the least leakage with SCC releasing less than 10% of their contents, which was not significant when compared to the leakage of control liposomes. Increasing the concentration of phosphatase to 2 units per nanomole of lipid led to an eightfold increase in leakage across all formulations. Interestingly, the concentration of phosphatase influenced both the leakage rate and the final extent of contents, which suggests a product inhibition type of phenomena. The inorganic phosphate produced as a result of dephosphorylation is known to inhibit alkaline phosphatases [164] and can partially explain the inhibition phenomena observed. It is also possible that as the system charge converts the phosphatases associate with patches of cationic lipids and is thereby removed from the reaction. Further experimentation is needed to support these hypotheses. Nevertheless, the fact that inactivated phosphatases did not trigger content release indicates that the leakage effect is a result of phosphatase catalyzed dephosphorylation.

Although this data provides evidence that indicates that SCC can be designed for phosphatase triggered release, further experimentation is needed to fully characterize the impact of lipid composition and phosphatase concentration on the triggered release kinetics of SCC. Factors that can influence SCC content release include: the rate of dephosphorylation, which is

dependent on the type of phosphatase (alkaline, acidic, tyrosine protein phosphatase, ser/thr protein phosphatase, etc.), the temperature of the media, the bilayer packing of SCC as a result of the lipid chain lengths in the bilayer the ratio of helper lipids to inverse PC, the rate of lipid aggregation rate as a result of divalent cations in solution, and the concentration of SCC liposomes in solution. This last point is of critical importance since bilayer destabilization requires inter-bilayer contact [68, 70]. Thus, studying the effect of liposome concentration on content release of SCC can provide further explanation of the roles of lipid aggregation, SCC destabilization, and membrane fusion. Finally, leakage of SCC under an osmotic gradient could provide further insights into the elastic deformation and critical failure of SCC carriers [165, 166]. Understanding these effects will provide additional information to enable engineers to optimize SCC formulations.

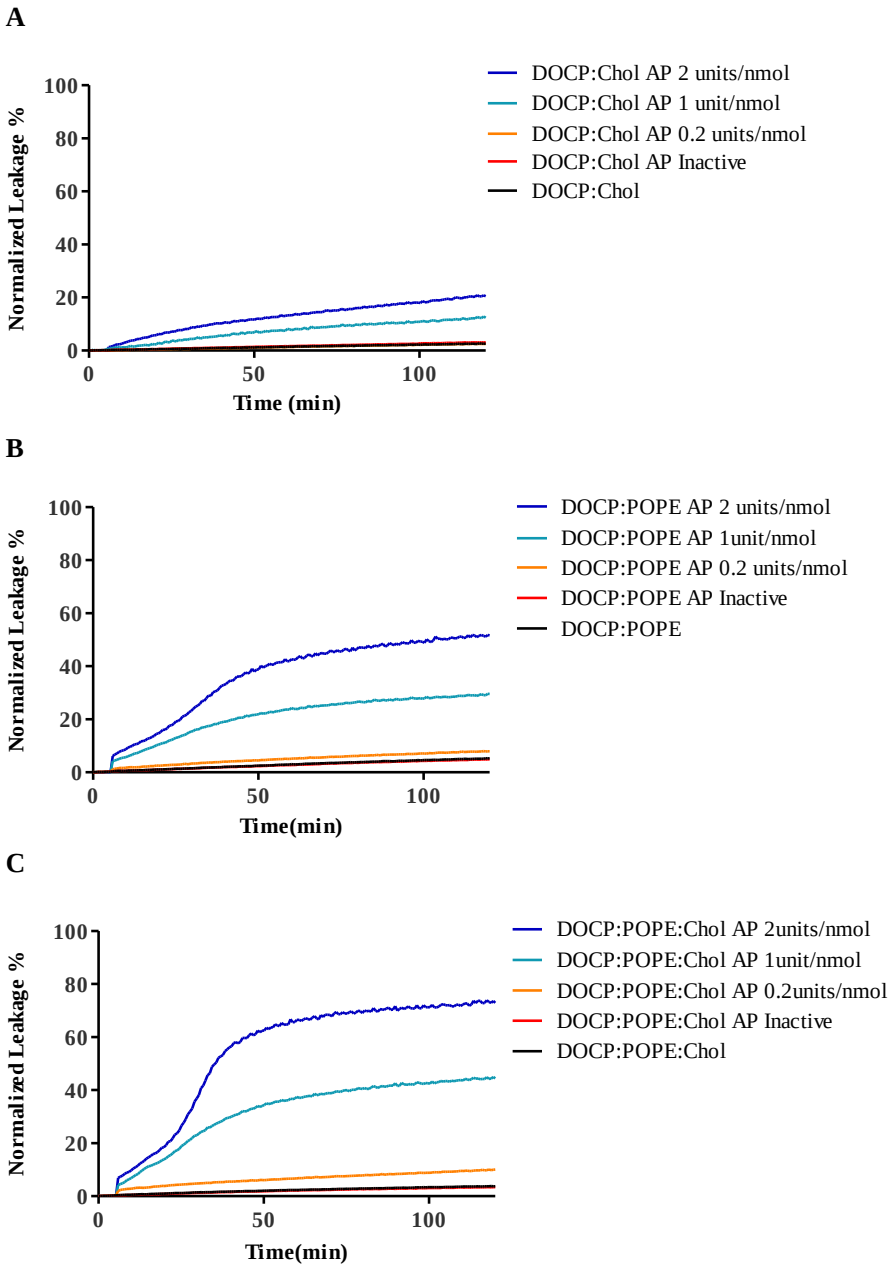

Figure 4.5: Content Release of SCC Formulations Triggered by Alkaline Phosphatase. SCC composed of DOCP:Chol (60:40 molar ratio), DOCP:POPE (60:40 molar ratio), DOCP:POPE:Chol (50:30:20 molar ratio)) were tested for their ability to trigger content release. Each SCC formulation encapsulated 100 mM CF. The release of CF from SCC was monitored in the presence and absence of alkaline phosphatase. Heat inactivated alkaline phosphatase (AP Inactive) was tested in all formulations and found to have no significant effect on triggering. The concentration of phosphatase is given as enzyme units per nanomole of lipid (unit/nmol). Content release experiments were performed at 37 ^{o}C in a Tris-buffered solution containing 145 mM NaCl, 5 mM Tris, and 0.1 mM $MgCl_2$ (pH7.4).

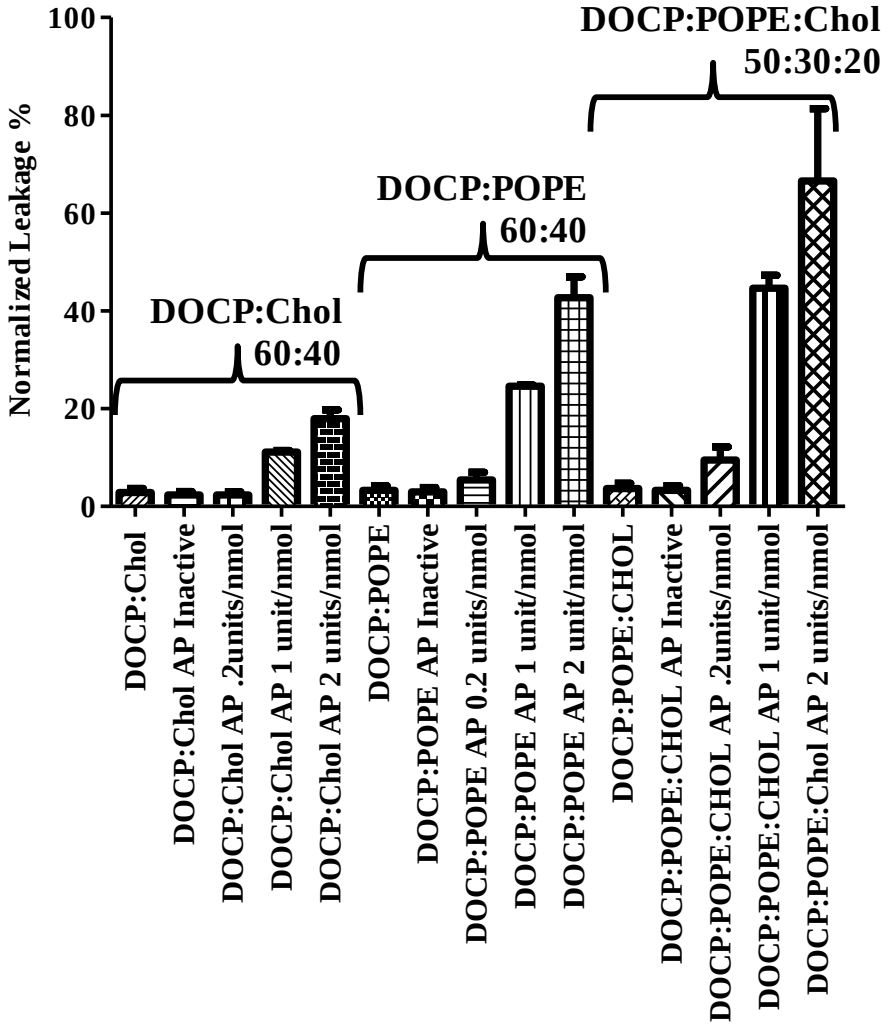

Figure 4.6 Effect of Lipid Composition on Triggered Release of SCC. SCC formulations containing phosphatidylethanolamine had the greatest content release, with DOCP:POPE:Chol SCC exhibiting the most leakage. The extent of content release from SCC upon phosphatase addition was monitored over 2 hours. Content release experiments were performed at 37 ^{o}C in a Tris-buffered solution containing 145 mM NaCl, 5 mM Tris, and 0.1 mM $MgCl_2$ (pH7.4).

4.3.3 Effect of PEG Shielding on Triggered Content Release

Sterically protective polymers, such as PEG, are covalently incorporated onto the bilayer to prolong the circulation time of liposomes [9, 32, 46] as they reduce the adhesion energy between liposomes and cells. Several triggerable liposomes have been designed by incorporating cleavable PEG lipids into the bilayer. These lipopolymers were reported to provide control for triggering alterations by pH, redox potential, and protease activity [71, 75, 79, 167, 168]. Furthermore, sterically protective polymers have been reported to suppress the binding of proteins on triggerable nanoparticles [71, 168]. However, there have also been reports of nanoparticles that make use of sterically protective polymers to enhance the trigger effect of enzymes like phospholipase [74, 75, 77, 169, 170]. It is thus of interest to understand what effect PEG shielding would have on triggering of SCC. Since the triggering mechanism of SCC relies on charge conversion at the bilayer interface, it was hypothesized that the incorporation into the bilayer of sterically protective polymers, like PEG, would result in a reduction of triggered content release.

To study this, DOCP:POPE (60:40 molar ratio) SCC encapsulating CF were formulated with 0%, 1% , 5%, and 10% PEG-DSPE lipid and were tested for phosphatase triggered content release, as described in section 4.3.2. It was observed that the effect of PEG inhibition is dependent upon its surface concentration (Figure 4.7). In the absence of PEG, SCC showed phosphatase dependent triggered release with SCC releasing 40% of their content in 1 hour (Figure 4.7d). Increasing the PEG mole ratio in the liposome to 1% reduced the trigger response by 50%, with SCC releasing 20% of their content in 1 hour. Increasing the PEG mole concentration to 5% dramatically reduced the trigger effect with SCC releasing only 7% in 1 hour. The extent of content release in SCC modified with PEG was also affected by the concentration of phosphatase. Increasing the concentration of phosphatase in the reaction mixture led to an increase in content release for all formulations that contained less than 10 mol% PEG.

Formulations with 10% PEG were found to be the most stable and were not affected by changes in phosphatase concentration. This suggests that PEG can be used to effectively modulate the triggered content release of SCC. Further experiments are required to determine if PEG also inhibits dephosphorylation and charge conversion of SCC. This can be readily done by quantifying the release of phosphates from pegylated SCC carriers when exposed to phosphatases. It would also be interesting to determine whether the effect is consistent across different types of phosphatases. The use of PEG as a modulator of phosphatase triggering is an important result of this study and has important implications for the design of *in vivo* SCC therapeutics for systemic administration.

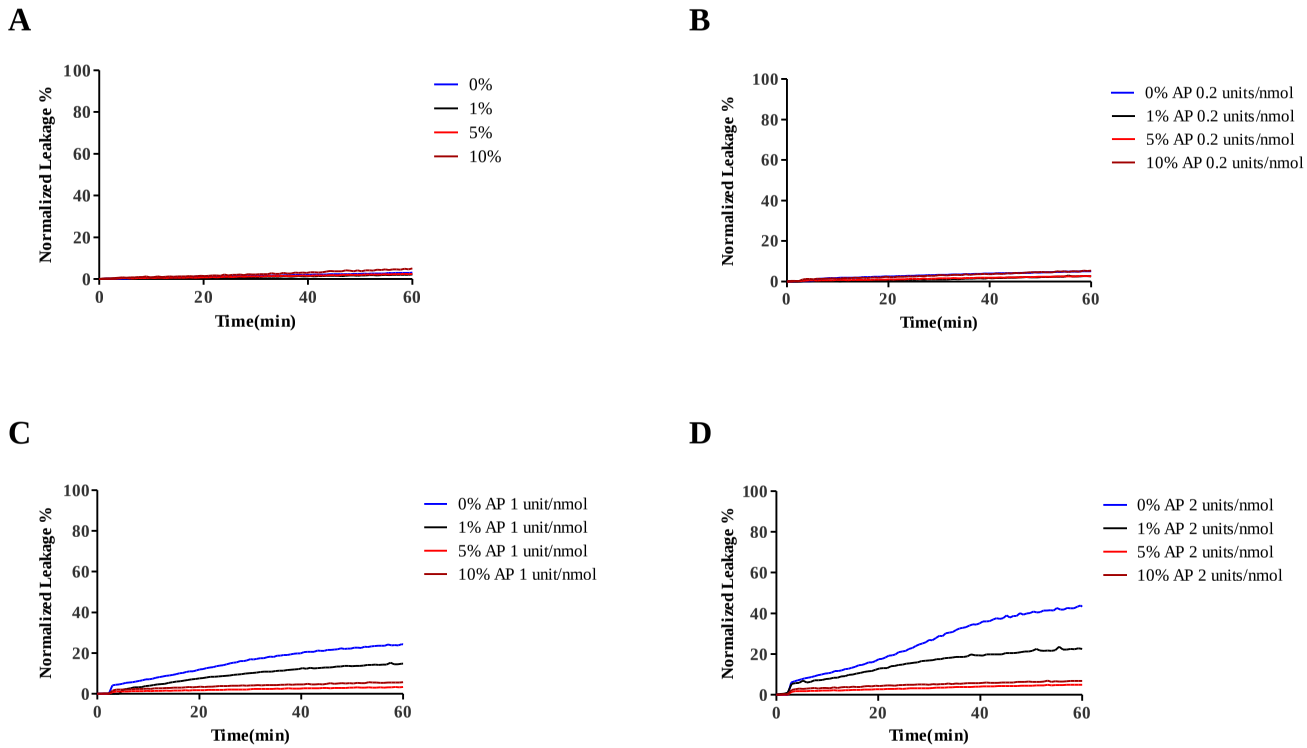

Figure 4.7 Effect of PEG on Triggered Content Release of SCC Formulations Containing Phosphatidylethanolamine. DOCP:POPE (60:40 molar ratio) SCC encapsulating CF were formulated with 0%, 1% , 5%, and 10% PEG-DSPE lipid and were tested for phosphatase triggered content release. The extent of content release in SCC modified with PEG was also modulated by the concentration of phosphatase. Phosphatase concentrations tested include: 0 units/nmol (A), 0.2 units/nmol (B), 1 unit/nmol (C) and 2 units/nmol (D).Content release experiments were performed at 37 ^{o}C in a Tris-buffered solution containing 145 mM NaCl, 5 mM Tris and 0.1 mM $MgCl_2$ (pH7.4).

4.3.4 Effect of Phosphatase Triggered Charge Conversion on Lipid Mixing

Surface charge converters would be particularly useful if they can mediate lipid mixing and endosomal or lysosomal escape. In order to do so, they must be effective at fusing with anionic membranes. Because charge conversion occurs at the head group, it was hypothesized that upon dephosphorylation the exposed cationic head group could mediate ion pairing with anionic membranes, and trigger membrane fusion.

To investigate if SCC are capable of mediating fusion with anionic membranes, fluorescence lipid mixing assays were performed in a FluoroLog-3 spectrofluorometer (Horiba Jobin Yvon, Edison, NJ). Lipid mixing was measured by fluorescence energy transfer [131] using a mixture of unlabeled (DOCP:DOPE in a 60:40 ratio) SCC and labeled anionic liposomes (POPG:DOPE in a 60:40 ratio with 1 mol % of both NBD-PE and Rho-PE). The liposomes were mixed at a 9:1 molar ratio and suspended in an acidic (pH 5.0) or a buffered solution (pH 6.8-7.4). Phosphatase was then added to the medium and the rate of lipid mixing was monitored for 1500 seconds by measuring the intensity change of NBD at 520 nm. Fluorescence intensity changes were normalized to the maximum fluorescence observed after surfactant lysis.

The rate of lipid mixing by SCC was greatest in acidic environments (pH 5.0), and in the presence of acid phosphatases (Figure 4.8). Significantly reduced lipid mixing was observed at physiological or alkaline pH. Both alkaline phosphatases tested, human alkaline phosphatase (Alkaline Placental Phosphatase Type XXIV, Sigma-Aldrich, St. Louis, MO) and calf intestine phosphatase (CIP, New England Biolabs, Ipswich, MA), had minimal effect on lipid mixing of SCC (Figure 4.8b). CIP was unsuccessful at mediating lipid mixing. HAP was able to mediate mixing to a greater extent than CIP, but the effect was small. Acid phosphatases (Sweet Potato Acid Phosphatase, Sigma-Aldrich, St. Louis, MO) were effective at triggering SCC and mediating lipid mixing. Triggering of SCC by acid phosphatase at pH 5 resulted in substantial lipid mixing. The extent of lipid mixing was measured at 50±10% and occurred relatively fast

(Figure 4.8a). Also, no significant lipid mixing was observed in the presence of heat-inactivated phosphatases. The findings suggest that triggered fusion is modulated by charge conversion as a result of phosphatase catalyzed dephosphorylation.

Further experimentation is needed to fully understand the effect of pH and phosphatase type on fusion of SCC liposomes. It is possible that lipid mixing is limited at neutral pH by the surface association of the negatively charged phosphatase with the newly formed cationic head group. This would shield the cationic patches on the surface of the SCC and limit their ion pairing with anionic vesicles. The isoelectric point of the phosphatases tested (pI 4.5-5) suggest that this shielding effect would be more pronounced at neutral pH. It is also possible, however, that a protein mediated fusion event is the cause for the accelerated rate of lipid mixing observed at acidic pH. Further experiments are required to test this hypothesis. Nevertheless, the data indicates that acid and alkaline phosphatases can mediate lipid mixing between SCC and anionic membranes. Hence, SCC might be able to fuse with endosomes or lysosomes and mediate cytosolic delivery of drugs.

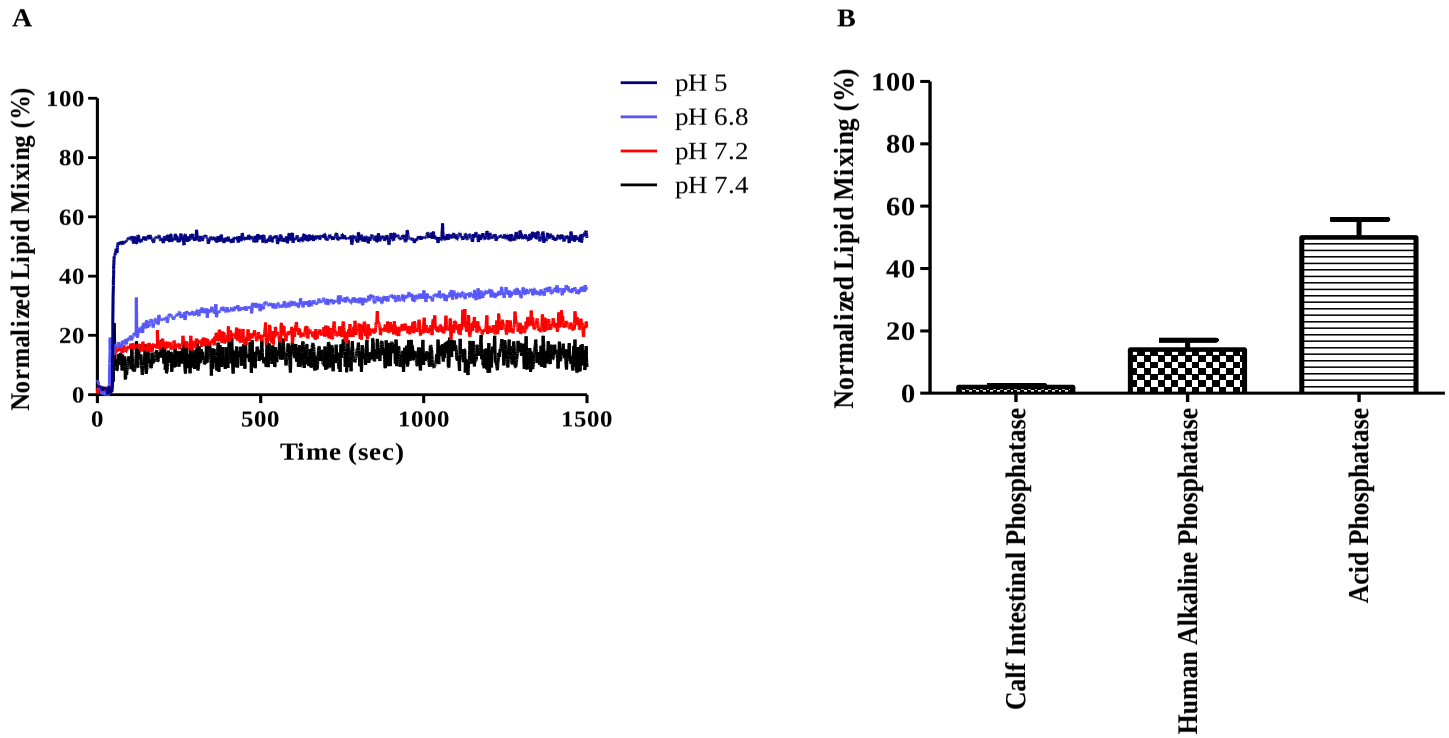

Figure 4.8 Lipid Mixing of SCC Formulations with Anionic Vesicles Triggered by Alkaline and Acid Phosphatases. A) The kinetics of phosphatase-induced lipid mixing from SCC liposomes is plotted as a function of pH. Lipid mixing was measured by fluorescence energy transfer [131] using a mixture of unlabeled (DOCP:DOPE in a 60:40 ratio) SCC and labeled anionic liposomes (POPG:DOPE in a 60:40 ratio with 1 mol % of NBD-PE and Rho-PE). The liposomes were mixed at a 9:1 molar ratio in an acidic (pH 5.0) or buffered neutral solution. Phosphatase (CIP, human alkaline phosphatase, or acidic phosphatase) was then added to the medium and the rate of lipid mixing was monitored by measuring the intensity change of NBD at 520 nm. Fluorescence intensity changes were normalized to the maximum fluorescence observed after surfactant lysis. B) Acid phosphatase induced the greatest lipid mixing effect relative to Calf Intestinal Phosphatase or Human Alkaline Phosphatase (from placenta). Data is plotted as the average of at least three runs.

4.3.5 Cytotoxicity of SCC in cultured cells

The unique biophysical properties of DOCP raised the prospect that this lipid might be useful for cytosolic delivery of SCC liposome contents. As a first toxicity screen, we examined the effects of DOCP SCC on the metabolic activity of B16F10 and HeLa cells using the MTT assay. No significant difference in cell toxicity, as compared to POPC, was observed at concentrations lower than 100 μM (Figure 4.9). Moreover, SCC showed no detectable cytotoxic effects at the highest concentration tested (200 μM) where the cell viability was 80±10%.

4.3.6 Cellular uptake of SCC in cultured cells

To quantify the extent of uptake between SCC and control liposomes, flow cytometry studies were performed on a FACSarray system (Becton Dickinson, CA). Fluorescently labeled DOCP SCC, cationic DOTAP, anionic POPG and zwitterionic POPC liposomes with 0.5 mol% Rho-PE were prepared by sonication and extrusion methods. B16F10 cells (0.5×10^5) were seeded in glass bottom dishes and grown to 70% confluency. Liposomes were then added to cells and incubated for 1, 2, 4, and 6 hours. After the incubation period, the unbound liposomes were removed from the cells by washing three times with HBSS media. After removal of unbound liposomes, the cells were detached from cell culture plates using calcium and magnesium free HBSS media and analyzed by FACS analysis. Cells were gated on FSC/SCC (forward scatter/ side scatter) to remove debris. The fluorescence from SCC containing Rho-PE was then measured using the mCherry emission channel. FACS analysis showed a time-dependent uptake for all formulations (Figure 4.10a). SCC had an accelerated rate of cellular association in the first 2 hours, followed by a slow increase over time. Interestingly, SCC showed greater accumulation than zwitterionic POPC at all time points, but reduced accumulation compared to anionic POPG liposomes and cationic DOTAP liposomes. The quantitative difference in uptake measured using FACS was confirmed by more qualitative measurements using fluorescence microscopy (Figure

4.10b-e). Fluorescence microscopy was performed using a Nikon Eclipse TS100 fluorescence microscope (Nikon, Tokyo, Japan), using the following filters: FITC (Excitation: 460 nm, Emission: 510 nm) and Texas Red (Excitation: 532 nm, Emission: 605 nm). Images were captured with a Spot RT MonoChrome digital camera using a 20X objective. DOTAP liposomes exhibited the highest level of cell associated liposome signal (Figure 4.10e).

4.3.7 Cytosolic delivery of FITC-Dextran by SCC

The ability of the SCC to charge convert, and fuse with adjacent anionic membranes in the presence of acidic phosphatases provides a valuable method for endosomal or lysosomal escape. In addition, the susceptibility towards acid phosphatase provides an enzyme trigger in diseases where phosphatases are upregulated such as prostate [138] and cervical cancer [139]. Hence, SCC could be useful carriers for siRNA or nucleic acid if they can effectively mediate cytosolic delivery. In order to do so, SCC need to be formulated with lipids that can promote lamellar to hexagonal phase transitions subsequent to the ion pairing of the newly generated cationic lipid and anionic lipids in the endosome or lysosome [171]. It was hypothesized that SCC formulated with DOCP, cholesterol, and phosphatidylethanolamine would be effective at mediating cytosolic delivery of macromolecules since acid phosphatases in the endosome would expose the cationic group needed for ion pairing with anionic phospholipids and the additional lipids, cholesterol and phosphatidylethanolamine, would promote a lamellar to hexagonal phase transition.

To test this hypothesis, FITC-Dextran was encapsulated in SCC. As a first screen, three SCC formulations were tested: DOCP:Chol (60:40 molar ratio), DOCP:DOPE (60:40 molar ratio) and DOCP:DOPE:Chol (40:30:30 molar ratio); all of which contained 0.5 mol% Rho-PE in the bilayer. FITC-Dextran was encapsulated by the reverse-phase evaporation method [172] for

achieving a high encapsulation efficiency and obtain a good payload for delivery. SCC containing FITC-Dextran were removed from FITC-Dextran by Sephadex G-75 gel filtration. FITC-Dextran SCC were then incubated with HeLa cells for various times and imaged for cytosolic delivery. Non-associated liposomes were removed from cells by washing three times with HBSS prior to imaging.

Cytosolic delivery of FITC-Dextran is assumed to have occurred if a diffuse and widespread fluorescent signal is observed throughout the cell. Cytosolic delivery of FITC-Dextran was observed in formulations containing phosphatidylethanolamine: DOCP:DOPE SCC and DOCP:DOPE:Chol SCC. DOCP:Chol SCC were unable to generate the diffuse cytoplasmic fluorescence. SCC formulations containing both DOPE and SCC showed the greatest cytoplasmic delivery (Figure 4.11). The delivery of FITC-Dextran was observed to be time-dependent. A minimum of 4 hours was required for a cytoplasmic delivery event to be observed. Earlier time points were characterized by a punctate green fluorescence which was co-localized with the Rho-PE probe of the SCC. This was evidence that the liposome and contents resided in intracellular compartments. After 4 hours, the extent of cytosolic delivery increased and achieved a maximum for overnight incubations (Figure 4.12).

At later time points, the fluorescently-labeled SCC preferentially accumulated in the perinuclear space of cells (Figure 4.12). This suggests that the SCC were sorted to lysosomal compartments. Moreover, the time lag prior to observing a strong diffuse FITC-Dextran signal in the cell suggests that acid phosphatases in the lysosome might be responsible for the triggering event that leads to cytoplasmic delivery. In addition, the extensive time delay between uptake and cytosolic delivery suggests that the local concentration of phosphatases is lower than needed for SCC to effectively charge convert. This is further supported by reports describing changes in the expression level of acid phosphatases as a result of cell cycle. The expression of acid phosphatases in HeLa cells appears to be greater during nuclear division than during interphase

[173]. Also, the lysosomal membrane becomes more permeable during cell division. Both of these factors could be responsible for the enhanced cytosolic delivery of FITC-Dextran observed at later time points. Further experiments are necessary to validate this hypothesis.

It is also a possibility that SCC might charge convert but the intracellular membrane may not have the appropriate anionic membrane composition that is fusion competent until the liposomes traffic to the perinuclear and presumably lysosomal location. Additional studies are needed to more precisely identify the compartments in which delivery occurs. Nevertheless, the potential of SCC as mediators of cytosolic delivery has been validated.

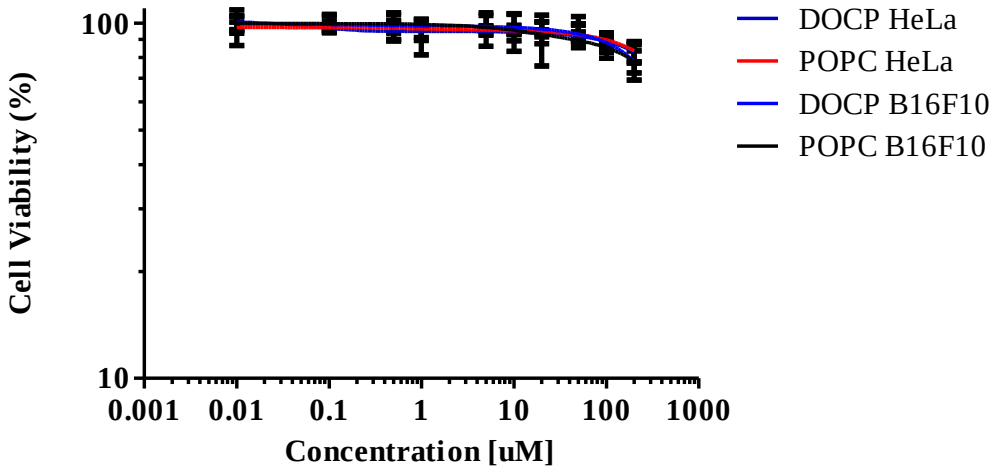

Figure 4.9 Cytotoxicity of DOCP SCC in Cultured Cells. DOCP SCC liposomes showed low levels of cytotoxicity as reveled by the MTT assay. B16F10 and HeLa cells were seeded into 96-well plates at a density of 9,000 cells per well and cultured for 24 hours. After 24 hours, the cell culture medium was replaced and the cells were incubated with increasing liposome concentration. Following a 24 hour incubation, the cells were analyzed for cytotoxicity using the MTT assay. Relative viability was calculated using 0% (wells without cells) and 100% (wells with untreated cells) controls. Data is presented as an average of four measurements.

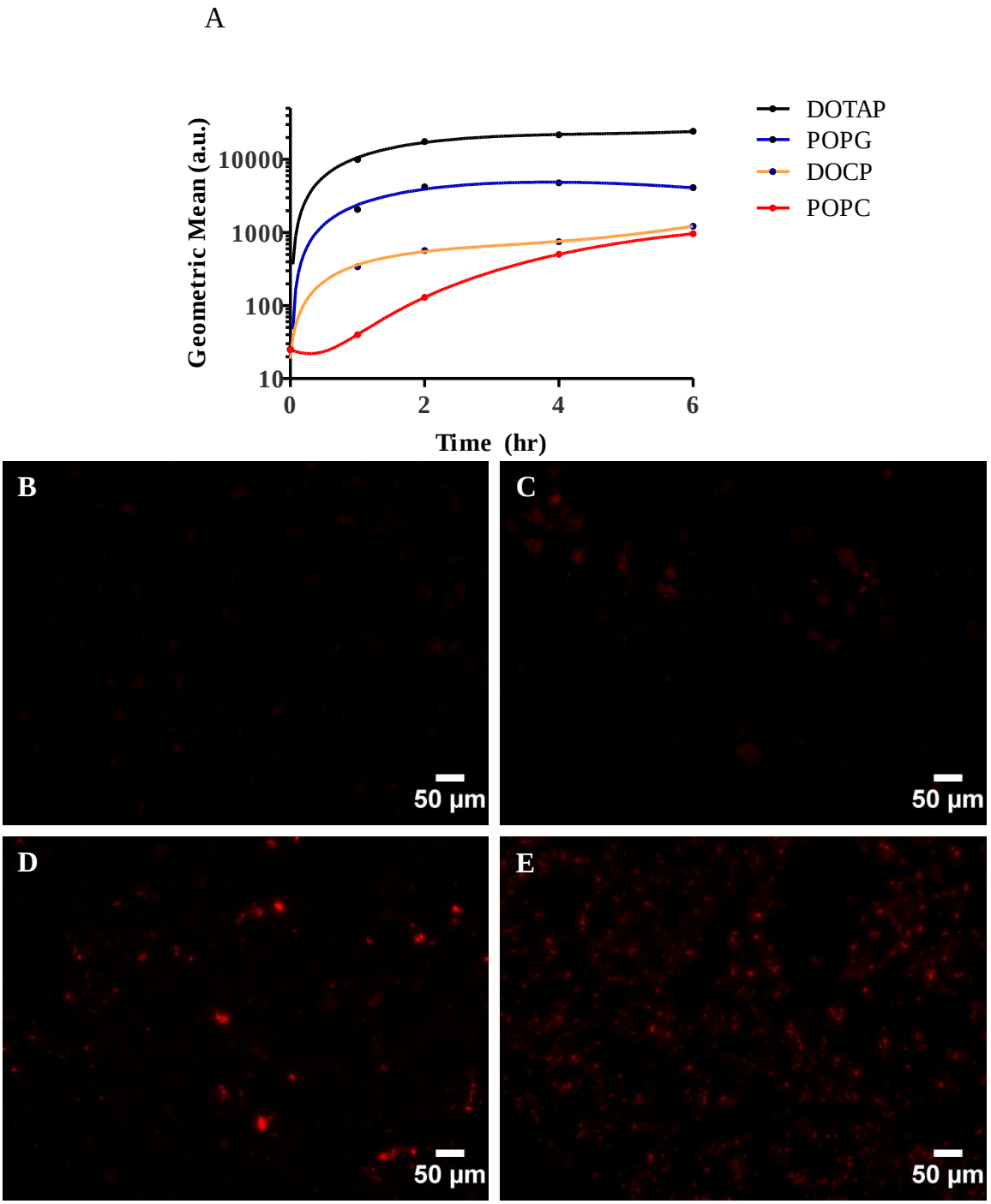

Figure 4.10: Cellular Association of DOCP SSC. A) B16F10 cells were incubated with 50 nanomoles of liposomes for 1, 2, 4, and 6 hours at 37°C and 5% CO_2. Cell association was then measured by FACS. A minimum of 10,000 events were collected by list-mode that consisted of side scatter, forward scatter, and fluorescence (mCherry) emission. The time-dependent uptake of fluorescently-labeled liposomes in B16F10 as measured by FACS is plotted. B-E) Fluorescence images of uptake in B16F10 cells are shown. A qualitative difference in uptake was apparent by fluorescence microscopy. Images of POPC (B), DOCP (C), POPG (D), and DOTAP (E) labeled with 0.5 mol% of Rho-PE are shown after a 2 hour incubation.

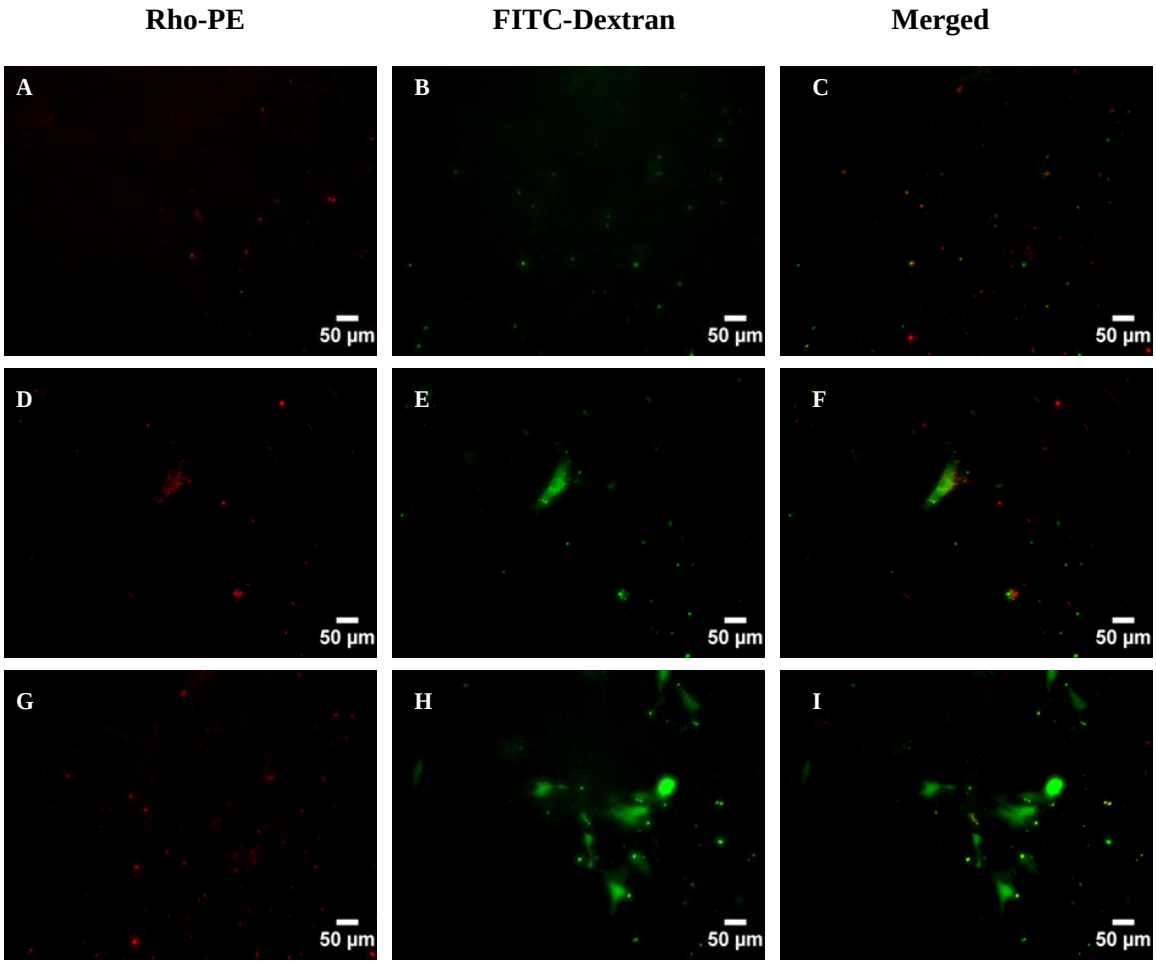

Figure 4.11 Efficiency of Cytosolic Delivery of FITC-Dextran by SCC Formulations. HeLa cells were incubated with 50 nanomoles of SCC for 4 hours at 37°C and 5% CO_2. SCC encapsulating 1 mM FITC-Dextran were formulated with DOCP:Chol (60:40 molar ratio) (A-C), DOCP:DOPE (60:40 molar ratio) (D-F), and DOCP:DOPE:Chol (40:30:30 molar ratio) (G-I). The fluorescent lipid Rho-PE (0.5 mol%) was used as liposomal marker (A, D, G).

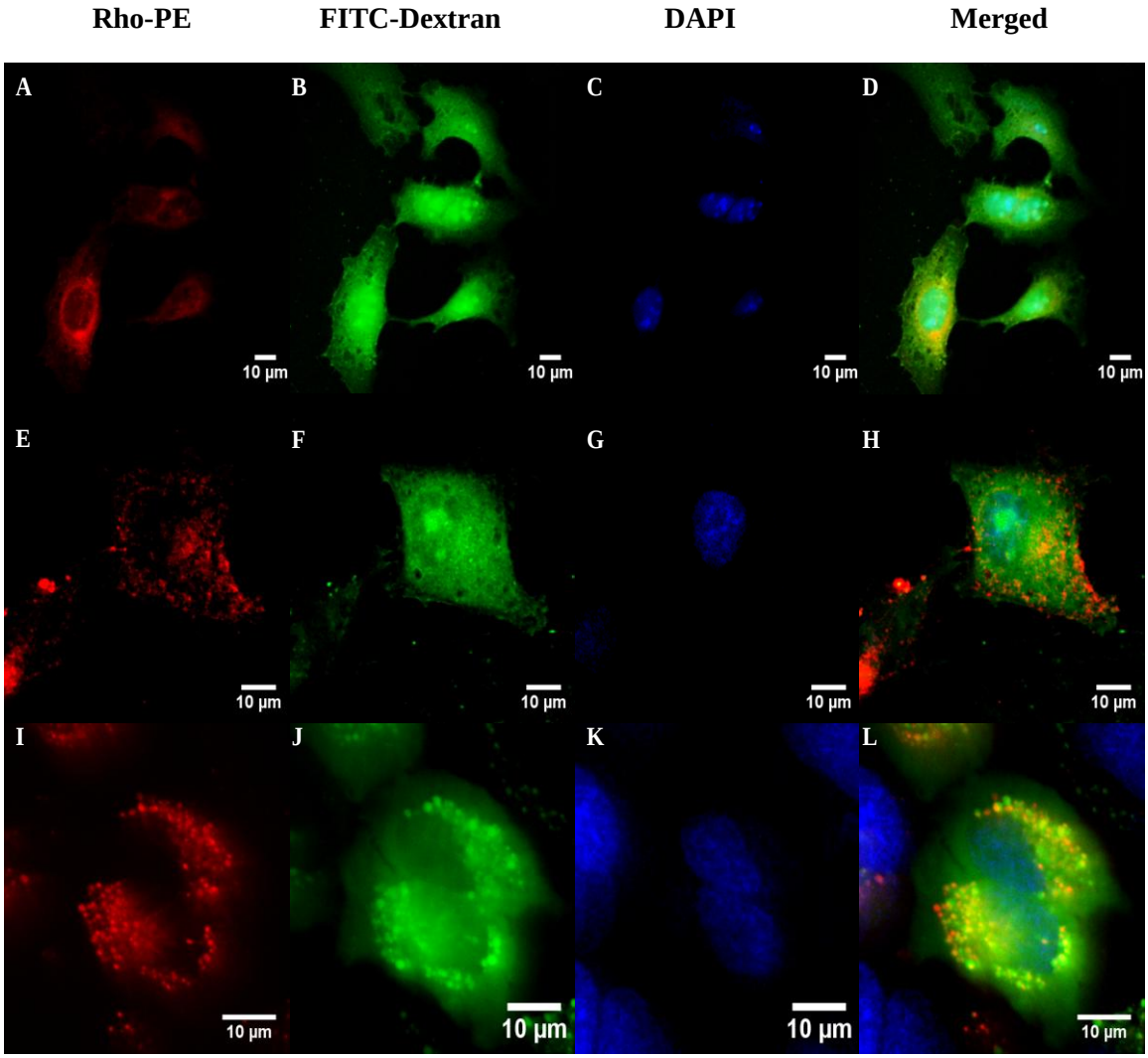

Figure 4.12: Cytosolic Delivery of FITC-Dextran after 24 Hours. Confocal images show uptake of SCC and cytoplasmic delivery of the macromolecule FITC-Dextran at 40x (A-D), 63x (E-H), and 100x (I-L) magnification. HeLa cells were incubated with 50 nanomoles of DOCP:DOPE:Chol (40:30:30 molar ratio) SCC encapsulating 1 mM FITC-Dextran (10kd) for 24 hours at 37°C and 5% CO_2. SCC were labeled with fluorescent lipids Rho-PE (0.5 mol%). A perinuclear localization is observed for SCC (A, E, I). Cytoplasmic delivery of FITC-Dextran is observed in most imaged cells (B, F, J). Dapi was used to stain the nuclei of the cells (C, G, K).

4.3.8 Towards the Design of Lipid-based Logic Gates

The molecular switch behavior of DOCP and the extended position of its phosphate provide a template for rationale trigger design. Subsequent modifications to the phosphate group, such as esterification, could provide greater trigger control of drug release, in addition to a second "logic" component. This is illustrated for instance in DOCPe, which is structurally analogous to DOCP but contains a phosphoester in place of the phosphate. DOCPe is a substrate for esterases but not a good substrate for phosphatases. However, when the ethyl group is removed by an esterase, the resulting DOCP becomes a substrate for a phosphatase. As a result, the system's dynamics of DOCPe mimics those of an "AND" gate, which is a logical conjunction that results in a "true" or a "1" if both of its inputs are "true", otherwise it results in a "false" or "0".

Charge conversion experiments with DOCPe were performed to confirm this "AND" gate behavior. At physiological pH and in a buffered solution of 25 mM NaCl and 5 mM Tris (pH 7.4), the lipid has a zeta potential of -25±7 mV [63]. Addition of esterase (Porcine Liver Esterase, Sigma Aldrich, St. Louis, MO) hydrolyses the ester in the phosphate group, lowering the surface charge to -60 mV, which is in accordance with the zeta potential of DOCP. Addition of phosphatase hydrolyses the head group phosphate and results in a similar charge conversion effect to DOCP as was illustrated in Figure 4.4. Thus, DOCPe SCC exhibit AND logic. If neither or only one of its inputs, phosphatase or esterase, is present in the reaction no charge conversion occurs and the system has an output of 0. However, if both of its inputs are present, then charge conversion proceeds and a cationic head group is generated. Hence the system has an output of 1. The potential for a double trigger is attractive since it could help overcome some of the limitations that DOCP SCC liposomes would have upon systemic administration. For instance, in prostate cancer, the high levels of prostatic acid phosphatase in circulation would induce premature drug release from DOCP SCC. However, premature drug release could be overcome with a system like DOCPe SCC which requires two inputs for triggering. This provides increased

trigger control, as well as a greater opportunity for DOCPe SCC liposomes to extravasate from circulation and accumulate in the tumor site. Thus, DOCPe SCC could be advantageous for minimizing off target effects in brain drug delivery since both esterases and alkaline phosphatases are over expressed in malignant brain tumors [174, 175]. Nevertheless, SCC are inherently limited for applications in which both levels of enzymes are over expressed in circulation.

4.4 Conclusion

SCC liposomes can be engineered with inverse-phosphocholine lipids for triggered charge conversion by phosphatases. The charge conversion properties of the system are analogous to the behavior of a logic switch, and are thus suitable for switching bilayers from lamellar to hexagonal phase when phosphatidylethanolamine lipids are present in the bilayer. Furthermore, this switch-like behavior facilitates triggered release and membrane mixing from SCC liposomes containing hexagonal phase competent lipids such as DOPE, POPE and Chol. SCC liposomes were effective at mediating cytosolic delivery of FITC-Dextran. Their low cytotoxicity and enhanced delivery properties make SCC liposomes a candidate for further *in vivo* delivery of genes, proteins, and siRNA.

SCC liposomes can also exhibit "AND" logic. This was demonstrated by formulating SCC with DOCPe, which requires the presence of both esterases and phosphatases for mediating an anionic to cationic conversion. Surface charge converters capable of "AND" logic are an attractive platform for designing carriers capable of sensing and distinguishing between different cellular zip codes. Efforts to improve SCC should be focused on optimizing the carrier composition and potentially incorporating additional stimulus responsive triggers into the bilayer.

4.5 Materials and Methods

4.5.1 Reagents

1-palmitoyl-2-oleyl-sn-glycero-3-phosphocholine (POPC), 1,2-dioleoyl-sn-glycero-3-phosphoethanolamine (DOPE), 1-palmitoyl-2-oleoyl-sn-glycero-3-phosphoethanolamine (POPE), 1-palmitoyl-2-oleyl-sn-glycero-3-phosphoglycerols (POPG), 1,2-dioleoyl-3-trimethylammonium-propane (chloride salt) (DOTAP), and 1,2-dipalmitoyl-*sn*-glycero-3-phosphoethanolamine-N-(lissamine rhodamine B sulfonyl) (ammonium salt) (Rho-PE) were obtained from Avanti Polar Lipids Inc. (Alabaster, Alabama). 5-FAM (carboxyfluorescein) was obtained from Anaspec (San Jose, CA). 3β-Hydroxy-5-cholestene (CHOL), and fluorescein isothiocyanate-dextran (FITC-Dextran, MW 10,000) were obtained from Sigma-Aldrich (St. Louis, MO). Solvents were purchased from VWR Scientific. All other chemicals were purchased from Sigma Aldrich. All reagents and solvents used were of analytical or HPLC grade. HPFC column purifications were performed on a Reveleris Flash System (Grace Division Biosciences) with pre-packed GraceResolv silica cartridges (67 Å, 40.5 μm). All buffers were made with MilliQ water and subsequently filtered through 0.1 μM filters.

4.5.2 Synthesis and Purification of DOCP

DOCP was synthesized by E. Perttu as previously described [63]. A 20 mM stock solution was then prepared in chloroform from stock material. A yellow color was visible in the solution suggesting trace amounts of iodine. As a result, the solution was extracted into chloroform in the presence of 20 mM sodium bisulfate. Briefly, 1 mL of 20 mM stock solution in chloroform was mixed with 1 mL of MeOH and 0.9 mL of 10 mM sodium bisulfate solution (pH 7.4). The solution was shaken and vortexed, and allowed to phase separate at -20 ^{o}C for 24 hours. The aqueous phase was removed and the organic phase was collected and dried by rotary evaporation and placed under high vacuum. Finally, the lipid film was re-suspended in water and

lyophilized. After lyophilization, a 20 mM stock solution was prepared and kept under argon at -20 ^{o}C.

4.5.3 Vesicle Preparation for Charge Conversion, Leakage and Lipid Mixing

Lipid stock solutions were prepared in chloroform ($CHCl_3$). Prior to use, glassware was rinsed in methanol (MeOH) and $CHCl_3$ and then dried. Liposomes were prepared by combining chloroform solutions of POPC in borosilicate glass tubes and drying them under reduced pressure using rotary evaporation. Residual solvent was removed overnight under high vacuum. For charge conversion assay, lipid films were rehydrated in buffer containing 25 mM NaCl and 5 mM Tris (pH 7.4). For leakage and lipid mixing assays, lipid films were hydrated in buffer, containing 145 mM NaCl and 5 mM Tris (pH 7.4), by intermittent vortexing and sonicated for 10 minutes under argon. Defined diameter liposomes were then formed by extruding 10 times through 100 nm polycarbonate membranes using a hand-held extruder (Avestin, Ottawa, Canada). Labeled liposomes for lipid mixing contained 1 mol % of NBD-PE and Rho-PE and were also prepared in buffer 145 mM NaCl and 5 mM Tris (pH 7.4). Liposomes containing CF were prepared as previously described [135]. Lipid formulations of POPC were dried down from chloroform stock solutions in a test tube to form a thin film. The thin film was rehydrated in a 100 mM CF solution containing 5 mM Tris buffer (pH 7.4). The solution was then sonicated for 10 minutes under argon, and the liposomes were extruded through 100 nm polycarbonate membranes. Free CF was removed by size exclusion chromatography (PD-10 sephadex column; GE Healthcare, Piscataway, New Jersey). The mobile phase for separation consisted of a 5 mM Tris buffer with 145 mM NaCl, pH 7.4. The encapsulated CF liposomes were capped with argon. All liposome preparations were sized using dynamic light scattering.

4.5.4 Triggered Charge Conversion Assay

Charge conversion was measured by two methods: (a) the time-dependent change in zeta potential of DOCP liposomes in the absence and presence of phosphatase, and (b) the time-dependent change in zeta potential of DOCP lipids treated with phosphatase as measured after lipid extraction and liposomal reconstitution. The method for **(a)** is as follows: 1 mL 100 µM DOCP liposome solutions were prepared in a 25 mM NaCl, 5 mM Tris buffer (pH 7.4) and placed in a glass cuvette. The solution was then warmed to 37 ^{o}C and 5 µL of Antartic Phosphatase (New England Biolabs, Ipswich, MA) was added to the solution. The reaction was allowed to proceed for set periods of time. Zeta potential measurements were collected at 0, 1, 2, 5, 10, 15, 20, 30, 45, and 60 minutes. To control for enzyme effects on zeta potential, charge conversion assays were run in the presence of denatured phosphatase. To do so, 5 µL of Antartic Phosphatase was added to 1 mL of 25 mM NaCl, 5 mM Tris buffer (pH 7.4) and the solution was heated in a glass vial for 20 minutes at 100 ^{o}C. The solution was then placed in a temperature controlled incubator and allowed to cool over 10 minutes to 37 ^{o}C. DOCP liposomes were then added to a final concentration of 100 µM and zeta potential was measured for each time point.

The method for **(b)** is as follows, 5 µL of Antartic Phosphatase was added to a 1 mL solution of 100 µM DOCP SCC solution that was prewarmed to 37 ^{o}C. The reaction was allowed to proceed for the given time intervals : 0, 1, 2, 5, 10, 15, 20, 30, 45, and 60 minutes. The reaction was stopped by extracting the liposomes in an organic:aqueous solution consisting of 1.1 mL chloroform, 1.1 mL methanol, and 1 mL liposome solution. The extracted solution was vortexed for 90 seconds and placed at -20 ^{o}C. The solution was allowed to phase separate, with the lipids partitioning into chloroform. The aqueous phase was removed by pipetting and transferred into a new vial. The solvent was then removed by rotary evaporation. The resulting thin lipid film was rehydrated in 1 mL of 25 mM NaCl, 5 mM Tris buffer (pH 7.4). The lipid

mixture was then sonicated for 10 minutes and the zeta potential for each time point was measured.

Charge conversion was calculated as the change in zeta potential relative to the initial zeta potential at the start of the incubation. Reported are the mean results of three separate lipid extractions, with 10 zeta reads as minimum. All zeta potential measurements were done with a zeta dip cell using a Zetasizer Nano-ZS (Malvern, Worcestershire, UK).

4.5.5 Phosphatase Triggered Content Release

100 nanomoles of SCC were re-suspended in 2 mL buffer containing 145 mM NaCl, 5 mM Tris and 0.1 mM MgCl2 (pH 7.4), and stirred at 37 ^{o}C in the presence or absence of phosphatase. The assays were done in either a FluoroLog-3 spectrofluorometer (Horiba Jobin Yvon, Edison, NJ) equipped with a temperature controlled stage (LFI-3751) and a 450-W xenon light source and a magnetic stirrer or in a TECAN multi-plate reader with built-in shaker. For all experiments, the temperature stage and buffers were warmed to 37 ^{o}C 10 minutes prior to the start of the run. A baseline reading was first done to determine the emission minimum of the solution. Then, alkaline phosphatase (Calf Intestine Phosphatase (CIP) or Antarctic Phosphatase (AP)) was added in different amounts to the solution and the intensity change was recorded over time. The release of CF from the liposomes was monitored, with the excitation and emission wavelengths set to 485 nm and 520 nm, respectively. Runs were done in triplicate and data was analyzed in Matlab. For all experiments, percent CF leakage values were calculated by measuring the total CF released, and normalized to the maximum intensity after the liposomes were lysed with C12E10 surfactant and adjusted for background fluorescence as follows:

$$CF(\nabla) = \frac{CFintensity(\nabla) - background(\nabla)}{detergent(\nabla) - background(\nabla)}$$ *where ∇ represents emission wavelength.*

4.5.6 Phosphatase Triggered FRET Lipid Mixing

Membrane fusion was measured by changes in fluorescence intensity resulting from fluorescence resonance energy transfer between the head group labeled probes NBD-PE and Rho-PE as previously described [136] using a Fluorolog-3 spectrofluorometer (Horiba Jobin Yvon, Edison, NJ). Two sets of liposomes set were prepared: unlabelled DOCP:DOPE (60:40 ratio) liposomes, and labeled POPG:DOPE (60:40) liposomes with 1% mol NBD-PE and Rho-PE. Two buffers were primarily used during the assay and adjusted for the different pH: a Tris-buffered solution containing 145 mM NaCl, 5 mM Tris (pH 7.4) and a Citrate-buffered solution containing 145 mM NaCl, 5 mM citrate (pH 5.5). A mixture of unlabeled and labeled liposomes at a 9:1 molar ratio of 100 μM total lipid concentration were re-suspended in 2 mL of buffer. The samples were placed incubated at 37 ^{o}C for 10 minutes before the start of the run while stirring. The baseline NBD emission was first recorded, and then alkaline (Calf Intestine Phosphatase (CIP), New England Biolabs, Ipswich, MA and Human Alkaline Phosphatase Type XXIV, Sigma Aldrich, St. Louis, MO) or acidic phosphatase (Acid Phosphatase from Sweet Potato, Sigma Aldrich, St. Louis, MO) at a concentration of 2 units per nanomole of lipid was added to the solution. The change in NBD emission intensity was then monitored with excitation wavelength set to 467 nm and emission at 520 nm, with slits at 3 nm. Lipid mixing was then calculated by measuring the change in NBD fluorescence intensity, and normalized to the maximum intensity after the liposomes were lysed with $C_{12}E_{10}$ surfactant, and adjusted for background fluorescence as follows:

$$Lipid\ Mixing(\nabla) = \frac{NBDintensity(\nabla) - background(\nabla)}{detergent(\nabla) - background(\nabla)}\ where\ \nabla \text{ represents } emission\ wavelength$$

Background fluorescence from vesicles containing 1 mol % of NBD-PE and Rho-PE in a 1:9 mixture with non-probe-containing vesicles was set to 0% lipid mixing and 100% lipid

mixing was set to 100% lipid mixing. The addition of phosphatase did not alter the fluorescence of the probes.

4.5.7 Cell Culture

B16F10 murine melanoma cell and HeLa cell line were obtained from the UCSF Cell Culture Facility. B16F10 cells were maintained in RPMI 1640 medium containing 10% (v/v) CultraPure fetal bovine serum (Axenia Biologix, Dixon, CA), 25 mM hepes and 1% penicillin-streptomycin. HeLa cells were maintained in Eagle Modified media containing at least 10% (v/v) CultraPure fetal bovine serum, 5 mM Hepes, and 1% penicillin-streptomycin. Cells were cultured with complete medium at 37 ^{o}C in a humidified atmosphere of 5% CO_2 in air. Media was filtered through a 0.1 μM filter prior to use. Experiments were performed with cells harvested from subconfluent cultures using 0.05% trypsin and re-suspended in complete medium prior to plating.

4.5.8 Microscopy

Fluorescence microscopy was performed using a Nikon Eclipse TS100 fluorescence microscope (Nikon, Tokyo, Japan), using the following filters: FITC (Excitation: 460 nm, Emission: 510 nm) and Texas Red (Excitation: 532 nm, Emission: 605 nm). Images were captured with a Spot RT MonoChrome digital camera using a 20X objective. Spot software (Diagnostic Instruments, Sterling Heights, MI) was used for data capture and Image J was used for post processing overlays and pseudocoloring.

Spinning disk confocal images were acquired using a Zeiss Axiovert 200 M microscope with a 40x/1.3 NA oil objective, a 63x/1.4 NA oil objective, or a 100x/1.4 NA oil objective, Andor iXon 887 EMCCD Camera, Prior Proscan III stage, Yokogawa CSU-10 spinning disk with 488 nm and 561 nm laser lines modulated by a Neos AOTF (Solamere Technology Group, Salt

Lake City, Utah). Cells were kept at 37 ^{o}C using a Zeiss objective and sample heater. Metamorph (Molecular Devices, Sunnyvale, CA) was used to control the microscope, as well as for image acquisition and processing.

4.5.9 Cytotoxicity Assay

Cytotoxicity of liposomes was determined by the MTT assay (Sigma, St. Louis, USA). B16F10 and HeLa cells were seeded into 96-well plates at a density of 9,000 cells per well and cultured for 24 hours. After 24 hours the cell culture medium was replaced and the cells were incubated with increasing liposome concentration in 100 μL cell culture medium. After a 24 hour incubation, the medium was replaced by RPMI 1640 containing 0.5 mg/mL MTT (3-(4,5-dimethylthiazol-2-yl)-2,5-diphenyl tetrazolium bromide) (Sigma, St. Louis, USA). After 4 hours incubation at 37 °C, the medium was aspirated and formazane crystals were dissolved in 200 μL DMSO per well. Measurements were taken using a micro plate reader at a wavelength of 570 nm, with a background correction at 690 nm. Relative viability was calculated using 0% (wells without cells) and 100% (wells with untreated cells) controls, and data is presented as an average of four measurements.

4.5.10 Liposome Uptake Assay

B16F10 cells (0.5 x 10^5) were plated separately in Fluorodish glass bottom dishes (World Precision Instruments, Sarasota, FL) and grown to 70% confluency at 37 ^{o}C and 5% CO_2 in medium (RPMI 1640 with 10% (v/v) FBS). The cell monolayer was rinsed with FBS-free medium and then medium containing 50 nanomoles of fluorescently-labeled liposomes with 0.5 mol% Rho-PE was added. Cells were incubated for 1, 2, 4, and 6 hours at 37 ^{o}C and 5% CO_2. Fluorescence microscopy was then used to image the wells. Flow cytometric analysis (FACS

analysis) for liposomes fluorescence was also performed using a FACSArray BioAnalyzer system (Becton Dickinson, CA). A minimum of 10,000 events were collected by list-mode data that consisted of side scatter, forward scatter and fluorescence (green, yellow, mCherry, DsRed) emission. Data was analyzed using FlowJo software (Ashland, OR). The geometric mean of mCherry emission was used to quantify the amount of liposomal uptake at different time points and for the different lipopeptide surface densities.

4.5.11 FITC-Dextran Cytosolic Delivery Assay

DOCP, DOPE, POPE, and Chol stock solutions were prepared in chloroform and used for liposome formulations. 0.5 mol% Rho-PE was added to all solutions. Lipids were dried by a combination of rotary evaporation and high vacuum, and hydrated in buffer containing FITC-Dextran by reverse phase evaporation method (REV) as previously described [67, 172]. Briefly, lipid films were prepared from lipid stock solutions and dried down by rotary evaporation and overnight vacuum treatment. The films were rehydrated in 1 mL of diethyl ether (distilled over sodium bisulfate). The solution was sonicated for 60 seconds under argon, and vortexed. Then, 0.5 mL of a 50 mM solution of FITC-Dextran (10kd MW) containing 145mM NaCl, 5mM Tris (pH 7.4) was added. The resulting emulsion was sonicated for 2 minutes, and vortexed. Then, the emulsion was evaporated in a rotary evaporator at 37 ^{o}C under reduced pressure until a stable gel formed. Upon gel formation, the solution was briefly vortexed and treated again by rotary evaporation until a gel to liquid transition occurred. All liposomal formulations were extruded through 200 nm pores. Free FITC-Dextran was then removed by Sephadex G-75 (1 x 20 cm) gel filtration. The mobile phase for separation consisted of a 5 mM Tris buffer with 145 mM NaCl (pH 7.4).

For delivery assays, B16F10 cells (0.5×10^5) or HeLa cells were plated in Fluorodish glass bottom dishes (World Precision Instruments, Sarasota, FL) and grown to 70% confluency at 37 ^oC and 5% CO_2 in medium (RPMI 1640 with 10% (v/v) FBS). The cell monolayer was rinsed with FBS-free medium and medium containing 50 nanomoles of liposomes was added. Cells treated with liposomes encapsulating FITC-Dextran were incubated at 37 ^oC and 5% CO_2 up to 24 hours. At the end of the incubation, the medium was removed and the cells were washed three times with 1mL HBSS. The cells were then counterstained with DAPI. Confocal and fluorescence microscopy was then used to image the wells.

Chapter 5: Mathematical Insights for Brain Drug Delivery by Local Convection and Retro-Convection

5.1 Abstract

Delivery of drugs and macromolecules into the brain is a challenging problem, due in part to the blood-brain barrier. In this chapter, we focus on the possibilities and limitations of two infusion techniques devised to bypass the blood-brain barrier: convection enhanced delivery (CED) and retro-convection enhanced delivery (R-CED). CED infuses fluid directly into the interstitial space of brain or brain tumor; whereas R-CED removes fluid from the interstitial space which results in the transfer of drugs from the vascular compartment into the brain or brain tumor. Both techniques have shown promising results for the delivery of small and macromolecules into large volumes of tissue. Theoretical approaches of varying complexity have been developed to better understand and predict brain interstitial pressures and drug distribution for these techniques. These theoretical models of flow and diffusion can only be solved explicitly in simple geometries, and spherical symmetry is usually assumed for CED, while axial symmetry has been assumed for R-CED. This chapter summarizes features of these models and provides physical arguments and numerical simulations to support the notion that spherical symmetry is a reasonable approximation for modeling CED and R-CED. We also explored the potential of multi-catheter arrays for delivering and compartmentalizing drugs in the brain interstitial area using CED and R-CED.

5.2 Introduction

Primary malignant brain tumors are a significant therapeutic challenge in spite of substantial advances in tumor imaging, neurosurgery, and radiation therapy. The efficacy of potent chemotherapy drugs is limited by biochemical and physiological barriers, including: poor drug delivery to the brain tumor mass and its peripheral regions [176-178], rapid clearance from the brain extracellular space [179], high intratumor pressure [180], and toxicity to normal brain tissue. More effective patterning of fluid movement through the tumor or diversion of fluid from entering normal brain parenchyma could improve brain tumor therapy.

Over the past decade, convection enhanced delivery (CED), employing a positive pressure infusion directly into the brain, has shown promising results in both animal models and clinical trials [181-184]. CED distributes macromolecules, proteins, and particulate therapies into large volumes of tissue [185-187]. Retro-convection enhanced delivery (R-CED), which removes interstitial fluid through a microdialysis catheter [188], has been introduced to deliver drugs into brain tumors [189]. Continuous flow of a high molecular weight hyperosmotic polymer solution drives fluid flow from the interstitial space and out of the brain. This removal of interstitial fluid induces a retro movement of fluid from the capillaries into the tissue enabling the extravasation of drugs and nanoparticles into the brain, as illustrated in Figure 5.1. The availability of CED and R-CED provides tools to pattern interstitial flow through the brain if these techniques are simultaneously applied from different catheters.

Computational and mathematical modeling can be used to gain further insights into the physiological complexities that these techniques face. Theoretical approaches of varying complexity, ranging from analytical to finite element models, have been developed to better understand and predict the interstitial distribution of material infused by CED [190-195]. These models have also been used to predict features such as the interstitial fluid pressure, interstitial fluid velocity, tissue swelling, and the transvascular fluid exchange rate during CED. Although

these models do not recapitulate all aspects of fluid distribution in the brain following CED, they are instructive regarding what might be achieved in fluid patterning by a multi-catheter infusion protocol.

Recently, mathematical models of R-CED were developed to analyze the driving forces behind R-CED [196]. The study showed that drug concentration near the catheter is enhanced when drug cannot permeate through the catheter membrane, but such enhancement is marginal when drug is permeable or semi permeable to the membrane. Removal of drug into the catheter largely defeats the purpose of R-CED, which is to draw drug into brain or tumor tissue from the capillaries.

Analytical models of flow and diffusion for both CED and R-CED can only be solved explicitly in simple geometries, and spherical symmetry is usually assumed for CED, while axial symmetry was assumed by Wang and Olbricht for R-CED [196]. Real systems are more complicated. CED catheters typically deliver drug through the open end of a shaft, while R-CED microdialysis membranes are tubes of finite extent.

In this chapter, we provide physical arguments and supporting numerical studies indicating that spherical symmetry is a reasonable approximation in many cases. We also explore the potential benefits of fluid delivery through multiple catheters. For example, drug-free fluid flow out of one catheter can be used to divert drug-containing fluid delivered from another catheter, offering protection to tissue surrounding the first catheter. Thus, drug delivered near tumor/tissue interface might, in principle, be localized on the tumor side.

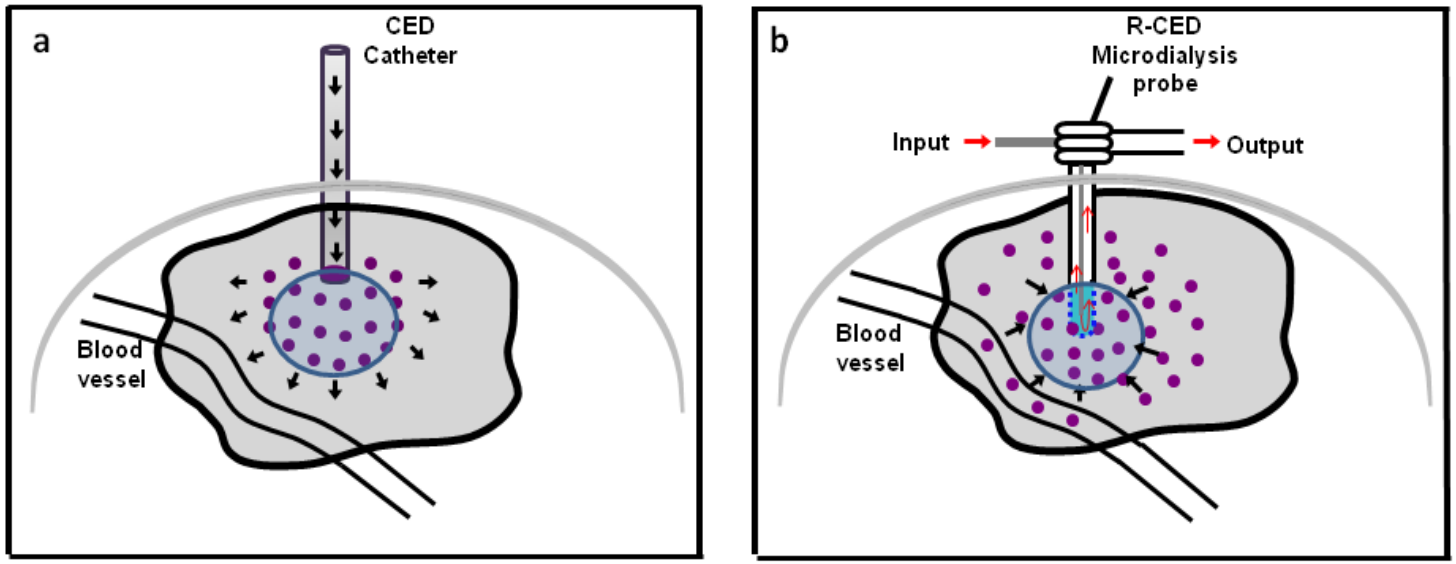

Figure 5.1 Illustration of Fluid Movement in the Brain under the Influence of CED or R-CED. A) A CED catheter is implanted into the brain and a solution is perfused under a positive pressure (black arrows). The therapeutic solution convects in response to the pressure field. This allows permeation and distribution of the therapeutic agent contained in the solution into the region of interest. **B)** To remove fluid from the brain, a hyperosmotic solution is perfused into the brain using a microdialysis probe. The microdialysis membrane separates the hyperosmotic perfusate from the brain interstitial. Fluid then flows from the blood into the ISF and towards the microdialysis probe as diagrammed with the black arrows. The fluid then exits through the output tube of the probe [197].

5.3 Mathematical Modeling of CED and R-CED

This section describes the mathematical models and numerical simulation techniques used to gain additional insight into the physiological complexities that CED and R-CED system face in the brain. Fluid balance equations at the catheter tip interface, as well as mathematical models for spherical symmetry approximations and non-spherical geometries are detailed.

5.3.1 Fluid Balanced Equations

The simplified mathematical model for extravascular flow assumes the tissue to be a rigid homogenous porous medium that is uniformly perfused by capillaries [194]. Pores contain interstitial fluid (ISF) and extracellular matrix (ECM). In the present section we consider flow from or into catheter tips of defined geometries under CED or R-CED conditions, for catheters embedded in a homogeneous tissue such as brain parenchyma or tumor. We consider relatively short infusion times, during which infusion or removal of fluid dominates interstitial fluid flow turnover processes. We also disregard tissue stress and strain fields developed near the CED and R-CED catheters [192], and capillary compressibility.

Due to the strong suppression of fluid inertia by the highly reticulated tissue, with fluid flowing through ECM, we utilize a simplified modeling approach in which fluid flow through tissue is described by Darcy's law,

$$\bar{u} = -K\nabla p \tag{1}$$

and the continuity equation for fluid flow,

$$-\varphi\nabla \bullet \bar{u} - \varphi L_{pc} s(p - p_e) = 0 \tag{2}$$

where p is the interstitial hydraulic pressure at a given location, $\bar{u}$ is the local (vector) fluid velocity, p_e is the Starling pressure of the capillary bed calculated according to Starling's law:

$p_e = p_c + \sigma(\pi - \pi_c)$, where p_c and π_c are the intercapillary hydraulic and osmotic pressures, π is the interstitial osmotic pressure, and σ is the reflection coefficient of the capillary wall, φ is the volume fraction of tissue available for interstitial flow, *s* is capillary surface are per unit volume of tissue, *K* is the hydraulic conductivity of interstitial space, and L_{pc} is the hydraulic permeability coefficient of the capillary walls.

The parameters p_e, φ, *s*, *k*, and L_{pc} are all assumed to be constant for a given tissue (e.g. brain parenchyma, tumor). The velocity vector $\overline{u}$ is taken as a volume averaged field variable, and volume averaging effects are introduced at the level of the Darcy coefficient, *K*. Combining equations (1) and (2) yields the equation for the difference between interstitial and effective Starling capillary pressure, $\tilde{p} = p - p_e$,

$$\nabla^2 \tilde{p} = \kappa^2 \tilde{p} \qquad (3)$$

where $\kappa = \sqrt{L_{pc} s / K}$ has units of inverse distance.

Equation (3) is of the Helmholtz type. In the absence of fluid exchange between tissue and capillaries ($L_{pc} = 0$), it reduces to Laplace's equation: $\nabla^2 \tilde{p} = 0$. More detailed treatments also consider drug transport by diffusion and exchange across capillary walls. Since the focus is fluid flow, these contributions to drug transport will not be considered.

5.3.2 CED and R-CED from a spherically symmetric catheter tip

We first assume that the flow of a drug solution through an ideal catheter with tip radius R_m and center at the origin *Q* is spherically symmetric. Using spherical coordinates, its position can be represented by:

$$r = (x, y, z), |r| = \sqrt{x^2 + y^2 + z^2}, \bar{i}_r = r/|r|$$

and its velocity field around the source by:

$$\bar{u} = u_r \bar{i}_r, \quad r > R_m.$$

By rearranging equations (3) and (1), the following differential equations are obtained:

$$\frac{\partial^2 \tilde{p}}{\partial r^2} + \frac{2}{r}\frac{\partial \tilde{p}}{\partial r} = \kappa^2 \tilde{p} \qquad r > R_m \tag{4}$$

$$u_r = -K\frac{\partial \tilde{p}}{\partial r} \qquad r > R_m \tag{5}$$

Fluid flow continuity at the tip/tissue interface prescribes the boundary condition:

$$Q = 4\pi R_m^2 \varphi u_r(R_m) = -4\pi R_m^2 \phi K \left.\frac{\partial \tilde{p}}{\partial r}\right|_{r=R_m} \tag{6}$$

Far from the tip, the interstitial and capillary fluids are in Starling equilibrium, i.e.

$$\tilde{p}(r) \to 0, \quad r \to \infty \tag{7}$$

The solution to Eqs. (4)-(7) is

$$\tilde{p} = \left[\frac{Q}{4\pi\phi K r}\right]\left\{\frac{e^{-\kappa(r-R_m)}}{1+\kappa R_m}\right\} \qquad r > R_m \tag{8}$$

$$u_r = \left[\frac{Q}{4\pi\phi r^2}\right]\left\{\left(\frac{1+\kappa r}{1+\kappa R_m}\right)e^{-\kappa(r-R_m)}\right\} \quad r > R_m \tag{9}$$

The terms in the square brackets refer to pressure and flow that would occur in the absence of fluid exchange between tissue and capillaries, i.e. κ=0, (Laplace equation solution).

The terms in the curly brackets quantifies the relative effects of fluid exchange compared to interstitial flow. These terms rapidly decay to zero for $r>>1/\kappa$ and limit the region of influence of a catheter to a few screening lengths.

Equations (8) and (9) are analogous to the Debye-Hückel linearized theory of the screened electrical potential and field around a charged spherical particle. Pursuing this analogy, $1/\kappa$ is recognized as a "screening length" over which flow across capillary walls buffers perturbations in pressure due to infusion. As the screening length increases, more fluid flow is directed through the tissue and less is lost to capillaries, resulting in higher interstitial pressures and velocities.

The model exhibits two length scales, R_m and $1/\kappa$, affecting the shapes of pressure and velocity profiles. Taking κ as the scaling parameter, and defining the dimensionless variables $\rho=\kappa r$, $\rho_m=\kappa R_m$, $\hat{p} = 4\pi\varphi K\tilde{p}/q$ and $\hat{u}_r = 4\pi\varphi K R_m^2 u_r/q$, Eqs. (8) and (9) simplify to

$$\hat{p} = \frac{e^{-\rho_m(\rho/\rho_m - 1)}}{(1+\rho_m)\rho_m(\rho/\rho_m)} \quad ; \quad \hat{u}_r = \frac{(1+\rho)e^{\rho_m(\rho/\rho_m - 1)}}{(1+\rho_m)\rho_m^2(\rho/\rho_m)^2} \quad \rho/\rho_m > 1 \qquad (10)$$

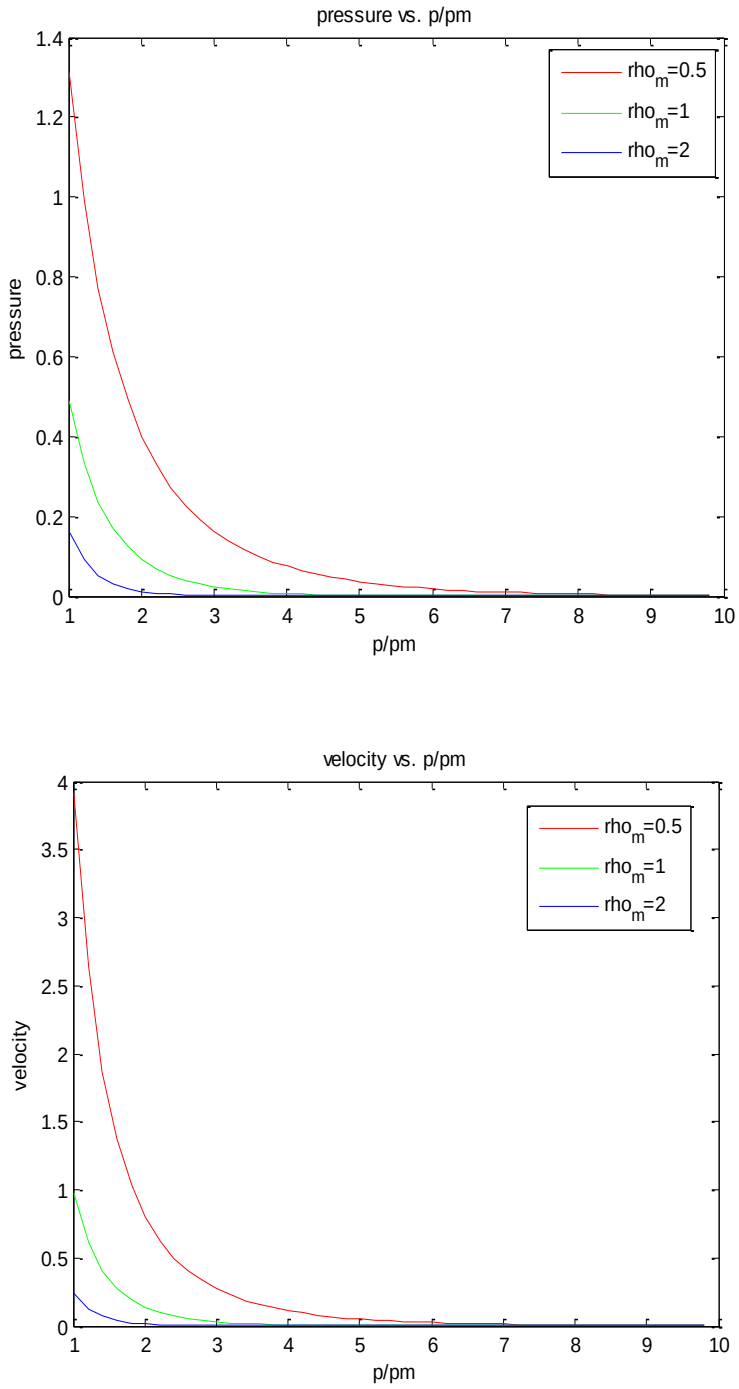

Figure 5.2: Plots of $\hat{p}$ and $\hat{u}_r$ as a Function of $\rho/\rho_m(=r/R_m)$. The top plot shows a family of pressure fields parameterized by ρ_m. As ρ_m increases both the velocity and the pressure are significantly reduced.

When tip radius is significantly smaller that the screening length, i.e. $\kappa R_m << 1$, Eqs. (8) and (9) simplify to $\tilde{p} = q\kappa e^{-\kappa r} / 4\pi\phi K(\kappa r)$ and $u_r = [q\kappa^2 / 4\pi\phi(\kappa r)^2](1+\kappa r)e^{-\kappa r}$, respectively, for $r > R_m$. In this case, pressure and velocity at a point beyond the tip surface decay according to the number of screening lengths the point lies away from the center of the tip.

To be more precise, we note that $\rho_m = \kappa R_m = R_m/(1/\kappa)$ is the ratio of the catheter radius to the pressure/velocity decay length. When this parameter is small ($\kappa R_m << 1$), Eqs. (8) and (9), simplify to $\tilde{p} = (q/4\pi\phi K r)e^{-\kappa r}$. In a similar manner, let L_m be the largest length parameter of the catheter tip where outflow occurs, such as tip length or radius. We assert that when $\lambda = \kappa L_m << 1$, neither the shape of the catheter outlet nor the presence of the catheter shaft significantly affects the pressure and velocity surrounding the catheter, except where $r < L_m$.

To model R-CED, we must include the effects of the dialysis membrane, whose hydraulic permeability will be denoted by L_{pm}. We retain spherical symmetry in the model, and assume that this simplification will not lead to great error. Taking the intercapillary Starling pressure as reference, and assuming that the osmolyte (e.g. high MW dextran) cannot permeate through the dialysis membrane but all other solutes can, the relevant pressure inside the catheter lumen is $\tilde{p}_l = p_l - \pi_l - p_e$, where the subscript *l* refers to the lumen. For R-CED, this pressure will be negative. Flow continuity at the membrane/tissue interface warrants that

$$L_{pm}[\tilde{p}_l - \tilde{p}(R_m)] = -\varphi K \left.\frac{d\tilde{p}}{dr}\right|_{r=R_m} \qquad (11)$$

Replacing Eq. (6) with Eq. (11), the pressure and velocity fields surrounding a spherical R-CED catheter become

$$\tilde{p} = (1-\theta)\ \frac{R_m}{r}\ e^{-\kappa(r-R_m)}\tilde{p}_l \quad ; \quad u_r = (1-\theta)K\frac{R_m}{r^2}\ \frac{1+\kappa r}{1+\kappa R_m}\ e^{-\kappa(r-R_m)}\tilde{p}_l \quad r > R_m \qquad (12)$$

where

$$\theta = \frac{1}{1 + L_{pm} R_m / \varphi K (1 + \kappa R_m)} \tag{13}$$

is the fraction of Starling pressure that is dissipated in the membrane. The cases $\theta = 0$ and $\theta = 1$ correspond, respectively, to membrane and tissue control of R-CED flow. For $\kappa R_m << 1$, Eq. (12) simplifies to

$$\tilde{p} = (1 - \theta)(R_m / r) e^{-\kappa r} \tilde{p}_l \tag{14}$$

$$u_r = (1 - \theta) K (R_m / r^2)(1 + \kappa r) e^{-\kappa r} \tilde{p}_l . \tag{15}$$

5.3.3 Non-spherical catheter tips

Having derived equations for the idealized geometry, we now ask if tip geometry can impact drug delivery at the catheter-tissue interface. For CED, delivery is through the open end of a narrow shaft. For R-CED, tubular microdialysis membranes are used, and Wang and Olbricht's work assumed cylindrical geometry. Calculations based on this assumption are strictly correct only for catheters with large axis to radius ratios, or when looking at tissue that is very close to the catheter. We now argue that spherical symmetry often provides a useful and reasonably accurate approximation for CED and R-CED. This observation has analogies in colloid science: the precise shape of charged colloidal particles has little bearing on electrical potentials far from particle surfaces [198, 199].

Let *d* be the largest length scale of the catheter tip, such as its radius or half its length. Also, let the radial coordinate, *r*, be a suitably chosen centroid of the catheter tip. Then our

hypothesis is that spherical symmetry will apply for $r>d$, and that Eqs. (8), (9) and (12) are reasonable approximations. For $r<d$, shape effects are more important.

To support this assertion, several cases were studied in the COMSOL 3.5a simulation environment (COMSOL, Inc., Burlington MA). COMSOL was used to solve partial differential equations, subject to appropriate boundary conditions, using the finite element method. This method, despite its approximations, is preferred over analytic solutions. Even for the simple case of two ideal spherical catheters delivering fluid at the same rate, superposition does not provide a correct solution since each catheter's presence perturbs the flow pattern generated by the other catheter. In electrostatics, the analogy is that colloidal particles polarize each other, thus altering the fields they each generate. Self consistent solutions in either case involve infinite series, which are solved approximately by making added assumptions that permit cutoff after a small number of terms [198]. Perturbative corrections should become less significant, and superposition solutions should become more accurate, with increasing distance between catheters.

To solve PDE's in COMSOL, a finite domain corresponding to tissue is prescribed, as is the geometry of the catheter(s). The type of equation (usually Helmholtz in the present case) is then selected, and boundary conditions are prescribed at the catheter surfaces and at the edges of the domain. To minimize the effect of domain boundaries on the numerical solution, the domain should be large compared to catheter radius or length and distance between the catheters tip. In the present simulations, Dirichlet conditions (zero Starling pressure, similar to Eq. (7)) are prescribed at the domain boundary. Neumann conditions (pertaining to pressure gradients) are prescribed at catheter boundaries. Since we are only interested in patterns, no attempt was made to introduce physiological parameters, flows magnitudes, or specific Starling pressures.

As a first example, Figure 5.3 shows that a cubic tip, with fluid flowing uniformly and equally out of each face, is surrounded by a spherical pressure field, except at the edge of the tip

where the shape influences the flow. Thus, the use of spherical approximation is justifiable. We then wanted to test the effect of fluid flow when two catheters are placed side by side and separated by a sufficient distance that their interaction is small, assuming that equal flow emerges from the two tips. We observed that the two objects produce essentially identical pressure and flow fields away from their surfaces, while fields near the surfaces depend on shape. Figure 5.4 shows simulations of delivery from a shaft, with unidirectional flow to the lumen, which opens at its end into the tissue. The outer body of the shaft is impermeable to fluid flow. For simplicity, flow inside the shaft is modeled as plug instead of Poisseiulle flow. This demonstrates that a nearly spherically symmetric pressure/flow profile develops soon after fluid leaves the catheter tip, even though the tip itself is circular and shaft's wall blocks fluid flow. Intuitively, as one moves farther away from the tip, the surface area of the isobar becomes larger compared to the cross sectional area of the shaft. The shaft therefore becomes much less important in "shaping" the front. Figure 5.5 displays the flow pattern into a cylinder, representing R-CED into a microdialysis membrane. The axial/radial ratio is 8. Close to the membrane, the (negative) pressure contours are nearly cylindrical, but they round out as one moves away from the tube. With a smaller value of κ (larger $1/\kappa$), more such contours would be discernable.

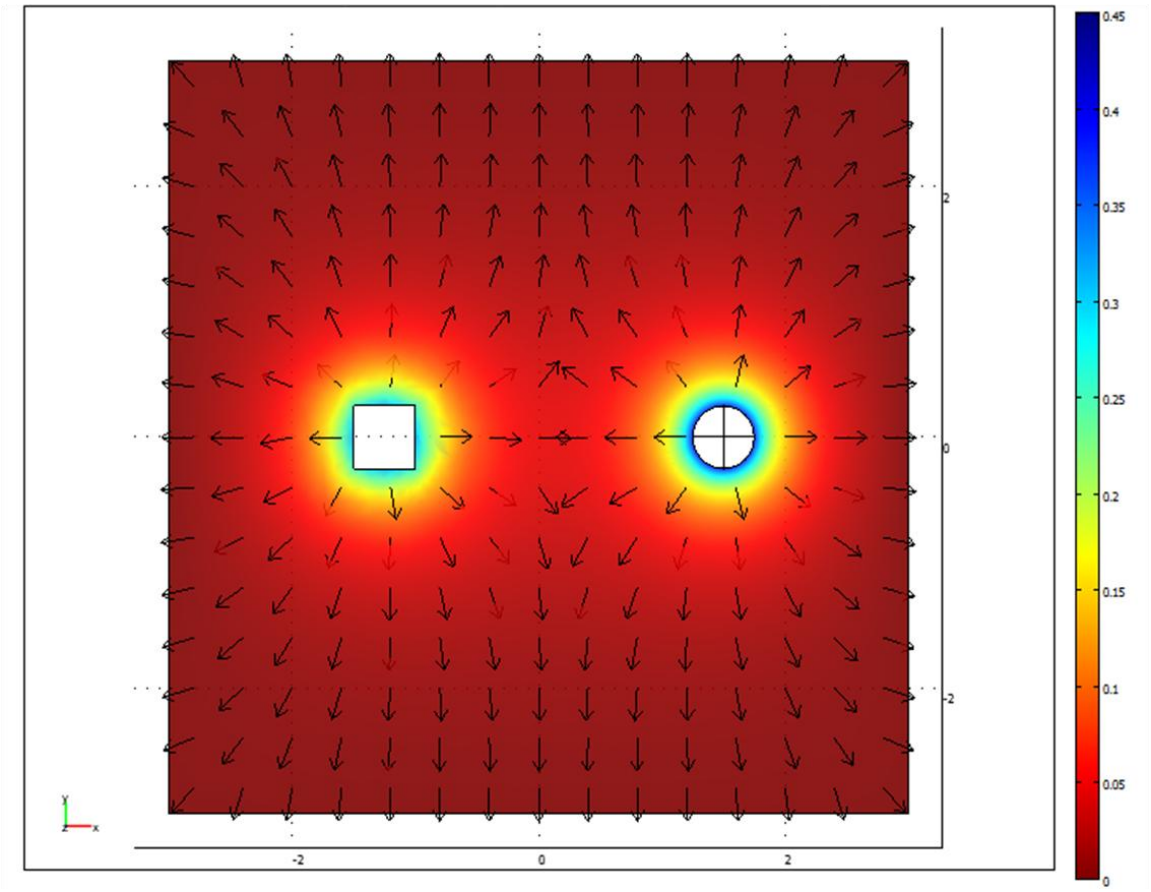

Figure 5.3: Finite Element Analysis of Spherical and Cubic "Model" Catheter Tips. We designed objects with equal diameter and set boundary conditions such that the flux emitting from the cube and the sphere are the same, and κR_m=0.25. Pressure variations are represented by color changes and the arrows correspond to the direction of the velocity field with normalized magnitudes.

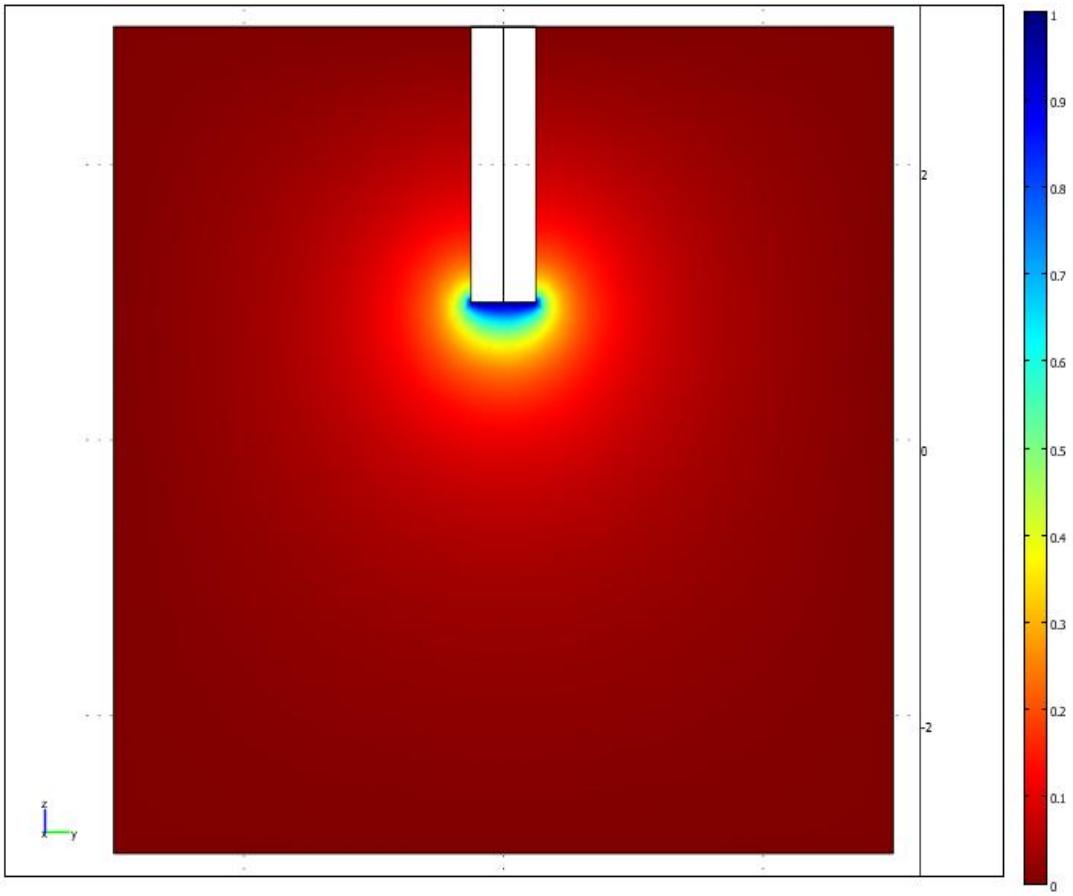

Figure 5.4: Finite Element analysis of a CED catheter tip fed by unidirectional plug flow. κR_m =0.5 as in Figure 5.3. Pressure variations are represented by color changes.

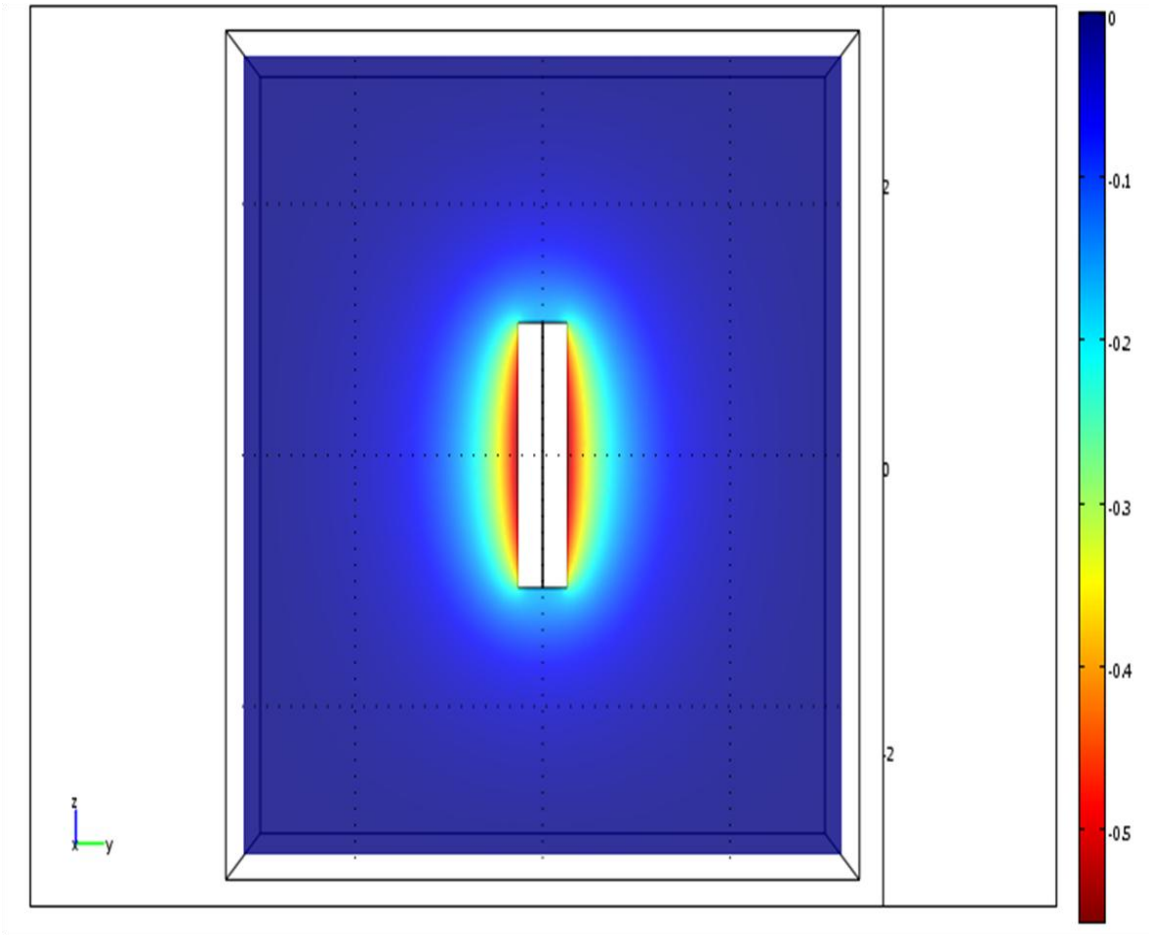

Figure 5.5: Finite Element Analysis of R-CED Flow. κR_m=0.5 as in Figure 5.3 & 5.4. κd=4. The shaft tips are to be impermeable, and the surrounding edges were modeled as model membranes. Relative pressures are mostly negative close to the membrane where reverse flow is being generated.

5.3.4 Multiple Catheter Delivery

In the previous sections it was shown that catheter shape has little effect on pressure and flow profiles once fluid moves a sufficient distance from the catheter tip. We now consider the effects of flow from one catheter on flow from a second catheter. The simplest situation is two identical catheters placed at a distance from each other in a medium (tissue) with uniform properties. Suppose that one catheter delivers drug, while the other delivers a drug-free, blank solution. If flows from the two catheters are equal, then the flows will collide at the "mirror" plane perpendicular the two catheters, and proceed along that plane. This phenomenon is illustrated by the flow arrows in Figure 5.3. Now suppose that flow from the "blank" catheter is stronger. Then, the fluids will collide along a surface that is closer to and bent around the drug-delivering catheter. If the former and latter catheters are placed properly placed inside and outside the tumor, and flows are properly selected, based on the tissue properties of tumor and brain parenchyma, it seems possible to focus drug delivery within the tumor and substantially reduce exposure in the parenchyma. Conversely, flow of a radio protective agent from outside the tumor could be "steered away" from tumor tissue by flow of blank solution from a catheter inside the tumor.

A second possible dual probe configuration would involve convective drug delivery from one catheter and fluid removal by the other. Note that the latter catheter is not used in the same way as has been previously considered for R-CED, since drug is not being pulled out of the circulation through capillaries, but rather is supplied by the delivery catheter. In this case, flows are predicted from the delivery catheter to the removal catheter, with a pattern resembling the alignment of iron filings over two-pole magnet. For reasons already identified by Wang and Olbricht, this technique seems less promising than dual CED, since it is more difficult to pull osmotically than it is to push hydraulically, and since drug will be lost into the removal catheter, unless that catheter is impermeable to drug.

5.4 Conclusion

This chapter focused on the convective aspects of CED and R-CED in the brain. We have argued that for many situations, both of these modalities can be modeled reasonably well using simple spherically symmetric solutions to the Helmholtz equation which accounts for pressure and flow fields around single catheters. While real catheters may have different shapes, spherical fronts develop away from the catheter. Because the spherical shells grow as one moves away from the central source, the pressure and flow fields for most of the affected tissue are relatively insensitive to catheter shape, provided boundary conditions such as total flow are properly set. This simplifies calculations.

We have also demonstrated the effect of dual catheters in shaping the flow fields, and argued that by this means one might steer chemotherapy out of regions of the brain where toxic side effects could occur. Of course, one might consider the effects of multiple catheters in generating drug delivery patterns, subject to surgical constraints.

In addition to drug localization, drug patterning by multiple catheters could be useful when drug should be distributed through an entire brain region while sparing critical tissues. This could be accomplished by infusing a non-toxic saline solution into the critical area while simultaneously infusing the drug into the larger regional space.

In order to enable such combination therapies, it will be necessary to know the tissue properties in advance of pattern planning or to use real time imaging [184, 200] such that the infusion flow rates could be altered based on the distribution of the ongoing infusion.

We conclude by suggesting further strategies which use CED and R-CED. In one example, a rapidly eliminated blood brain barrier permeable drug could be administered systemically and a saline solution could be infused into the tumor. The pressure of the saline infusion would reduce drug extravasation into the tumor but would have no such effect in normal

tissue. Potential applications, including the infusion of radio- or cryoprotectants [201], whereby protectant would accumulate in normal tissue, but tumor would remain susceptible to radiation or cryo therapies.

Parameters governing transport in the brain may be susceptible to manipulation, allowing for alteration in drug distribution. For example, interstitial hydraulic conductivity might be altered using enzymes such as hyaluronidase to degrade the extracellular matrix [202]. Capillary permeability, on the other hand, might be altered by angiogenesis regulators such as VEGF. Such alterations, in addition to changing the region of influence of a catheter, might alter the pressure requirements on the catheter to establish a desired drug distribution.

5.5 Methods

5.5.1 Finite Element Analysis: COMSOL Modeling

R-CED and CED systems were modeled using the COMSOL Multiphysics package, 3.5a release. The simulations were performed using the classical partial differential equation (PDE) package. The Helmholtz Equation module was selected from the PDE package, which is designed to support the numerical modeling of partial differential equations of space and pressure. As illustrated in Figure 5.6, COMSOL simulations were setup within a three-dimensional environment using a 6 x 6 cube as the boundary edges of the system.

R-CED and CED catheters were represented in the system with spheres and/or cubes placed at specific distances within the environment to mimic catheter placement and generate pressure and velocity plots. The objects created were $1/20^{th}$ the volume of the outer cube. The diffusion, absorption and source coefficients of the subdomain setting:

$$-\nabla \bullet (c\nabla u) + au = f$$

were modified accordingly to reflect the absorption and diffusion conditions of the system, and if the outer cube boundaries were acting as a fluid source or drain. Each outer face was treated assuming Dirichlet boundary condition:

$$hu = r$$

where h was set to 1 and u and r were set to 0. Each face of the inner cube or sphere was treated assuming the Neumann boundary condition:

$$n \bullet (c\nabla u) + q \bullet u = g$$

where q is set to 0 and g is set to 1 or -1 depending if the object is a source (CED) or a sink (R-CED). The system was then simulated and plots, isosurfaces, and streamlines were generated for all cases simulated using COMSOL postprocessing module.

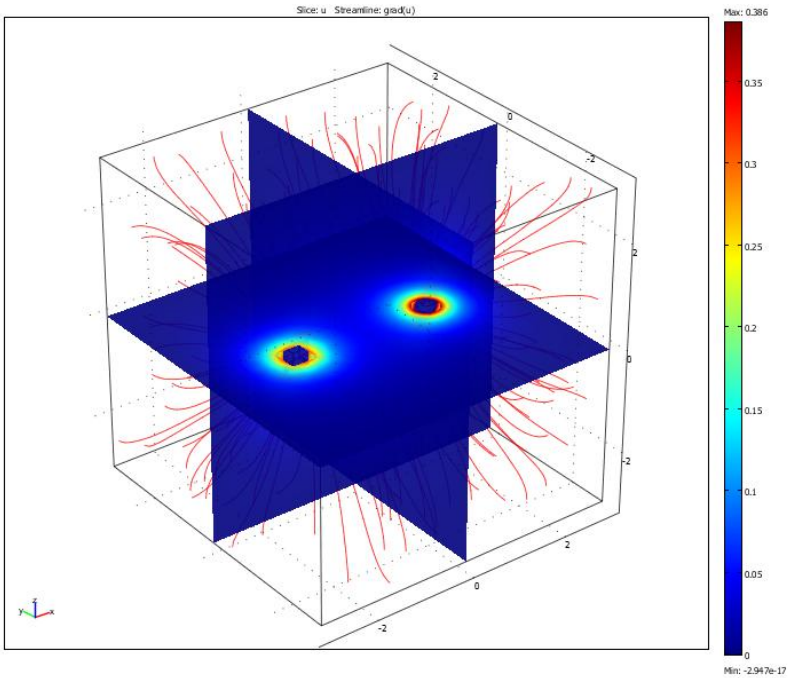

Figure 5.6: Three-Dimensional Representation of the COMSOL Modeling Environment. The figure shows the 6x6 cube used to simulate CED and R-CED fluid flow. Pressure variations are represented by color changes and streamlines (red) correspond to the direction of the flow with normalized magnitudes.

Chapter 6: Concluding Remarks

In this dissertation, a biophysical approach was used to engineer triggerable liposomal systems capable of mediating cytosolic delivery of drugs. My intent was to extend the use of phosphatases as enzymatic triggers for drug delivery systems. I was motivated by the fact that very few drug delivery systems have been engineered for phosphatase triggering, even though phosphatases are both widespread in the body, but also over expressed in a number of life-threatening conditions.

Phosphatases can be thought of as polarity converters. They can effectively mediate the removal of hydrophilic phosphate masks to expose hydrophobic substrates. This polarity conversion can be exploited for engineering systems that make use of substrate masking as a trigger technique. As proof of principle, I designed phosphatase triggerable liposomes that mimicked the fusion machinery of viruses. These triggerable fusogenic liposomes (FTP) were designed by displaying phosphorylated fusion peptides on the surface of liposomes. The exposure of FTP to phosphatases triggered the system and induced a polarity reversal on the surface of the liposomes. Dephosphorylation of the phosphopeptides resulted in a gain of fusion potential and promoted their insertion into adjacent membranes. This elicited membrane fusion and content release of drugs.

In order to design FTP, I first had to gain control over the membrane destabilizing properties of fusion peptides. In Chapter 2, phosphorylated gp41 fusion peptides were designed to assess the inhibitory effects of phosphate groups on the membrane destabilizing properties of fusion peptides. I observed that two phosphates provided enough hydrophilicity and polarity to inactivate the peptides. The phosphorylated fusion peptides exhibited altered secondary structures and a reduced capacity to induce lipid mixing and liposomic disruption. However, they were excellent substrates for phosphatases. Phosphatases catalyzed the dephosphorylation of the

phosphopeptide, thereby regenerating the fusion sequence and exposing their membrane destabilizing domains. This elicits content leakage and lipid mixing of adjacent bilayers. The findings of Chapter 2 suggested that phosphorylated fusion peptides are suitable as triggerable components for FTP.

In Chapter 3, FTP were designed by displaying phosphopeptides on the surface of liposomes. It was hypothesized that phosphatase catalyzed dephosphorylation would activate the displayed fusogenic phosphopeptides and promote efficient membrane fusion of FTP with neighboring membranes. Surface displayed phosphopeptides were substrates for phosphatases. Furthermore, the anchoring of the peptide to the membrane promoted a stable secondary structure. An enhanced fusogenic potential was observed as a result of the localized concentration of peptides anchored to the surface of the FTP. The substantial enthalpic gain resulting from the displayed peptides partitioning into neighboring membranes resulted in efficient membrane fusion and content release. The promising results motivated the study of FTP in mammalian cells. FTP exhibited enhanced cellular accumulation and were effective at mediating cytosolic delivery. Interestingly, the time difference between cellular accumulation and cytosolic delivery indicated that the delivery occurred after internalization, and most likely in endosomes, rather than at the cell membrane. The potential of FTP to mediate cytosolic delivery is apparent and validates the utility of phosphates as substrates masks to engineer phosphatase triggerable liposomes.

Phosphatases can also be thought of as charge converters since dephosphorylation promotes a local charge conversion at the substrate. A gain in surface charge is achieved from the loss of the negative phosphate. This physico-electrical property can be used to design phosphate shielded cationic lipids that when dephosphorylated promote charge conversion and induce a "switch-like (on/off)" behavior. Properly engineered liposomes can exploit this charge effect to modulate lipid packing changes in the bilayer and induce membrane fusion and contents release of neighboring membranes.

In Chapter 4, proof-of-concept experiments were performed to elucidate the mechanism of charge conversion by phosphatase triggering. Surface charge converters (SCC) were engineered with inverse phosphocholine lipids, DOCP and DOCPe, and tested for their ability to charge convert. DOCP SCC were found to be excellent substrates for phosphatases. Acid and alkaline phosphatases readily acted on them, dephosphorylating their extended phosphate, and promoting charge conversion at the membrane interface. This resulted in an anionic to cationic conversion of the lipid head group. The net change in zeta potential as a result of dephosphorylation was found to be +80 mV, which is an impressive charge conversion for an enzymatically-active system. Furthermore, DOCP SCC formulated with phosphatidylethanolamine and cholesterol exhibited lipid mixing and content release characteristics. Triggered content release was observed in physiological conditions, whereas lipid mixing was enhanced in acidic conditions. Furthermore, SCC were effective at mediating endosomal escape and cytosolic delivery of macromolecules, validating their utility as delivery carriers. In addition to their "switch-like" behavior, SCC can be designed to exhibit AND logic if formulated with DOCPe. This is an interesting outcome of a head group substitution in which the phosphate is replaced by a phosphoester, providing a double trigger substrate. Thus, both esterases and phosphatase must act sequentially on the substrate in for charge conversion to occur.

Drug delivery to the brain, however, is one of the most challenging problems in drug delivery. Thus, theoretical models that can provide insights into the driving factors influencing drug delivery are beneficial. In Chapter 5, mathematical insights into the use of infusion techniques for brain delivery were provided. Furthermore, the effect of dual catheters and multi-catheters arrays in shaping fluid flow was demonstrated. The findings suggest that infusion techniques could be useful in selectively compartmentalizing drugs to regions of the brain affected by disease while steering drug away from healthy tissue. Thus, infusion techniques that

can selectively deliver phosphatase triggerable liposomes to affected areas of the brain could provide an unprecedented level of selectivity and efficacy for treating brain tumors. The double trigger feature of DOCPe SCC is highly attractive and could be advantageous for designing therapies against brain tumors, where both esterases and phosphatases are localized and over expressed.

In conclusion, the sine qua non for engineering triggerable phosphatase liposomes is to ensure that the trigger moieties are accessible and not sterically hindered to the phosphatase. In addition, triggering must elicit a local change in the physico-chemical or physico-electrical properties of the substrate in order to elicit membrane fusion or drug release. The principles and guidelines outlined throughout this thesis should serve as a guide for designing other enzymatically-active triggerable systems. Finally, the potential for treating diseases such as brain, prostate, and cervical cancer as well as heart failure and arthritis is truly appealing, and should be a motivation for engineering novel drug delivery systems that can overcome the challenges associated with the *in vivo* delivery of phosphatase triggerable liposomes.

References

1. Huang, Z., Jaafari, M. R., and Szoka, F.C., *Disterolphospholipids: non-exchangeable lipids and their application to liposomal drug delivery.* Angew Chem Int Ed Engl, 2009. **48**(23): p. 4146-4149.
2. Green, J.J., Langer, R., and Anderson, D.G., *A combinatorial polymer library approach yields insight into nonviral gene delivery.* Acc Chem Res, 2008. **41**(6): p. 749-759.
3. Lee, C.C., MacKay, J.A., Frechet, J.M., and Szoka, F.C., *Designing dendrimers for biological applications.* Nat Biotechnol, 2005. **23**(12): p. 1517-26.
4. Dalton, W.S., Grogan, T.M., Meltzer, P.S., Scheper, R.J., Durie, B.G., Taylor, C.W., Miller, T.P., and Salmon, S.E., *Drug-resistance in multiple myeloma and non-Hodgkin's lymphoma: detection of P-glycoprotein and potential circumvention by addition of verapamil to chemotherapy.* J Clin Oncol, 1989. **7**(4): p. 415-24.
5. Sharma, A., and Straubinger, R.M., *Novel taxol formulations: preparation and characterization of taxol-containing liposomes.* Pharm Res, 1994. **11**(6): p. 889-96.
6. von Hoff, D., Layard, M., Basa, P., Davis, H. L., von Hoff, A., Rozencweig, M., and Muggia, F.M., *Risk factors for doxorubicin-induced congestive heart failure.* Ann Intern Med, 1979. **91**(5): p. 710-17.
7. Constantinides, P.P., Tuastian, A., and Kessler, D.R., *Tocol emulsions for drug solubilization and parenteral delivery.* Adv Drug Deliv Rev, 2004. **56**(9): p. 1243-1255.
8. Guo, X., and Szoka, F.C., *Chemical approaches to triggerable lipid vesicles for drug and gene delivery.* Acc Chem Res, 2003. **36**(5): p. 335-341.
9. Torchilin, V.P., *Passive and active drug targeting: drug delivery to tumors as an example.* Handb Exp Pharmacol, 2010. **197**: p. 3-53.
10. Li, W., and Szoka, F.C., *Lipid-based nanoparticles for nucleic acid delivery.* Pharm Res, 2007. **24**(3): p. 438-49.
11. Yew, N.S., and Scheule, R.K., *Toxicity of cationic lipid-DNA complexes.* Adv Genet, 2005. **53**: p. 189-214.
12. Lockman, P.R., Koziara, J.M., Mumper, R.J., and Allen, D.D., *Nanoparticle surface charges alter blood-brain barrier integrity and permeability.* J Drug Target, 2004. **12**(9-10): p. 635-41.
13. Aleku, M., Schulz, P., Keil, O., Santel, A., Schaeper, U., Dieckhoff, B., Janke, O., Erduschat, J., Durieux, B., Roeder, N., Loeffler, K., Lange, C., Fechtner, M., Mopert, K., Fisch, G., Dames, S., Arnold, W., Jochims, K., Giese, K., Wiedemann, B.,Scholz, A., and Kaufmann, J., *Atu027, a liposomal small interfering RNA formulation targeting protein kinase N3, inhibits cancer progression.* Cancer Res, 2008. **68**: p. 9788-9798.
14. Strumberg, D., Schutlies, B., Traugott, U., Vank, C., Santel, A., Keil, O., Giese, K., Kaufmann, J., and Drevs, J., *Phase I clinical development of Atu027, a siRNA formulation targeting PKN3 in patients with advanced solid tumors.* Int J Clin Pharmacol Ther, 2012. **50**(1): p. 76-78.
15. Kong, G., Braun, R. D., and Dewhirst, M.W., *Hyperthermia enables tumor-specific nanoparticle deliery: effect of particle size.* Cancer Res, 2000. **60**(16): p. 4440-4445.
16. Hang, C., Zuckerman, J. E., Webter, P., and Davis, M. E., *Targeting kidney mesangium by nanoparticles of defined size.* PNAS, 2011. **108**(16): p. 6656-6661.
17. Seki, J., Sonoke, S., Saheki, A., Fukui, H., Sasaki, H., and Mayumi, T., *A nanometer lipid emulsion, lipid nano-shere (LNS), as a parenteral drug carrier for passive drug targeting.* Int J Pharm, 2004. **273**(1-2): p. 75-83.
18. Senior, J., and Gregoriadis, G., *Is half-life of circulating liposomes determined by changes in their permeability?* FEBS Lett, 1982. **145**(1): p. 109-14.

19. Kelly, C., Jeffries, C., and Cryan S.A., *Targeted liposomal drug delivery to monocytes and macrophages.* J Drug Deliv, 2011. **2011**: p. 727241-11.
20. Gabizon, A.A., Sheeda, H., and Zalipsky, S., *Pros and Cons of the Liposome Platform in Cancer Drug Targeting.* J Liposome Res, 2006. **16**: p. 175-183.
21. Ong, W., Yang, Y., Cruciano, A.C., and McCarley, R.L., *Redox-triggered contents release from liposome.* J Am Chem Soc, 2008. **130**(44): p. 14739-44.
22. Meers, P., *Enzyme-activated targeting of liposomes.* Adv Drug Deliv Rev, 2001. **53**(3): p. 265-72.
23. Wells, J., Sen, A., and Hui, S.W., *Localized delivery to CT-26 tumors in mice using thermosensitive liposomes.* Int J Pharma, 2003. **261**(1-2).
24. Hayashi, H., Kono, K., and Takagishi, T., *Temperature-controlled release property of phospholipic vesicles bearing a thermo-sensitive polymer.* Biochim Biophys Acta, 1996. **1280**(1): p. 127-134.
25. Shamay, Y., Adar, L., Ashkensay, G., and David, A., *Light induced drug delivery into cancer cells.* Biomaterials, 2011. **32**(5): p. 1377-86.
26. Febvay, S., Marini, D.M., Belcher, A.M., and Clapham, D.E., *Targeted cytosolic delivery of cell-impermeable compounds by nanoparticle-mediated light triggered endosome disruption.* Nano Lett, 2010. **10**(6): p. 2211-19.
27. Amstad, E., Kohlbrecher, J., Muller, E., Schweizer, T., Textor, M., and Reimhult, E., *Triggered release from liposomes through magnetic acutation of iron oxide nanoparticle containing membranes.* Nano Lett, 2011. **11**(4): p. 1664-70.
28. Ge, J., Neofytou, E., Cahill, T. J., Beygui, R. E., and Zaret, R. N., *Drug release from electric-field-responsive nanoparticles.* ACS Nano, 2012. **6**(1): p. 227-233.
29. Bangham, A.D., and Horne, R.W., *Negative staining of phospholipids and their structural modification by surface-active agents as observed in the electron microscope.* J Mol Biol, 1964. **8**(5): p. 660-668.
30. Bangham, A.D., Standish, M.M., and Watkins, J.C., *Diffusion of univalent ions across the lamellae of swollen phospholipids.* J Mol Biol, 1965. **13**(1): p. 238-252.
31. Sessa, G.a.W., G., *Phospholipid spherules (liposomes) as a model for biological membranes.* J Lipid Res, 1968. **9**(3): p. 310-18.
32. Torchilin, V.P., and Weissig, V., *Liposomes*. Second Edition ed. Liposomes, ed. V.P. Torchilin, and Weissig, V.2003, New York: Oxford University Press Inc. 396.
33. Li, W., and Szoka, F.C. , *Lipid-based nanoparticles for nucleic acid delivery.* Pharm Res, 2007. **24**(3): p. 438-449.
34. Bangham, A.D., Miller, N.G.A., Davies, R.J., Greenough, A., and Morley, C.J. , *Introductory remarks about artificial lung expanding compounds (ALEC).* Colloids and Surfaces, 1984. **10**: p. 337-341.
35. Maurer, N., Fenske, D.B., and Cullis, P.R., *Developments in liposomal drug delivery systems.* Expert Opin Biol Ther, 2001. **1**(6): p. 923-47.
36. Torchilin, V.P., *Tumor delivery of macromolecular drugs based on the EPR effect.* Adv Drug Deliv Rev, 2011. **63**(3): p. 131-35.
37. Maeda, H., *The enhanced permeability and retention (EPR) effect in tumor vasculature: the key role of tumor-selective macromolecular drug targeting.* Adv Enzyme Regul, 2001. **41**: p. 189-207.
38. Jain, R.K., *Transport of molecules, particles, and cells in solid tumors.* Annu Rev Biomed Eng, 1999. **1**: p. 241-263.
39. Palmer, T.N., Caride, V.J., Caldecourt, M.A., Twickler, J., and Abdullah, V. , *The mechanism of liposome accumulation in infarction.* Biochim Biophys Acta, 1984. **797**(3): p. 363-68.

40. Maeda, H., Sawa, T., and Konno, T., *Mechanism of tumor-targeted delivery of macromolecular drugs, including the EPR effect in solid tumor and clinical overview of the prototype polymeric drug SMANCS.* J Control Release, 2001. **74**(1-3): p. 47-61.
41. Frank, M.M., *The reticuloendothelial system and bloodstream clearance.* J Lab Clin Med, 1993. **122**(5): p. 487-488.
42. Harashima, H., Matsuo, and Kiwada, H., *Identification of proteins mediating clearance of liposomes using a liver perfusion system.* Adv Drug Deliv Rev, 1998. **32**(1-2): p. 61-79.
43. Miller, C.R., Bondurant, B., McLean, S.D., McGovern, K.A., and O'Brien, D.F., *Liposome-cell interaction in vitro: effect of liposome surface charge on the binding and endocytosis of conventional and sterically stabilized liposomes.* Biochemistry, 1998. **37**(37): p. 12875-83.
44. Szebeni, J., *The interaction of liposomes wih the complement system.* Crit Rev Ther Drug Carrier Syst, 1998. **15**(1): p. 57-88.
45. Semple, S.C., Chonn, A., and Cullis, P.R., *Interactions of liposome and lipid-based carrier systems with blood proteins: relation to clearance behavior in vivo.* Adv Drug Deliv Rev, 1998. **32**(1-2): p. 3-17.
46. Klibanov, A.I., Maruyama, K., Torchilin, V.P., and Huang, L., *Ampiphatic polyethyleneglycols effectively prolong the circulation time of liposomes.* FEBS Lett, 1990. **268**(1): p. 235-237.
47. Lasic, D.D., and Martin, F.J., *Stealth Liposomes*1995, Boca Raton: CRC Press.
48. Yuan, F., Leunig, M., Huang, S. K., Berk, D.A., Papahadjopoulos, D., and Jain, R.K., *Microvascular permeability and interstitial penetration of sterically stabilized (stealth) liposomes in a human tumor xenograft.* Cancer Res, 1994. **54**(13): p. 3352-56.
49. Liu, D., Mori, A., and Huang, L., *Role of liposome size and RES blockade in controlling biodistribution and tumor uptake of GM-1 containing liposomes.* Biochim Biophys Acta, 1992. **1104**(1): p. 95-101.
50. Fox, M.E., Szoka, F.C., and Frechet, J.M.J., *Soluble polymer carriers for the treatment of cancer: the importance of molecular architecture* Acc Chem Res, 2010. **42**(8): p. 1141-51.
51. Gabizon, A.A., *Pegylated liposomal doxorubicin: metamorphosis of an old drug into a new form of chemotherapy.* Cancer Invest, 2001. **19**: p. 285-294.
52. Kundson, W., *Tumor-associated hyaluronan. Providing an extracellular matrix that facilitates invasion.* Am J Pathol, 1996. **148**(6): p. 1721-1725.
53. Platt, V.M., and Szoka, F.C. Jr., *Anticancer therapeutics: Targeting macromolecules and nanocarriers to hyaluronan or CD44, a Hyaluronan receptor.* Mol Pharm, 2008. **5**(4): p. 474-86.
54. Eliaz, R.E., Szoka, F.C., *Liposome-encapsulated Doxorubicin Targeted to CD44: A strategy to kill CD44-overexpressing tumor cells.* Cancer Research, 2001. **61**: p. 2592-2601.
55. Byrne, J.D., Betancourt, T., and Brannon-Peppas, *Active targeting schemes for nanoparticle systems in cancer therapeutics.* Adv Drug Deliv Rev, 2008. **60**: p. 1615-1626.
56. Bartlett, D.W., Su, H., Hilderbrandt, I. J., Weber, W. A., and Davis, M.E., *Impact of tumor-specific targeting on the biodistribution and efficacy of siRNA nanoparticles measured by multimodality in vivo imaging.* PNAS, 2007. **104**(39): p. 15549-15554.
57. Xiong, X.B., Huang, Y., Lu, W.L., Zhang, X., Zhang, H., and Zhang Q., *Enhanced intracellular uptake of sterically stabilized liposomal doxorubicin in vitro resulting in improved antitumor activity in vivo.* Pharm Res, 2005. **22**(6): p. 933-39.
58. Kirpotin, D.B., Drummond, D.C., Shao, Y., Shalaby, M. R., Hong, K. L., Nielsen, U. B., Marks, J. D., Benz, C. C., and Park, J. W., *Antibody targeting of long-circulating lipidic*

nanoparticles does not increase tumor localization but does increase internalization in animal models. Cancer Res, 2006. **66**(13): p. 6732-6740.
59. Peer, D., Karp, J. M., Hong, S., Farokhzad, O. C., Margalit, R., and Langer, R., *Nanocarriers as an emerging platform for cancer therapy.* Nat Nanotechnol, 2007. **2**(12): p. 751-60.
60. Maruyama, K., Ishida, O., Takizawa, T., and Moribe, K., *Possibility of active targeting to tumor tissues with liposomes.* Adv Drug Deliv Rev, 1999. **40**(1-2): p. 89-102.
61. Drummond, D.C., Noble, C.O., Hayes, M.E., Park, J.W., and Kirpotin, D.B., *Pharmacokinetics and in vivo drug release rates in liposomal nanocarrier development.* J Pharm Sci, 2008. **97**(11): p. 4696-4740.
62. Webb, M.S., Saxon, D., Wong, F.M., Lim, H.J., Wang, Z., Bally, M.B., Choi, L.S., Cullis, P.R., and Mayer, L.D., *Comparison of different hydrophobic anchors conjugated to poly(ethylene glycol): Effects of the pharmacokinetics of liposomal vincristine.* Biochim Biophys Acta, 1998. **1372**(2): p. 272-82.
63. Perttu, E.K., Kohli, A.G., and Szoka, F.C., *Inverse-phosphocholine lipids: a remix of a common phospholipid.* J Am Chem Soc, 2012 **134**(10): p. 4485-8.
64. Ganta, S., Devalapally, H., Shahiwala, A., and Amiji, M., *A review of stimuli-responsive nanocarriers for drug and gene delivery.* J Control Release, 2008. **126**(3): p. 187-204.
65. Sasaki, K., Kogure, K., Chaki, S., Nakamura, Y., Moriguchi, R., Hamada, H., Danev, R., Nagayama, K., Futaki, S., and Harashima, H., *An artificial virus-like nano carrier system: enhanced endosomal escape of nanoparticles via synergistic action of ph-sensitive fusogenic peptide derivatives.* Anal Bioanal Chem, 2008. **391**(8): p. 2717-27.
66. Hafez, I.M., and Cullis, P.R., *Cholesteryl hemisuccinate exhibits pH sensitive polymorphic phase behavior*. Biochim Biophys Acta, 2000. **1463**(1): p. 107-114.
67. Chu, C.J., Dijsktra, J., Lai, M.Z., Hong, K., and Szoka, F.C., *Efficiency of cytoplasmic delivery by pH-sensitive liposomes to cells in culture*. Pharm Res, 1990. **7**(8): p. 824-34.
68. Bentz, J., Ellens, H., Lai, M.Z., and Szoka, F.C. Jr., *On the correlation between H_{II} phase and the contact-induced destabilization of phosphatidylethanolamine-containing membranes.* PNAS, 1985. **82**: p. 5742-5745.
69. Lai, M.Z., Vail, W. J., and Szoka, F.C., *Acid- and calcium-induced structural changes in phosphatidylethanolamine membranes stabilized by cholesteryl hemisuccinate.* Biochemistry, 1985. **24**(7): p. 1654-61.
70. Ellens, H., Bentz, J., and Szoka, F.C., *pH-induced destabilization of phosphatidylethanolamine-containing liposomes: role of bilayer contact.* Biochemistry, 1984. **23**(7): p. 1532-8.
71. Harris, T.J., von Maltzahn, G., Lord, M.E., Park, J.H., Agrawal, A., Min, D.H., Sailor, M.J., and Bhatia, S.N., *Protease-triggered unveiling of bioactive nanoparticles*. Small, 2008. **4**(9): p. 1307-1312.
72. Andresen, T.L., Thompson, D.H., and Kaasgaard, T., *Enzyme-triggered nanomedicine: drug release strategies in cancer therapy*. Mol Membr Biol, 2010. **27**(7): p. 353-63.
73. Millan, J.L., Fishman, W.H., and Stinson, R., *Biology of human alkaline phosphatases with special reference to cancer.* Crit Rev Clin Lab Sci, 1995. **32**(1): p. 1-39.
74. Jorgensen, K., Davidsen, J., and Mouritsen, O.G., *Biophysical mechanisms of phospholipase A2 activation and their use in liposome-based drug delivery*. FEBS Lett, 2002. **531**(1): p. 23-27.
75. Jorgensen, K., Vermeheren, C., and Mouritsen, O.G., *Enhancement of phospholipase A2 catalyzed degradation of polymer grafted PEG-liposomes: effects of lipopolymer-concentration and chain-length.* Pharm Res, 1999. **16**(9): p. 1491-1493.
76. Andresen, T.L., Mouritsen, O.G., Begtrup, M., and Jorgensen, K., *Phospholipase A2 activity: Dependence on liposome surface charge and polymer coverage.* Biophys J, 2002. **82**: p. 148A.

77. Andresen, T.L., Davidsen, J., Begtrup, M., Mouritsen, O.G., and Jorgensen, K., *Enzymatic release of antitumor ether lipids by specific phospholipase A_2 activation of liposome-forming prodrugs.* J Med Chem, 2004. **47**(7): p. 1694-703.
78. Sarkar, N.R., Rosendahl, T., Krueger, A.B., Banerjee, A.L., Benton, K., Mallik, S., and Srivastava, D.K., *'Uncorking' of liposomes by matrix metalloproteinaise-9.* Chem Commun, 2005. **8**: p. 999-1001.
79. Terada, T., Iwai, M., Kawakami, S., Yamashita, F., and Hashida, M., *Novel PEG-matrix metalloproteinase-2 cleavable peptide-lipid containing galactosylated liposomes for hepatocellular carcinoma-selective targeting.* J Control Release, 2006. **111**(3): p. 333-42.
80. Hatakeyama, H., Akita, H., Kogure, K., Oishi, M., Nagasaki, Y., Kihira, Y., Ueno, M., Kobayashi, H., Kikuchi, H., and Harashima, M., *Development of a novel systemic gene deliver system for cancer therapy with a tumor-specific cleavable PEG-lipid.* Gene Ther, 2007. **14**(1): p. 68-77.
81. Singh, N., Karambelkar, A., Gu, L., Lin, K, Miller, J.S., Chen, C.S., Sailor, M.J., and Bhatia, S.N., *Bioresponsive mesoporous silica nanoparticles for triggered drug release.* J Am Chem Soc, 2011. **133**(49): p. 19582-5.
82. Pak, C.C., Erukulla, R.K., Ahl, P.L., Janoff, A.S., and Meers, P., *Elastase activated liposomal delivery to nucleated cells.* Biochim Biophys Acta, 1998. **1419**(2): p. 111-26.
83. Virshup, D.M., and Shenolikar, S., *From promiscuity to precision: protein phosphatases get a makeover.* Mol Cell, 2009. **33**: p. 537-45.
84. Barford, D., Das, A.R., and Egloff, M.P., *The structure and mechanism of protein phosphatases: Insights into catalysis and regulation.* Annu Rev Biophys Biomol Struct, 1998. **27**: p. 133-64.
85. Barford, D., *Molecular mechanisms of protein serine/threonine phosphatases.* Trends Biochem Sci, 1996. **21**(11): p. 407-412.
86. Smith, S.W., Weiss, S.B., and Kennedy, E.P., *The enzymatic dephosphorylation of phosphatidic acids.* J Biol Chem, 1957. **228**(2): p. 915-22.
87. Poelstra, K., Bakker, W.W., Klok, P.A., Hardonk, M.J., and Meijer, D.K., *A physiologic function for alkaline phosphatase: endotoxin detoxification.* Lab Invest, 1997. **76**(3): p. 319-27.
88. Davis, S.C., and Szoka, F.C., *Cholesterol phosphate derivatives: synthesis and incorporation in to a phosphatase and calcium-sensitive triggered release liposome.* Bioconjugate Chem, 1998. **9**(6): p. 783-92.
89. Pawson, T., and Scott, J.D., *Signalling through scaffold, anchoring, and adaptor proteins.* Science, 1997. **278**(5346).
90. Schutkowski, M., Bernhardt, A., Zhen Zhou, X., Shen, M., Reimer, U., Rahfeld, J., Lu, K. P., and Fischer, G., *Role of phosphorylation in determining the backbone dynamics of the serine/threonine-proline motif and pin1 substrate recognition.* Biochemistry, 1998. **37**(16): p. 5566-75.
91. Moorhead, G.B.G., Trinkle-Mulcahy, L., and Ulke-Lemee, A., *Emerging roles of nuclear protein phosphatases* Nat Rev Mol Cell Biol, 2007. **8**(3): p. 234-44.
92. Dean, D.A., Urban, G., Aragon, I.V., Swingle, M., Miller, B., Rusconi, S., Bueno, M., Dean, N.M., and Honkanen, R.E., *Serine/threonine protein phosphatase 5 (PP5) participates in the regulation of glucocorticoid receptor nucleocytoplasmic shuttling.* BMC Cell Biol, 2001. **2**(6).
93. Swarup, G., Cohen, S., and Garbers, D.L., *Selective dephosphorylation of proteins containing phosphotyrosine by alkaline phosphatases.* J Biol Chem, 1981. **256**(15): p. 8197-201.
94. Rigden, D.J., *The histidine phosphatase superfamily: structure and function.* Biochem J, 2008. **409**(2): p. 333-48.

95. Bull, H., Murray, P.G., Thomas, D., Fraser, A.M., and Nelson, P.N., *Acid phosphatases.* Mol Pathol, 2002. **55**(2): p. 65-72.
96. Rooseboom, M., Commandeur, J. N. M., and Vermeulen, N. P . E, *Enzyme-catalyzed activation of anticancer prodrugs.* Pharm Rev, 2004. **56**(1): p. 53-102.
97. Calabro-Jones, P.M., Farhey, R.C., Smoluk, G.D., and Ward, J.F., *Alkaline phosphatase promotes radioprotection and accumulation of WR-1065 in V79-171 cells incubated in medium containing WR-2721.* Int J Radiat Biol Relat Stud Phys Chem Med, 1985. **47**: p. 23-27.
98. Senter, P.D., *Activation of pro-drugs by antibody-enzyme immunoconjugates: a new approach to cancer therapy.* FASEB J, 1990. **4**(2): p. 188-93.
99. Senter, P.D., Schreiber, G. J., Hirschberg, D. L., Ashe, S. A., Hellstrom, K. E., and Hellsrom, I., *Enhancement of the in vitro and in vivo antitumor activities of phosphorylated mytomicin C and etoposide derivatives by monoclonal-antibody alkaline phosphatase conjugates.* Cancer Res, 1989. **49**(21): p. 5789-92.
100. Wallace, P.M., and Senter, P.D., *In vitro and in vivo activities of monoclonal-antibody alkaline phosphatase conjugates in combination with phenol mustard phosphate.* Bioconjug Chem, 1991. **2**(5): p. 349-52.
101. Vrudhula, V.M., Senter, P.D., Fischer, K.J., and Wallace, P.M., *Prodrugs of doxorubicin and melphalan and their activation by a monoclonal antibody-penicillin-G amidase conjugate.* J Med Chem, 1993. **36**(7): p. 919-23.
102. Cho, A., Ochoa Lara, K.L., Yatsimirsky, A.K., and Eliseeve, A.V., *Phosphatase-triggered guest release from a cyclodextrin guest complex.* Org Lett, 2000. **2**(12): p. 1741-3.
103. Jahn, R., Lang, T., and Sudhof, T.C., *Membrane fusion.* Cell, 2003. **112**(4): p. 519-533.
104. Earp, L.J., Delos, S.E., Park, H.E., and White, J.M., *The many mechanisms of viral membrane fusion proteins.* Curr Top Microbiol Immunol, 2005. **285**: p. 25-66.
105. Chernomordik, L.V., and Kozlov, M. M., *Membrane hemifusion: Crossing a chasm in two leaps.* Cell, 2005. **123**: p. 375-382.
106. Chernomordik, L.V., Zimmerberg, J., and Kozlov, M. M., *Membranes of the world unite!* J Cell Biol, 2006. **175**(2): p. 201-207.
107. Rand, R.P., and Parsegian, V.A., *Hydration forces between phospholipid bilayers.* Biochim Biophys Acta, 1989. **988**: p. 351-76.
108. Weissenhorn, W., Hinz, A., and Gaudin. Y., *Virus membrane fusion.* FEBS Lett, 2007. **581**(11): p. 2150-55.
109. Li, Y., Han, X., and Tamm, L.K., *Thermodynamics of fusion peptide-membrane interactions.* Biochemistry, 2003. **42**(23): p. 7245-51.
110. Harrison, S.C., *Viral membrane fusion.* Nat Struct Mol Biol, 2008. **15**(7): p. 690-698.
111. Kozlov, M.M., Leikin, S.L., Chernomordik, L.V, Markin, V.S., and Chizmadzhev, Y.A., *Stalk mechanism of vesicle fusion. Intermixing of aqueous contents.* Eur Biophys J, 1989. **17**(3): p. 121-129.
112. Weissenhorn, W., Dessen, A., Harrison, S.C., Skehel, J.J., and Wiley, D.C., *Atomic structure of the ectodomain from HIV-1 gp41.* Nature, 1997. **387**(6631): p. 426-430.
113. Dalgleish, A.G., Beverley, P.C., Clapham, P.R., Crawford, D.H., Greaves, M.F., and Weiss, R.A., *The CD4 (T4) antigen is an essential component of the receptor for the AIDS retrovirus.* Nature, 1984. **312**: p. 763-767.
114. Kowalski, M., Potz, J., Basiripour, L., Dorfman, T., Goh, W. C., Terwilliger, E., Dayton, A., Rosen, C., Hasltine, W., and Sodroski, J., *Functional regions of the envelope glycoprotein of human immunodeficiency virus type 1.* Science, 1987. **237**(4820): p. 1351-1355.
115. Munoz-Barroso, I., Durrell, S., Sakaguchi, K., Appella, E., and Blumenthal, R., *Dilation of the human immunodeficiency virus-1 envelope glycoprotein fusion pore revealed by*

the inhibitory action of a synthetic peptide from gp41. J Cell Biol, 1998. **140**(2): p. 315-23.
116. Freed, E.O., Delwart, E.L., Buchschacher, G.L., Jr., and Panganiban, A.T., *A mutation in the human immunodeficiency virus type 1 transmembrane glycoprotein gp41 dominantly interferes with fusion and infectivity.* PNAS, 1992. **89**(1): p. 70-4.
117. Mobley, P.W., Waring, A.J., Sherman, M.A., and Gordon, L.M., *Membrane interactions of the synthetic N-terminal peptide of HIV-1 gp41 and its structural analogs.* Biochim Biophys Acta, 1999. **1418**(1): p. 1-18.
118. Tristam-Nagle, S., and Nagle, J.F., *HIV-1 fusion peptide decreases bending energy and promotes curved fusion intermediates.* Biophys J, 2007. **93**(6): p. 2048-55.
119. Lorin, A., Charloteaux, B., Lins, L., Stroobant, V., and Brasseur, R., *Determination of the minimal fusion peptide of HIV, SIV and BLV fusion glycoproteins*, in *Peptides for Youth: Advances in Experimental Medicine and Biology*2009.
120. Jaroniec, C.P., Kaufman, J.D., Stahl, S.J., Viard, M., Blumenthal, R., Wingfield, P.T., and Bax, A., *Structure and dynamics of micelle-associated human immunodeficiency virus gp41 fusion domain.* Biochemistry, 2005. **44**(9): p. 16167-80.
121. Peisajovich, S.G., Epand, R.F., Pristker, M., Shai, Y., and Epand, R.M., *The polar region consecutive to the HIV fusion peptide participates in membrane fusion.* Biochemistry, 2000. **39**: p. 1826-33.
122. Gallaher, W.R., *Detection of a fusion peptide sequence in the transmembrane protein of human immunodeficiency virus.* Cell, 1987. **50**(3): p. 327-328.
123. Pereira, F.B., Goni, F.M., Muga, A., and Nieva, J.L., *Permeabilization and fusion of uncharged lipid vesicles induced by the HIV-1 fusion peptide adopting an extended conformation: dose and sequence effects.* Biophys J, 1997. **73**(4): p. 1977-86.
124. Cheng, S.F., Chien, M.P., Lin, C.H., Chang, C.H., Lin, C.H., Liu, Y.T., and Chang, D.K., *The fusion peptide domain is the primary membrane-inserted region and enhances membrane interaction of the ectodomain of HIV-1 gp41.* Mol Membr Biol, 2010. **27**(1): p. 31-44.
125. Torres, O., and Bong, D., *Determinants of membrane activity from mutational analysis of the HIV fusion peptide.* Biochemistry, 2011. **50**(23): p. 5195-207.
126. Pritsker, M., Rucker, J., Hoffman, T.L., Doms, R.W., and Shai, Y., *Effect of nonpolar subsitutions of the conserved Phe11 in the fusion peptide of HIV-1 gp41 on its function, structure, and organization in membranes.* Biochemistry, 1999. **38**(35): p. 11359-71.
127. Delahunty, M.D., Rhee, I., Freed, E.O., and Bonifacino, J.S., *Mutational analysis of the fusion peptide of the human immunodeficiency virus type 1: identification of critical glycine residues.* Virology, 1996. **218**(1): p. 94-102.
128. Schaal, H., Klein, M., Gehrmann, P., Adams, O., and Scheid, A., *Requirement of the N-terminal amino acid residues of gp41 for human immunodeficiency virus type-1 mediated cell fusion.* J Virol, 1995. **69**(6): p. 3308-14.
129. Chang, D.K., Cheng, S.F., and Chien, W.J., *The amino-terminal fusion domain peptide of human immunodeficiency virus type 1 gp41 inserts into the sodicum dodecyl sulfate micelle primarily as a helix with a conserved glycine at the micelle-water interface.* J Virol, 1997. **71**: p. 6593-602.
130. Kliger, Y., Aharoni, A., Rapaport, D., Jones, P., Blumenthal, R., and Shai, Y., *Fusion peptides derived from the HIV type 1 glycoprotein 41 associate with phospholipid membranes and inhibit cell-cell fusion.* J Biol Chem, 1997. **272**(21): p. 13496-13505.
131. Parente, R.A., Nir, S., and Szoka, F.C., *pH dependent fusion of phosphatidylcholine small vesicles.* J Biol Chem, 1988. **263**(10): p. 4724-30.
132. Du, J.T., Li, Y. M., Ma, Q.F., Qiang, W., Zhao, Y.F., Abe, H., Kanazawa, K., Qin, X.R., Aoyagi, R., Ishizuka, Y., Nemoto, T., and Nakanishi, H., *Synthesis and conformational*

properties of phosphopeptide related to the human tau protein. Regul Pept, 2005. **130**(1-2): p. 48-56.
133. Ramelot, T.A., and Nicholson, L. K., *Phosphorylation-induced structural changes in the amyloid precursor protein cytoplasmic tail detected by NMR.* J Mol Biol, 2001. **307**(3): p. 871-84.
134. Savitsky, A., and Golay, M.J.E., *Smoothing and differentiation of data by simplified least squares procedures.* Anal Chem, 1964. **36**(8): p. 1627-39.
135. Ohno, H., Ukaji, K., and Tsuchida, E., *Temperature dependence of the leakage of carboxy fluorescein from an inner aqueous phase of liposomes or mixed liposomes.* J Col Int Sci, 1987. **120**(2): p. 486-494.
136. Struck, D.K., Hoekstra, D., and Pagano, R.E., *Use of resonance energy transfer to monitor membrane fusion.* Biochemistry, 1981. **20**(14): p. 4093-99.
137. Elegbede, A.I., Banerjee, J., Hanson, A. J., Tobwala, S., Ganguli, B., Wang, R., Lu, X., Srivastava, D. K., Mallik, S., *Mechanistic studies of the triggered release of liposomal contents by matrix metalloproteinase-9.* J Am Chem Soc, 2008. **130**(32): p. 10633-10642.
138. Ercole, C.J., Lange, P.H., Mathisen, M., Chiou, R.K., Reddy, P.K., and Vessella, R.L., *Prostatic specific antigen and prostatic acid phosphatase in the monitoring and staging of patients with prostatic cancer.* J Urol, 1987. **138**(5): p. 1181-4.
139. Markovic, O., and Markovic, N., *Cervical acid phosphatase: a biomarker of cervical dysplasia and a potential surrogate endpoint for colposcopy.* Dis Markers, 2003. **19**(6): p. 279-86.
140. Kellet, K.A.B., Williams, J., Vardy, E. R. L. C., Smith, A. D., and Hooper, N.M., *Plasma alkaline phosphatase is elevated in Alzheimer's disease and inversely correlates with cognitive function.* Int J Mol Epidemiol Genet, 2011. **2**(2): p. 114-21.
141. Neumann, J., Maas, R., Boknik, P., Jones, L.R., Zimmermann, N., and Scholz, H., *Pharmacological characterization of protein phosphatase activities in preparations from failing human hearts.* J Pharmacol Exp Ther, 1999. **289**(1): p. 188-93.
142. Seol, J.W., Lee, H.B, Kim, N.S., and Park, S.Y., *Tartare-resistant acid phosphatase as a diagnostic factor for arthritis.* Int J Mol Med, 2009. **24**(1): p. 57-62.
143. Rautio, J., Kumpulainen, H., Heimbach, T., Oliyai, R., Oh, D., Jarvinen, T., and Savolainen, J., *Prodrugs: design and clinical applications.* Nat Rev Drug Discov, 2008. **7**(3): p. 255-70.
144. Watson, D.S., and Szoka Jr., F.C., *Role of lipid structure in the humoral immune response in mice to covalent lipid-peptides from the membrane proximal region of HIV-1 gp41.* Vaccine, 2009. **27**(34): p. 4672-83.
145. Brune, M., Hunter, J. L., Corrie, J. E. T, and Webb, M. R., *Direct, real-time measurement of rapid inorganic phosphate release using a novel fluorescent probe and its application to actomyosin subfragment 1 ATPase.* Biochemistry, 1994. **33**: p. 8262-8271.
146. Li, J., Zheng, L., King, I., Doyle, T.W., and Chen, S., *Synthesis and antitumor activities of potent inhibitors of ribonucleotide reductase: 3-Amino-4-Methylpyridine-2-Carboxaldehyde-Thiosemicarbazone (3-Amp), 3-Amino-Pyridine-2-Carboxylaldehyde-Thiosemicarbazone (3-Ap) and its water-soluble prodrugs.* Cur Med Chem, 2001. **8**(2): p. 121-133.
147. Fens, M.H., Hill, K.J., Issa, J., Ashton, S.E., Westwood, F.R., Blakey, D.C., Storm, G., Ryan, A.J., and Schiffelers, R.M., *Liposomal encapsulation enhances the antitumor efficacy of the vascular disrupting agent ZD6126 in murine B16.F10 melanoma.* Br J Cancer, 2008. **99**(8): p. 1254-1264.
148. Yang, Q., Larsen, S.K., Mi, Z., Robbins, P.D., and Basse, P.H., *PTD-mediated loading of tumor-seeking lymphocytes with prodrug-activating enzymes.* AAPS J, 2008. **10**(4): p. 614-21.

149. Rokhlin, O.W., and Cohen, M.B., *Differential sensitivity of human prostatic cancer cell lines to the effects of protein kinase and phosphatase inhibitors.* Cancer Lett, 1995. **98**(1): p. 103-10.
150. Muller, W.J., Zen, K., Fisher, A.B., and Shuman, H., *Pathways for uptake of fluorescently labeled liposomes by alveolar type II cells in culture.* Am J Physiol, 1995. **269**(1): p. L11-19.
151. Guo, X., MacKay, J. A., and Szoka, F.C. Jr., *Mechanism of pH-triggered collapse of phosphatidylethanolamine liposomes stabilized by an ortho ester polyethyleneglycol lipid.* Biophys J, 2003. **84**(3): p. 1784-1795.
152. Kinsky, S.C., Loader, K.E., and Benson, A.L., *An alternative procedure for the preparation of immunogenic liposomal model membranes.* J Immunol Methods, 1983. **65**(3): p. 295-306.
153. Bowman, R.E., and Wolf, R.C., *A rapid and specific ultramicro method for total serum cholesterol.* Clin Chem, 1962. **8**(3): p. 302-309.
154. Vogel, K., Wang, S., Lee, R.J., Chmielewski, J., and Low, P.S., *Peptide-mediated release of folate targeted liposome content from endosomal compartments.* JACS, 1996. **118**(7): p. 1581-86.
155. Martin, B., Aissaoui, A., Sainlos, M., Oudrhiri, N., Hauchecorne, M., Vigneron, J.P., Lenh, J.M., and Lehn, P., *Advances in cationic lipid-mediated gene delivery.* Gene Ther Mol Biol, 2003. **7**: p. 273-89.
156. Felgner, J.H., Kumar, R., Sridhar, C.N., Wheeler, C.J., Tsai, Y.J., Border, R., Ramsey, P., Martin, M., and Felgner, P.L., *Enhanced gene delivery and mechanism studies with a novel series of cationic lipid formulations.* J Biol Chem, 1994. **269**(4): p. 2550-2561.
157. Legendre, J.Y., and Szoka Jr., F.C., *Delivery of plasmid DNA into mammalian cell lines using pH-sensitive liposomes: comparison with cationic liposomes.* Pharm Res, 1992. **9**(10): p. 1235-42.
158. Epand, R.M., and Bottega, R., *Modulation of the phase transition behavior of phosphatidylethanolamine by cholesterol and oxysterols.* Biochemistry, 1987. **26**(7): p. 1820-1825.
159. Demel, R.A., Bruckdorfer, K. R., and Van Deenen, L. L. M., *The effect of sterol structure on the permeability of liposomes to glucose, glycerol and Rb.* Biochim Biophys Acta, 1972. **255**(1): p. 321-330.
160. Papahadjopoulos, D., Nir, S., and Ohki, S., *Permeability properties of phospholipid membranes: effect of cholesterol and temperature.* Biochim Biophys Acta, 1972. **266**(3): p. 561-83.
161. Ohki, S., *The electrical capacitance of phospholipid membranes.* Biophys J, 1969. **9**(10): p. 1195-1205.
162. Cullis, P.R., and De Kruijff, B., *Polymorphic phase behaviour of lipid mixtures as detected by 31P NMR. Evidence that cholesterol may destabilize bilayer structure in membrane systems containing phosphatidylethanolamine.* Biochim Biophys Acta, 1978. **507**(2): p. 207-18.
163. Szoka, F., Jr., and Papahadjopoulos, D., *Comparative properties and methods of preparation of lipid vesicles (liposomes).* Annu Rev Biophys Bioeng, 1980. **9**: p. 467-508.
164. Fernley, H.N., and Walker, P. G., *Studies on alkaline phosphatase. Inhibition by phosphate derivatives and the substrate specificity.* Biochem J, 1967. **104**(3): p. 1011-8.
165. Mui, B.L., Cullis, P.R., Evans, E.A., and Madden, T.D., *Osmotic properties of large unilamellar vesicles prepared by extrusion.* Biophys J, 1993. **64**(2): p. 443-53.
166. Shoemaker, S.D., and Vanderlick, T.K., *Stress-induced leakage from phospholipid vesicles: effect of membrane composition.* Ind Eng Chem Res, 2002. **41**(3): p. 324-29.

167. Zalipsky, S., Qazen, M., Walker, J. A., Mullah, N., Quinn, Y. P., and Huang, S. K., *New detachable poly(ethylene glycol) conjugates: cysteine-cleavable lipopolymers regenerating natural phospholipid, diacyl phosphatidylethanolamine.* Bioconjugate Chem, 1999. **10**(5): p. 703-7.
168. Harris, T.J., von Maltzahn, G., Derfus, A.M., Rusolahti, E., and Bhatia, S.N., *Proteolytic actuation of nanoparticle self-assembly.* Angew Chem Int Ed Engl, 2006. **45**(19): p. 3161-3165.
169. Zhang, J.X., Zalipsky, S., Mullah, N., Pechar, M., and Allen, T.M., *Pharmaco attributes of dioleoylphosphatidylethanolamine/cholesterylhemisuccinate liposomes containing different types of cleavable lipopolymers.* Pharmacol Res, 2004. **49**(2): p. 185-98.
170. Kirpotin, D., Hong, K., Mullah, N., Papahadjopoulos, D., and Zalipsky, S., *Liposomes with detachable polymer coating: destabilization and fusion of dioleoylphosphatidylethanolamine vesicles triggered by cleavage of surface-grafted poly(ethylene glycol).* FEBS Lett, 1996. **388**(2-3): p. 115-18.
171. Xu, Y., and Szoka Jr., F.C., *Mechanism of DNA release from cationic liposome/DNA complexes used in transfection.* Biochemistry, 1996. **35**(18): p. 5616-23.
172. Szoka, F.C., and Papahadjopoulos, D., *Procedure for preparation of liposomes with large internal aqueous space and high capture by reverse-phase evaporation.* PNAS, 1978. **75**(9): p. 4194-98.
173. Maggi, V., *A study of lysosomal acid phosphatase during mitosis in HeLa cells.* J Royal Micros Soc, 1966. **85**(3): p. 291-295.
174. Cohen, R.B., Nachlas, M.M., and Seligman, A., *Histochemical demonstration of esterase in malignant brain tumors.* Cancer Res, 1951. **11**(9): p. 709-711.
175. Guner, G., Kokoglu, E., and Guner, A., *Acid and alkaline phosphatase activities in homogenates and subcellular fractions of human brain tumors.* Cancer Lett, 1985. **29**(3): p. 339-43.
176. Tunggal, J.K., Cowan, D.S., Shaikh, H., and Tannock, I.F., *Penetration of anticancer drugs through solid tissue: a factor that limits the effectiveness of chemotherapy for solid tumors.* Clin Cancer Res, 1999. **5**(6): p. 1583-6.
177. Groothuis, D.R., Benalcazar, H., Allen, C. V., Wise, R. M., Dills, C., Dobrescu, C., Rothholtz, V., Levy, R. M., *Comparison of cytosine arabinoside delivery to rat brain by intravenous, intrathecal, intraventricular and intraparenchymal routes of administration.* Brain Res, 2000. **856**(1-2): p. 281-90.
178. Huynh, G.H., Deen, D. F., and Szoka, F. C., Jr., *Barriers to carrier mediated drug and gene delivery to brain tumors.* J Control Release, 2006. **110**(2): p. 236-59.
179. Groothuis, D.R., Vavra, M. W., Schlageter, K. E., Kang, E. W., Itskovich, A. C., Hertzler, S., Allen, C. V., Lipton, H. L., *Efflux of drugs and solutes from brain: the interactive roles of diffusional transcapillary transport, bulk flow and capillary transporters.* J Cereb Blood Flow Metab., 2007. **27**(1): p. 43-56.
180. Chen, M.Y., Lonser, R. R., Morrison, P. F., Governale, L. S., and Oldfield, E. H., *Variables affecting convection-enhanced delivery to the striatum: a systematic examination of rate of infusion, cannula size, infusate concentration, and tissue-cannula sealing time.* J Neurosurg, 1999. **90**(2): p. 315-20.
181. Lopez, K.A., Waziri, A. E., Canoll, P. D., and Bruce, J. N., *Convection-enhanced delivery in the treatment of malignant glioma.* Neurol Res, 2006. **28**(5): p. 542-8.
182. Hall, W.A., Rustamzadeh, E., Asher, A. L., *Convection-enhanced delivery in clinical trials.* Neurosurg Focus, 2003. **14**(2): p. E2.
183. Raghavan, R., Brady, M. L., Rodriguez-Ponce, M. I., Hartlep, A., Pedain, C., and Sampson, J. H., *Convection-enhanced delivery of therapeutics for brain disease, and its optimization.* Neurosurg Focus, 2006. **20**(4): p. E12.

184. Voges, J., Reszka, R., Gossmann, A., Dittmar, C., Richter, R., Garlip, G., Kracht, L., Coenen, H. H., Sturm, V., Wienhard, K., Heiss, W. D., and Jacobs, A. H., *Imaging-guided convection-enhanced delivery and gene therapy of glioblastoma.* Ann Neurol, 2003. **54**(4): p. 479-87.
185. Bobo, R.H., Laske, D. W., Akbasak, A., Morrison, P. F., Dedrick, R. L., and Oldfield, E. H., *Convection-enhanced delivery of macromolecules in the brain.* PNAS, 1994. **91**(6): p. 2076-80.
186. Krauze, M.T., Forsayeth, J., Park, J. W., and Bankiewicz, K. S., *Real-time imaging and quantification of brain delivery of liposomes.* Pharm Res, 2006. **23**(11): p. 2493-504.
187. MacKay, J.A., Deen, D. F., and Szoka, F. C., Jr., *Distribution in brain of liposomes after convection enhanced delivery; modulation by particle charge, particle diameter, and presence of steric coating.* Brain Res, 2005. **1035**(2): p. 139-53.
188. DiResta, G.R., Lee, J., Healey, J.H., Levchenko, A., Larson, S.M., and Arbit, E., *"Artificial lymphatic system": a new approach to reduce interstitial hypertension and increase blood flow, pH and pO2 in solid tumors.* Ann Biomed Eng, 2000. **28**(5): p. 543-55.
189. Huynh, G.H., T. Ozawa, D.F. Deen, and F.C. Szoka, Jr., *Retro-convection enhanced delivery to increase blood to brain transfer of macromolecules.* Brain Res, 2007. **1128**(1): p. 181-90.
190. Baxter, L.T., and Jain, R.K., *Transport of fluid and macromolecules in tumors. I. Role of interstitial pressure and convection.* Microvasc Res, 1989. **37**(1): p. 77-104.
191. Kalyanasundaram, S., Calhoun, V. D., and Leong, K. W., *A finite element model for predicting the distribution of drugs delivered intracranially to the brain.* Am J Physiol, 1997. **273**(5 Pt 2): p. R1810-21.
192. Basser, P.J., *Interstitial pressure, volume, and flow during infusion into brain tissue.* Microvasc Res., 1992. **44**(2): p. 143-65.
193. Levin, V.A., Patlak, C. S., and Landahl, H. D., *Heuristic modeling of drug delivery to malignant brain tumors.* J Pharmacokinet Biopharm, 1980. **8**(3): p. 257-96.
194. Morrison, P.F., Laske, D. W., Bobo, H., Oldfield, E. H., and Dedrick, R. L., *High-flow microinfusion: tissue penetration and pharmacodynamics.* Am J Physiol, 1994. **266**(1 Pt 2): p. R292-305.
195. Smith, J.H., and Humphrey, J. A., *Interstitial transport and transvascular fluid exchange during infusion into brain and tumor tissue.* Microvasc Res, 2007. **73**(1): p. 58-73.
196. Wang, P., and Olbricht, W.L., *Retro-convection enhanced drug delivery: a computational study.* Ann Biomed Eng, 2010. **38**(8): p. 2512-9.
197. Motion, J.P., Huynh, G. H., Szoka, F. C., Jr., and Siegel, R. A., *Convection and retro-convection enhanced delivery: some theoretical considerations related to drug targeting.* Pharm Res, 2011. **28**(3): p. 472-9.
198. Verwey, E.J.W., and Overbeek, J.Th.G., *Theory of the Stability of Lyophobic Colloids*2000, Mineola, NY: Dover Publications.
199. Gueron, M., Weisbuch, G., *Polyelectrolyte Theory.I.Counterion Accumulation, Site-Binding and Their Insensitivity to Polyelectrolyte Shape in Solutions Containing Finite Salt Concentrations.* Biopolymers, 1980. **19**: p. 353-83.
200. Saito, R., Krauze, M. T., Bringas, J. R., Noble, C., McKnight, T. R., Jackson, P., Wendland, M. F., Mamot, C., Drummond, D. C., Kirpotin, D. B., Hong, K., Berger, M. S., Park, J. W., and Bankiewicz, K. S., *Gadolinium-loaded liposomes allow for real-time magnetic resonance imaging of convection-enhanced delivery in the primate brain.* Exp Neurol, 2005. **196**(2): p. 381-9.
201. Levi, M.S., Brimble, M. A., *A review of neuroprotective agents.* Curr Med Chem, 2004. **11**(18): p. 2383-97.

202. Neeves, K.B., Sawyer, A. J., Foley, C. P., Saltzman, W. M., and Olbricht, W. L., *Dilation and degradation of the brain extracellular matrix enhances penetration of infused polymer nanoparticles.* Brain Res, 2007. **1180**(14): p. 121-132.

Publishing Agreement

It is the policy of the University to encourage the distribution of all theses, dissertations, and manuscripts. Copies of all UCSF theses, dissertations, and manuscripts will be routed to the library via the Graduate Division. The library will make all theses, dissertations, and manuscripts accessible to the public and will preserve these to the best of their abilities, in perpetuity.

Please sign the following statement:

I hereby grant permission to the Graduate Division of the University of California, San Francisco to release copies of my thesis, dissertation, or manuscript to the Campus Library to provide access and preservation, in whole or in part, in perpetuity.

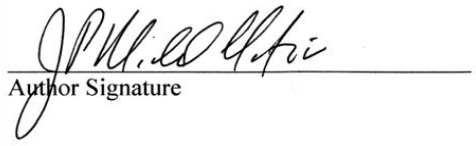

Author Signature

March 20th, 2012

Date